RECEIVED
LAWRENCE
RADIATION LABORATORY

UCRL-20682

DOCUMENTS SECTION

A STUDY OF THE REACTIONS $K^- p \rightarrow \Sigma^{\pm}\pi^{\mp}(\pi^0)$ BETWEEN 1.1 AND 1.7 GeV/c

Daniel Frederick Kane, Jr.
(Ph. D. Thesis)

April 1971

AEC Contract No. W-7405-eng-48

TWO-WEEK LOAN COPY

This is a Library Circulating Copy which may be borrowed for two weeks. For a personal retention copy, call Tech. Info. Division, Ext. 5545

LAWRENCE RADIATION LABORATORY
UNIVERSITY of CALIFORNIA BERKELEY

UCRL-20682

DISCLAIMER

This document was prepared as an account of work sponsored by the United States Government. While this document is believed to contain correct information, neither the United States Government nor any agency thereof, nor the Regents of the University of California, nor any of their employees, makes any warranty, express or implied, or assumes any legal responsibility for the accuracy, completeness, or usefulness of any information, apparatus, product, or process disclosed, or represents that its use would not infringe privately owned rights. Reference herein to any specific commercial product, process, or service by its trade name, trademark, manufacturer, or otherwise, does not necessarily constitute or imply its endorsement, recommendation, or favoring by the United States Government or any agency thereof, or the Regents of the University of California. The views and opinions of authors expressed herein do not necessarily state or reflect those of the United States Government or any agency thereof or the Regents of the University of California.

TABLE OF CONTENTS

		Page
Abstract		iv
I.	Introduction	1
II.	Experimental Procedures	4
	A. K^- Beam Design	4
	B. Bubble Chamber Characteristics	6
	C. Data Reduction	7
	D. Cutting and Weighting	10
	E. Efficiency Corrections	16
III.	Experimental Results	19
	A. Cross Sections	19
	B. Two Body Final States	21
	1. Angular Distributions	21
	2. Polarizations	23
	3. Legendre Coefficients	24
	C. Three Body Final States	26
	1. Dalitz Plots	27
	2. Invariant Mass-Squared Distributions	28
IV.	Partial Wave Analysis of $\pi^{\pm}\Sigma^{\mp}$	31
	A. Theoretical Basis	31
	B. Procedure	36
	C. Results	41
V.	Interpretation of Partial Waves	53
	A. The Resonance Model	53
	B. SU(3) Symmetry Classifications	58
	C. Comments on New Resonant States	64

Page

VI. Acknowledgments 66

VII. References and Footnotes 67

VIII. Tables 74

IX. Figure Captions 100

X. Figures 105

A STUDY OF THE REACTIONS $K^-p \to \Sigma^{\pm}\pi^{\mp}$ (π^0) BETWEEN 1.1 AND 1.7 GeV/c

Daniel Frederick Kane, Jr.

Lawrence Radiation Laboratory
University of California
Berkeley, California

April 1971

ABSTRACT

We present new data for the reactions $K^-p \to \Sigma^{\pm}\pi^{\mp}$ (π^0) for laboratory momenta between 1.1 and 1.7 GeV/c: angular distributions, polarizations, and Legendre coefficients for $\Sigma^{\pm}\pi^{\mp}$; Dalitz plots and invarient mass-squared plots for $\Sigma^{\pm}\pi^{\mp}\pi^0$; and cross sections for all reactions.

For the two body final states we also present a partial wave analysis. We have developed a new technique for finding new resonant structure when some resonances are well known, using non-resonant parameterizations in such a way that the appropriate resonances are suggested by the data. Applying this technique to the data of this and a related experiment (starting from the well established resonances - $\Sigma(1765)$, $\Lambda(1815)$, $\Lambda(1830)$, $\Sigma(2030)$, and $\Lambda(2100)$, we find independent evidence for several resonances not previously well established. In particular, we confirm the presence of resonances in the F15 and D13 waves between 1.9 and 2.0 GeV.

We have also looked at the couplings for resonances associated in representations of the SU(3) group. The quality of fit to SU(3) symmetric couplings depends on the assumed energy dependence of the resonant width. Since the best fit occurs for an energy dependence which seems to disagree with the energy dependence required for the partial wave analysis, we propose that the couplings are affected by SU(3) symmetry breaking.

I. INTRODUCTION

The data for this experiment were drawn from approximately three quarters of a million triads on 528 rolls of film. Each triad is three views of the Berkeley 25-inch Bubble Chamber, filled with liquid hydrogen; each was taken as a beam of K^- mesons entered during pressure expansion. The particles in the beam interacted with the protons in the chamber, and the basic object of the experiment was to study the forces involved in these interactions. All charged particles leave tracks of bubbles in the liquid; and, because the chamber was in a magnetic field, these tracks were curved. This curvature yields information on the momenta of the charged particles involved in the interaction. In addition, the density of bubbles in the track yields information for distinguishing particles of different rest mass.

In particular this experiment is concerned with the reactions

$$K^- p \rightarrow \pi^{\pm}\Sigma^{\mp} \ (\pi^0)$$

followed by

$$\Sigma^{\mp} \rightarrow \pi^{\mp} n \quad \text{or} \quad \Sigma^{+} \rightarrow \pi^{0} p \quad .$$

The sigma is a short-lived particle which almost always decays within the chamber. The visual topology--incoming beam track and two outgoing tracks, one of which "kinks"--occurred on the average once in twenty-five triads. Experiments studying these reactions at energies partially overlapping our range have been reported.[1-4]

Of the four known microscopic forces--the strong interaction, the electro-magnetic interaction, the weak interaction, and gravity--only the

electromagnetic interaction is well enough understood to have a detailed, coherent mathematical formulation. The decay of the sigma involves the weak interaction, about which sufficient is known experimentally for the purposes of this study. Our main concern here is the primary reaction, which proceeds via the strong interaction. A few general characteristics of this force are well established; beyond that there are at the present time a proliferation of theoretical models which attempt to account for various aspects of the observed phenomena. The model most appropriate for the energy range of this experiment is the resonance model, which pictures the strong interaction as proceeding by the formation and rapid decay of an intermediate particle. This particle, or resonance, decays so rapidly that it is detected only by the way its decay products are distributed; the strong force is observed only by the type and distribution of the outgoing particles. In particular it has been suggested that for two body final states such as ours, the strong interaction may be completely accounted for by resonance effects.[5] If a resonance is truely an independent particle, we expect it to be seen in more than one reaction. This experiment cannot by itself study this matter; however, it does add to the store of observations upon which this study must be based.

The following discussion proceeds from the directly observed to the model dependent interpretations. Section II describes how the data were brought into usable form. Section III presents the direct experimental results: the cross sections (probabilities) for the reactions and the distributions of the final state particles.

Section IV exploits the well-established properties of the strong interaction to represent the two body final states in a generally useful form--the partial waves. Finally, Section V attempts to interpret these partial waves in the context of the different models. The data for the three body final states are incomplete, and no analysis is attempted. These data are included here because the experimental procedure described in Section II is indistinguishably applicable to both two and three body final states, and because a simple, partial interpretation can be and is presented.

The primary concern here is to present the experimental results, along with some appropriate interpretation. We shall endeavor to describe the underlying physical concepts, skip over the details of derivation by referring to the literature, and present the exact formulae used in analysis or interpretation.

II. EXPERIMENTAL PROCEDURES

A. K^- Beam Design

The two-stage separated beam for the 25-inch bubble chamber, shown in Fig. 1, was designed for a wide variety of experiments. The use of a target in the external proton beam of the Bevatron made this secondary beam independent of the Bevatron field and allowed for the selection of positive or negative particles. Five bending magnets and a momentum slit allowed the selection of beam momenta varying from less than 1.0 BeV/c to greater than 3.0 BeV/c, with momentum bites typically ± 1%. The electrostatic separators (spectrometers in figure) with two mass slits eliminated undesired particles. Twelve quadrupole magnets and a vertical collimator shaped the beam for most efficient momentum selection and mass separation. The slits and collimator were made of uranium and were variable for different beam configurations. While taking film, the chamber was a peripheral user of the Bevatron; a rapid beam ejector furnished the primary protons. Whenever possible two RBEs were used--before and after major users got beam; the chamber could pulse twice per Bevatron cycle and, at this rate, take about a thousand triads per hour. Finally, a beam destroyer magnet swept the primary beam off the target when the number of beam particles entering the chamber reached the desired level.

The specific problems for the K^- beam were obtaining sufficient flux and eliminating the π^- flux. The number of K^- particles in a beam drops exponentially with a mean decay length depending on momentum: as the beam momentum ranged from 1.7 down to 1.1 BeV/c, the beam line

effectively increased from three to five decay lengths. Obtaining sufficient flux was the more difficult problem at the lower momenta where the decay loss was greater. The π^- flux was about one hundred times greater than the K^- flux at the production target and decayed much more slowly. The electrostatic separators, in two stages, diverted the π^- beam away from the median plane: the distance, Δ, between the two beams in the mass slit depending inversely on the momentum, p:[6]

$$\Delta \sim \frac{V\ell}{d} \frac{m_k^2 - m_\pi^2}{2p^3}$$

Here m_k and m_π are the respective masses and V, ℓ, and d are the voltage, length and plate separation of the separator involved. Separating the π^- beam from the K^- beam was the more difficult problem at the higher momenta. To solve these problems, the beam optics were designed to trade, at lower momenta, effective separation for flux. The separators were always run at maximum voltage. At lower momenta, where the center to center separation was larger, the beam size was magnified, allowing more of the angular divergence from the production target to be accepted into the beam. The K^- flux, determined from the tau decay mode, averaged roughly 9 to 11 particles per exposure. The exact contamination of the beam at the bubble chamber, less than 10% π^- or μ^-, was not critical since normalization was not determined by a beam count. Details, both for the overall beam and for the K^- beam, have been written up in technical notes.[7]

The film was taken during the period from May, 1968 to July, 1969 with the K^- beam tuned to fifteen different momenta. Table I shows the normalization within the beam phase space and chamber volume cuts. The momenta were determined from the fitted tau decays. Although some of the momenta were essentially the same, it was necessary to treat the subsets separately since the beam profiles were different. For explanation of terminology for and discussion of the cuts, see Section II-D. The significance of the microbarn equivalent is discussed in Section III-A. Further details about the normalization have been written up in a technical note.[8]

B. Bubble Chamber Characteristics

The bubble chamber, as a detection device, is based on the principle of ions triggering bubble formation in a super-heated liquid. The 25-inch bubble chamber filled with hydrogen had a density of .0603 gm/cm^3 (measured by range of stopping μ's). A signal from the Bevatron started a relaxation of the pressure, causing the liquid to become superheated; the beam entered the chamber before the pressure reached minimum. After a delay of about two milliseconds the lights were flashed, recording a triad, and the pressure restored. The density of bubbles depended on the position of the beam in the pressure valley; their size depended on the light delay. These parameters were maintained such that the bubbles would be about .4 mm in diameter with a density of 10-12 bubbles per centimeter at minimum ionization. The ionization caused by a given particle depends on its velocity, β:[9]

$$-\frac{dE}{dx} = \frac{k}{\beta^2} \left| \ln \frac{k'}{1-\beta^2} - \beta^2 \right|$$

is the ionizing energy lost by the particle per unit length. While the curvature of a track determines the particle's momentum, particles of different mass would have different velocities and hence different bubble densities. For example, a 1.0 BeV/c proton (p) causes ionization roughly twice that of a 1.0 BeV/c pion (π). One view of a typical event is shown in Fig. 2.

C. Data Reduction

There were four stages in the reduction of the data from visual patterns on film to physically meaningful numbers, namely momenta and angles. The first two stages, scanning the film for events having the desired pattern and then measuring these events, were accomplished using the COBWEB system of on-line scan tables and Franckensteins.[10] Scanners sent to an IBM 7044 computer, via teletype, information concerning each event's type and location (roll, frame, grid positions). All events with kinking tracks were taken. At a later time when the roll was on a Franckenstein for measurement, the computer transported the film to the proper frame and drove the stage to the fiducials and vertices. Operators did the final centering. Track following was used on long tracks, while the connecting track was often measured in the two point mode. A pulse height indicator was used to measure the projected bubble density as an indication of the ionization. Measuring rates averaged about twenty events per hour for this event type. The final two stages

of data reduction, geometrical reconstruction from the known locations of fiducials in three views and then kinematic fitting to reaction hypotheses, used the programs of the Data Handling Group, FOG and CLOUDY, respectively, executed on an IBM 7094.[11] The measured momentum of the beam track was modified by an edited value obtained by fitting highly constrained $\Lambda\pi^+\pi^-$ events. Usually no information was available for the connecting track, so two starting values were obtained assuming the visible decay particle was forward or backward in the center of mass; a simultaneous fit to both vertices was then used.

For most events, fitting was restricted to the hypotheses of interest. Initially a sample of data with negative track kinking was fitted as well to K^- hypotheses to look at the problem of ambiguities (particularly $K^-\pi^+n$ fitting $\Sigma^-\pi^+\pi^0$). Events that were ambiguous were studied on the scan table. From this it was estimated that excluding any event with a lifetime greater than .6 nsec. would leave a contamination of roughly 1/2%. This would exclude some sigmas, but weighting would account for them (see below). Therefore, any event was excluded from further consideration if: a) the connecting track was well measured (error on momentum relatively small); and b) the lifetime as determined from the measured momentum, and assuming it was a sigma, was greater than .6 nsec. This applied to positive kinking tracks as well, since there were also positive and negative pion decays. All events of this type which did fit the sigma hypothesis well were looked at on the scan table. The number that were truely sigmas was roughly that expected from the known lifetime. On the basis of the remainder it could be estimated that there remained a K^- contamination of 1/2% for

$\pi^+\Sigma^-$ and 2% for $\pi^+\Sigma^-\pi^0$. By fitting to the $K^+\Xi^-$ hypothesis, all events in which the three outgoing momenta were roughly coplanar, a 4% contamination of the $\pi^+\Sigma^-$ topology was eliminated. Negative kinking events, which did not fit the sigma hypotheses and were not beyond the lifetime cut, were also tried as Ξ^-K^+; if they fit well, they were excluded from further consideration.

The data reduction of tens of thousands of events required a great deal of bookkeeping and event selection techniques. Information from scanning, measuring, and geometrical reconstruction stages went onto "master list" tapes using the BOOKY program on the CDC 6600.[12] Events that were selected as unambiguous good fits or as beyond the lifetime cut were so flagged on the master list. All other events became candidates for remeasure. Logical selection of events used another program of the Data Handling Group, FAIR. In particular, there were two main classes of kinematic ambiguities: for the Σ^+ both π^+ decay and p decay hypotheses gave good fits, for $\pi^\pm\Sigma^\mp\pi^0$ both starting values led to good but significantly different fits. For the decay ambiguities the ionization information from the Franckensteins was sufficient for resolution in 30% of the cases;[13] most of the rest could be resolved visually by scanners. The three-body ambiguities could often be resolved on the basis of the ionization of the sigma. In all cases the scanners sent the event back for remeasurement if discrimination did not involve a factor of two between the bubble densities required by the fitted momenta. Along with this ionization scan the scanners looked at all events not measured, sometimes correcting clerical mistakes such as wrong event type or wrong frame number (grid positions identified events;

wrong numbers were often adjacent or from wrong view), sometimes rejecting the event as unmeasurable or failing scanning criteria. Such events, as well as the resolved ambiguities, were eliminated from or corrected on the remeasure candidates. Roughly 25% of the events were remeasured and went through the FOG-CLOUDY-FAIR system and an ionization scan. The overall statistics are given in Table II.

D. Cutting and Weighting

In order to normalize the numbers of events to the beam path length, it was necessary to make cuts in the beam phase space and chamber volume; these cuts are given in Table I. The phase space cuts, position at chamber window (YEND, ZEND) and entrance angle (ALFE, BETE), determine a swath as the beam passes through the chamber, hence the chamber volume is established by the initial and final locations along the beam direction (XVTX). These cuts were determined from the distributions for the tau decays, where necessary for each momentum; events were accepted within three standard deviations of the mean for determining cross sections, within 4.5 standard deviations otherwise. The distributions in YEND and XVTX were not gaussian; a comparison of the tau and sigma distributions is given in Fig. 3. Not all sigmas decayed inside the chamber, so it was necessary to establish an acceptance volume for the decay vertex (X2, Y2, Z2). This was chosen to be a cylinder 43 centimeters in diameter and 15 centimeters in height; the distribution of events with respect to this volume is shown in Fig. 4.

The scanners, who were looking for kinking two prongs, were unable to find all sigma events: sometimes the kink was not obvious,

either because the connecting track was too short or too long or because the deflection of the decay track was not noticeable. These losses are related to the lifetime and decay angular distributions of the sigma and can be corrected without biasing the study of the forces at the primary vertex. Those events determined to be subject to loss were cut from the sample and the others were weighted individually according to the fraction of the lifetime and decay distributions so eliminated.

The lifetime of the sigma in its rest frame is distributed exponentially, the number decaying in an interval $d\tau$ at a time τ being

$$dN = N^{o} \exp(-\tau/\tau_{m})\, d\tau$$

Here τ_m is the mean lifetime and the original number, N^o, is unity for weighting individual events. Duration in the rest frame is translated into distance traveled in the lab frame by the product of the time dilation factor and the velocity. The same product translates rest mass, m_Σ, into lab momentum, P_Σ; hence, if the momentum remains constant, the distance between production and decay vertices, L, is

$$L = \frac{P_\Sigma}{m_\Sigma}\, \tau$$

The momentum does change, however, as energy is lost by ionization; so when studying the lifetime distribution, an accurate integration was used to determine τ from the track length and the production momentum. The distribution of lifetimes was indeed exponential, within statistics, in a limited range excluding both large and small values, Fig. 5. The

mean lifetimes, calculated using a maximum likelihood technique, were determined for the sample of events passing all cuts.[14] These are given in Table III for each topology.

It was necessary to cut out events decaying within a certain distance L_{MIN}. For each event this was translated into a minimum lifetime

$$\tau_{MIN} = \frac{m_\Sigma}{P_\Sigma} L_{min} \quad .$$

The production momentum was used. There was a slight tendency for vertex disassociation when the connecting track was very long; a maximum length cut, L_{MAX}, was established. Also there was a cut directly on the lifetime, τ_k, to eliminate meson contamination. Hence it was necessary to choose a minimum from the upper cuts on the lifetime:

$$\tau_{MAX} = \text{MIN}\left(\frac{m_\Sigma}{P_\Sigma} L_{MAX}, \frac{m_\Sigma}{P_\Sigma} L_{POT}, \tau_k\right).$$

The maximum length and the potential length to the wall of the decay volume, L_{POT}, were translated using the production momentum. This was, although not strictly correct, a sufficient approximation in relevant cases: if the sigma had a high momentum (minimal ionization loss) or the event occurred very close to the wall, the momentum could change but insignificantly. In other cases τ_k was the minimum. The fraction, f_τ, of the lifetime distribution falling within the limits is

$$f_\tau = \exp(-\tau_{MIN}/\tau_m) - \exp(-\tau_{MAX}/\tau_m) \quad .$$

For purposes of weighting, the mean lifetimes were taken from a large statistics experiment:[15]

$$\tau_{\Sigma^-} = 1.47$$

$$\tau_{\Sigma^+} = 0.80$$

The decay angular distribution of the sigma is isotropic in two properly chosen variables. The direction of the decay in the sigma's rest frame can be correlated only with the sigma's spin direction. This may in turn be correlated with a direction perpendicular to the sigma's line of flight (production normal or decay normal).[16] However, the distribution of the angle between the decay direction and the line of flight averages over any such effect. Similarly the angle between two planes about the line of flight, the one containing the decay direction, the other containing an arbitrary, chamber fixed z-axis, is unaffected. These two variables, δ and ϕ respectively, are, when transformed to the rest frame, the polar and azimuthal angles in which the decay distribution should be isotropically distributed. The events missing from these distributions, Fig. 6, were those with imperceptible kinks. This made it necessary to determine a minimum acceptable δ, δ_c. Also certain regions of ϕ, decay toward or away from the cameras, were particularly subject to loss.

The cut on the variable δ must be transformed into the rest frame (ϕ is invariant under this transformation). The Lorentz variables, η and γ, are respectively the momentum and energy of the sigma divided by its rest mass.

$$P \sin \delta = p^* \sin \delta^*$$

$$P \cos \delta = \eta E^* + \gamma p \cos \delta^*$$

The constants, p^* and E^*, are the momentum and energy of the decay particle in the rest frame; the momentum in the lab frame, P, cancels in the succeeding derivation. The relation of the cuts in the variable $c = \cos \delta^*$ to the cut angle, δ_c, is

$$c^{\pm} = \frac{-T^2 R \pm \sqrt{1 + T^2(1 - R)}}{1 + T^2}$$

$$T = \gamma \tan \delta_c \quad , \quad R = \frac{\eta E^*}{\gamma P^*}$$

This transformation of the angle is presented graphically in Fig. 7. That, for $\Sigma^+ \to p\, \pi^0$, small δ can correspond to both forward and backward decays in the rest frame is evidenced by the loss specific to this decay type, as shown in Fig. 6. The fraction of the distribution, f_δ, not cut out of the sample is

$$f_\delta = \frac{1}{2}(c^+ - c^-) \qquad R > 1.$$

$$f_\delta = \frac{1}{2}(c^+ + 1.) \qquad R \leq 1.$$

since c is evenly distributed between -1. and +1. The case in which the radical is negative, corresponding to the confinement of all lab decay angles within the cut, was avoided (see below).

The distribution in ϕ was folded and a cut, ϕ_c, made on the

deviation from the nearest of 0°, 180°, or 360°. The fraction of the distribution accepted, f_{ϕ}, was simply

$$f_{\phi} = 1. - \phi_c/90.$$

The three variables--τ, δ, and ϕ--were uncorrelated; therefore, the fraction of the overall distribution which passed all cuts was the product of the individual fractions. Weighting each event passing all cuts by

$$\frac{1}{f_{\tau} \cdot f_{\delta} \cdot f_{\phi}}$$

should then give a statistically accurate, for sufficiently large samples, representation of the actual number of events. As the extent of the cut is increased, a point should be reached at which the weighted number of events ceases to change: the increase in the weights just accounts for the events newly cut. This was in fact the case, and this technique was used to determine the appropriate cuts.

A separate set of cuts was determined for each of the three decay types: $\Sigma^- \rightarrow \pi^- n$, $\Sigma^+ \rightarrow \pi^+ n$, and $\Sigma^+ \rightarrow p\pi^0$. The Σ^- differs significantly in its mean lifetime, the p decay in the transformation properties of the angle. For determining the overall numbers of events (i.e. for cross sections), the appropriate value for the cut in a given variable was taken to be that value for which the increase in the weighted number of events became negligible. For distributions in which the relative numbers of events were of sole importance, these cuts could be relaxed somewhat. Since the loss of events depended only on sigma momentum and chamber geometry, the effect of cutting and weighting was studied as a

function of sigma momentum. For production angular distributions and invariant mass-squared distributions, the cuts were chosen such that the further increase in the weighted numbers of events was statistically the same for all sigma momenta. For polarization of the Σ^+ even the relative numbers were not involved; essentially all good $\Sigma^+ \rightarrow p\pi^0$ were accepted. This decay type was not used for any other purpose, however, since for very high sigma momenta all decays were confined to small forward lab angles. With all events cut out, repopulation by weighting was impossible. The cuts used in the final analysis are given in Table IV; the numbers of events in three classes-failing beam phase space or chamber volume cuts, passing these but failing length or angle cuts, and passing all cuts--are given in Table V.

E. Efficiency Corrections

Not all of even the most obvious events are found during a single scan; furthermore, not all of the good events get through the data reduction to be used in the data analysis. The cross sections, representing absolute numbers of events, must be corrected both for scanning efficiency and for what will be called "through-put efficiency." In order to avoid over-correcting, these efficiencies were determined for the class of events passing all cuts.

Slightly over half the film was scanned a second time. All events found on only one scan were checked, and events either unmeasurable or failing scanning criteria were eliminated (these correspond to "measure reject sustained" in Table II). From the remaining events a scanning efficiency could be determined for all events. This was done for each

beam momentum, the results varying from 88% to 95% for a single scan. The good events found only on the second scan were also measured and made available for analysis. Thus it was possible to determine the scanning efficiency for all events passing all cuts. The results, varying from 95% to 98% for a single scan, were significantly different and represent the scanning efficiency for obvious events. The efficiencies for momenta scanned only once were determined from the efficiencies for individual scanners; the scanning efficiencies for two scans were never less than 99%. The results are given in Table VI.

Events were considered "good" fits, and hence used in the data analysis, if their chi-square for goodness of fit was less than 19 for the four constraint fit or less than 11 for the one constraint fit (missing neutral). As can be seen from Table II, roughly half of the events remeasured met these criteria. This suggests that the chi-square is not a good statistical indicator, presumably because of the difficulty in measuring this event type. One estimate of the through-put efficiency assumes that all events which fit represent all true events--some true events fail to fit while some fits are fakes.[17] Still there remain some 1800 events, considered satisfactory on the rescan, which did not have a fit attempted (remeasure, FOG, or CLOUDY rejects). Assuming the fraction of these that would fit is the same as for the other remeasures gives a second estimate of the through-put efficiency. The values used in the analysis were intermediate between these two, with errors reflecting their difference. Since the former could be determined both for all events and for events satisfying all cuts, a difference of about 1%, the final values included this adjustment. The data were handled

in four batches; a through-put efficiency was determined for each batch, as shown in Table VI.

III. EXPERIMENTAL RESULTS

A. Cross Sections

In the discussion of experimental procedure, the subsets of data have been designated by laboratory momentum, P_{LAB}. However, a more meaningful designation is the center of mass energy, E_{cm}, which is the square root of the Lorentz invariant

$$s = (P_{K^-} + P_p)^2$$

Here P_{K^-} and P_p are the four-momenta of the beam particle and the target particle respectively. Designation by E_{cm} will be used hereafter. Also, although it was necessary to treat the data in fifteen distinct subsets because of the different beam profiles, some subsets have essentially the same momenta and will be combined for all further considerations. In one case three subsets have almost identical momenta; in two cases two subsets have been combined because their means are within one standard deviation. This is shown in Fig. 8, which gives the distribution of fitted momenta for both τ decays and Σ events. For the former, the outgoing tracks are all well measured and the fit tends to constrain the beam momentum to its correct value. This is not as true for Σ events, especially those with a missing neutral. Hence, in general the peaks are narrower for the Σ events than for the τ decays. In particular for the two cases mentioned, the Σ events show a double peak but the τ decays not. (This indicates that the use of a beam edit (see Section II-C) distorts the results of the kinematic fitting. At the 1% level, however, this was considered tolerable.)

The cross section for a given reaction is just the number of such events with the dependence on beam and target densities removed. The product of cross section, beam path length, and number density of target particles yields the number of actual events (not all of which are observed). The microbarn equivalent, μ, is inversely related to path length and number density; it gives the cross section, in microbarns, represented by a single event. The cross section, σ, for a given subset, i, is given by

$$\sigma_i = \frac{\mu_i w_i}{f\, s_i t_i}$$

Here w_i is the weighted number of events after cuts, s_i and t_i are the scanning and through-put efficiencies (expressed as fractions), and f is the fraction going into the decay state used.[18] The s_i and t_i are expressed in Table VI as percentages, the μ_i are given in Table I. The error on the cross section combines the statistical uncertainty, based on the unweighted number of events, with the uncertainties in the other factors. These other uncertainties were not negligible in some cases. Where subsets were combined the microbarn equivalent was determined from the sum of the path lengths, the combined efficiencies were the appropriately weighted mean of the individual efficiencies.[19] The energy was determined from a similar mean of the momenta. Table VII gives the resulting cross sections (in millibarns), which are also shown in Fig. 9 along with results from other sources.

B. Two Body Final States

Neglecting the spin of the baryons, there are only two independent variables in the case of two body final states. There are four four-momenta, each restricted by a mass constraint; conservation of energy-momentum imposes four constraints, and the space-time frame invariance imposes a further six constraints.[20] In terms of Lorentz invariants two standard choices are the variable s described previously and

$$t = (P_{K^-} - P_{\pi^\pm})^2$$
$$= m_K^2 + m_{\pi^\pm}^2 - 2\,(E_{K^-}\,E_{\pi^\pm} - k_{K^-}\,k_{\pi^\pm}\cos\theta)$$

For a given center of mass energy, $E_{cm} = \sqrt{s}$, the energies, $E_{K,\pi}$, and magnitues of momenta, $k_{K,\pi}$, are determined. Hence $\cos\theta$, where θ is the angle between the incoming beam direction and the direction of the outgoing pion in the center of mass, is an equivalent variable. It is convenient to use $\cos\theta$ because distributions in this variable can be expanded in the orthonormal series of functions, the Legendre polynomials. The energy dependence of the data is probably best summarized, in the energy range here considered, by the coefficients of this expansion. The spin of the baryons should not be neglected: although the target protons were unpolarized, the sigmas may be produced in a polarized state. The three following subsections present the numerical distributions in $\cos\theta$, the polarizations in different regions of $\cos\theta$, and the Legendre expansion coefficients.

1. Angular Distributions

The first step in determining the angular distributions was simply to count the numbers of events, weighted and unweighted, in twenty equal

bins of cos θ at each energy. These results--the raw data--are given in Tables VIII-A and B. Normally the error for each bin would be the statistical uncertainty based on the unweighted number of events. For a given energy, i, and bin, j,

$$\Delta w_{ij} = \frac{w_{ij}}{\sqrt{n_{ij}}}$$

Without normalizing, the distribution is just the weighted numbers of events, w_{ij}; n_{ij} are the unweighted numbers. However for a chi-squre fitting procedure, such as that described in Section IV, the errors should be Gaussian. For large n_{ij} the above error approaches the Gaussian error desired; however, for our limited amount of data, many bins fall below a reasonable cutoff.

Rather than going to larger bins in general, we have decided to combine bins, where necessary, in such a way as to preserve structure. The combining of bins was performed by the computer--not only to avoid a tedious chore, but more importantly to avoid any introduction of bias by visual determination of structure. The computer was given an algorithm, the coding for which is listed in a technical note.[21] Briefly, if a single bin fell below the limit, it was combined with the smaller of the adjacent two. If a string of bins fell below the limit, they were combined successively until the total surpassed the limit; this continued until any remainder had to be added to the first bin beyond the string. This procedure was tried from either end and also from the center progressing in both directions. Whichever of these possibly three binning arrangements gave the smallest

$$\sum_i (n_i - n_L)^2$$

was used, where the sum is over the totals, n_i, which surpassed the limit n_L. We used a minimum of $n_L = 9$ except at the two highest energies.

The final results for the angular distributions are given in Fig. 10; the error bars indicate how the bins were combined and the approximately Gaussian errors ascribed to the totals for each combination of bins.

2. Polarizations

It is possible that the sigma particles are produced with their spins preferentially aligned along the normal to the production plane, along $\vec{k}_K \times \vec{k}_\pi$ (see section IV-A). This may be observed because the sigma decays via the parity non-conserving weak interaction; the distribution of the direction of the decay baryon is given by

$$f(\theta, \cos\chi)\, d\cos\chi = A\,(1 + \alpha P(\theta)\cos\chi)\, d\cos\chi$$

where χ is the polar angle between the decay baryon and spin directions, A and α are constants.[22] The polarization, P, may depend on the production angle, θ. This was in fact observed in the case $\Sigma^+ \to \pi^0 p$, where $\alpha \sim -1.0$; for $\Sigma^\pm \to \pi^\pm n$ the known values of α are approximately zero and in our data the distributions in $\cos\chi$ are everywhere consistent with this.

Although it was impossible to know the spin direction, the precession of the spin between production and decay vertices was negligible in the magnetic fields used. Hence we took χ to be, using azimuthal symmetries at both production and decay, the angle between the proton direction and the production normal--both in the sigma rest

frame. For a given combination of bins in cos θ we determined

$$P = \frac{3\sum_i \cos \chi_i}{\alpha N}$$

where the sum is over the N events in the combination of bins. The error is given by[23]

$$\Delta P = \frac{3 - Q}{\alpha^2 N}$$

where

$$Q = \mathrm{MIN}\ [(\alpha P)^2,\ 1.].$$

The sums of polar cosines ($\Sigma \cos \chi_i$) and numbers of events (N) are given in Table VIII-C for each of twenty bins in cos θ. The bins were combined according to the previously mentioned algorithm with a minimum (except at the two highest energies) $n_L = 20$. The final results are given in Fig. 11. An absolute value greater than 1. is not physical but is a result of limited statistics. However, it was felt that resetting such values to ± 1. would be a less valid representation in view of the relatively large errors. For estimating the error, which should be based on the true polarization, this limitation was used.

3. Legendre Coefficients

In view of the theoretical considerations presented in Section IV-A, it is best to expand the angular distribution in the standard Legendre polynomials, and to expand in the first associated Legendre polynomials a distribution which is the product of the angular distribution and the polarization. For this purpose the angular distributions were normalized such that the zeroeth order coefficient in

the expansion was

$$A_o = \frac{\sigma}{4\pi\lambda\!\!\!^{-2}}$$

Here σ is the cross section corresponding to the angular distribution in question; $2\pi\lambda\!\!\!^{-}$ is the center of mass wave length for the input channel at the given energy. The coefficients were obtained by a linear fit requiring simple matrix inversion. It was found that our data were consistent with expansion through seventh order. When eighth and ninth order were added, the probability of fit tended to fall and all coefficients remained unchanged within errors. In particular, the eighth and ninth order coefficients were consistent with zero at all energies.

The Legendre coefficients for the angular distributions, A_n, are given in Tables IX-A,B. For the product distribution a problem arises. Generally the polarizations are binned too coarsely to permit expansion through seventh order. Expanding to a lower order would ignore some information from the more finely binned angular distribution. For this purpose only, the polarizations were determined for the same bin structure as the corresponding angular distributions. To average out fluctuations, the polarization was not determined from just the events in the particular combination of bins; it included information, symmetrically and with successively less weight, from up to three adjacent bins. Details of this procedure are given in a technical note.[21] It should be emphasized that the independence of the various bits of information is not strictly preserved in this process. The expansion coefficients for the product distributions, B_N, are given in Table IX-C.

(The zeroeth order polynomial is identically zero; the first column is included only for consistency.)

The dashed curves in Figs. 11 and 12 show the resultant functional representation of the data. In the case of the polarizations there are occasional wild gyrations. These occur where the expansion in the A_n approximates zero (see Fig. 12-B) and the expansion in the B_n is varying, not necessarily rapidly. (The polarization is represented by the ratio of the latter to the former.) In the physical theory below, the A_N and B_N depend on the same set of parameters in such a way that this cannot happen. The curves are omitted at 1.952 and 1.970 GeV; these two energies were combined to obtain the coefficients at 1.961 GeV. Both had insufficient data to be fit to seventh order, while requiring $n_L = 9$; also the angular distributions and polarizations were not very different between the two. The same was true for the angular distributions ($\pi^+\Sigma^-$ events) at the two highest energies; however, since they were at the upper end of our data, these two were not combined. The binning limit had to be lowered to 4 for 1.644 GeV and 6 for 1.694 GeV.

In the final analysis only fits directly to the angular distributions and polarizations carry full statistical significance. Still, fitting to the Legendre coefficients--although they represent the data only with some goodness of fit and although the B_n are not strictly independent--is much faster and therefore advisable in the search mode.

C. Three Body Final States

When a third particle is added to the final state, there are three additional variables (e.g., the four momentum constrained to known mass).

A complete description of these data will not be given here; however, the distribution in three variables has a ready interpretation and will be displayed. These variables are the total energy in the center of mass, E_{cm}, and the two invariants

$$m_o^2 = (P_{\pi^\mp} + P_{\Sigma^\pm})^2$$

$$m_\pm^2 = (P_{\Sigma^\pm} + P_{\pi^o})^2$$

Since these two are squares of the rest energies of subsystems, they are called invariant mass-squareds.

1. Dalitz Plots

A scatter plot in two invariant mass-squareds is termed a Dalitz plot. For a given value of E_{cm} the points are kinematically confined within a boundary given by the curves for $\cos\psi = \pm 1$

$$m_\pm^2 = E_{cm}^2 + m_{\Sigma^\pm}^2 - m_o^2 - 2\,(E_{\pi^\mp}\,E_{\pi^o} - k_{\pi^\mp}\,k_{\pi^o}\cos\psi)$$

Here the energies and momentum magnitudes, E and k, of the mesons are determined in the $(P_{\Sigma^\pm} + P_\pi)$ rest frame. These boundaries are shown with the scatterplots in Fig. 13. Several values of E_{cm} are included per plot to make the structure in m_o^2 and $m_\pm^2$ more apparent; this is possible because of the independence of the variables. The events from both $\Sigma^+ \to \pi^o p$ and $\Sigma^+ \to \pi^+ n$ are scatter-plotted in Fig. 13-B.

The structure in the plots is the bands which are more densely populated than the rest of the bounded region. If the center of mass distribution of the three final state particles were isotropic, the

distribution in two invariant mass-squareds would be flat: the points would be evenly distributed within the boundary.[24] The plots in Fig. 13 do not give a completely accurate picture since they are necessarily of unweighted events; the weight depends essentially on the laboratory momentum of the sigma and does vary systematically across the narrow direction of the bounded region. This is shown in Table X, which combines all center of mass energies. Still the weight does not vary greatly nor account for the noticeable disparities in density. Clearly certain values of invariant mass-squared are preferred; this may be interpreted as quasi-two body final states in which one of the particles is unstable and decays immediately.

2. Invariant Mass-Squared Distributions

The distribution in one of the invariant mass-squareds might be considered a projection of the Dalitz plot into that coordinate. Both invariant mass-squared distributions are so shown, with the proper orientation, in Fig. 13. These histograms are of weighted events, and in Fig. 13-B only the $\Sigma^+ \rightarrow \pi^+ n$ events are included. Such distributions may be deceptive, however, in the case of an elongated Dalitz boundary: a concentration in one invariant mass-squared may be reflected into a concentration in the other. There is also a third subsystem, $(P_{\pi^\mp} + P_{\pi^0})$, but our data show no evidence for a concentration in its invariant mass-squared.

To aid in the interpretation of these distributions, it is convenient to superimpose the shape the distribution would take for complete isotropy. Since each plot combines several values of E_{cm},

this curve is calculated for their mean value; also the same curve is used for both m_o^2 and $m_\pm^2$ distributions, neglecting the small mass difference between the neutral and the charged pions. The curves have been scaled by eye to approximate those regions apparently unaffected by the concentrations. This had to be done simultaneously for both distributions with due regard for possible reflections. It does not constitute a fit; the curves are merely visual aids.

There are several well-known unstable particles, or resonances, in this region. Their identifications, mass-squared values and widths, and fractional decays via the $\Sigma\pi$ channel include[25]

$\Sigma(1385)$	1.92 ± .05	.10
$\Lambda(1405)$	1.97 ± .06	1.00
$\Lambda(1520)$	2.30 ± .02	.41
$\Lambda(1670)$	2.79 ± .04	.45
$\Sigma(1670)$	2.79 ± .08	.40
$\Lambda(1690)$	2.86 ± .09	.40

There are others at higher invariant mass-squareds. The Σ resonances could appear either in $m_\pm^2$ or m_o^2, the Λ resonances only in m_o^2. Higher resonances are suppressed kinematically: the purely statistical probability for a reaction occurring is proportional to the center of mass momentum, which decreases as the masses of the particles increase. There is no clear evidence for even the last three resonances listed. At some energies there may be a possible enhancement around 2.0 GeV^2 in $m_\pm^2$, indicating presence of $\Sigma(1385)$. The major enhancements are near 2.0 and 2.3 GeV^2 in m_o^2; the $\Lambda(1405)$ and $\Lambda(1520)$ are clearly present. The resonant contributions vary with energy and with the charge of the

final state particles. From this can be inferred some information about the strong force in the quasi-two body reaction, but no analysis will be attempted here.

IV. PARTIAL WAVE ANALYSIS OF $\pi^{\pm}\Sigma^{\mp}$

A. Theoretical Basis

Although the strong interaction still eludes complete understanding, certain of its properties seem to be well established. These include the conservation of charge, hypercharge, and baryon number, which we have tacitly assumed even in the selection of reactions for study. Invariance under the transformations of the full Lorentz group (implying conservation of energy, momentum, and angular momentum), invariance under space reflection (conservation of parity), and invariance under time reversal also seem well established. The conservation of energy and momentum were used in the kinematic fitting. The situation for angular momentum and parity is complicated by the intrinsic spin-parity of the particles -- $1/2^+$ for p and Σ, 0^- for the K and π. Total angular momentum, J, is conserved but quantized to half integral multiples of the basic quantum. Since both initial and final states are intrinsically $1/2^-$, conservation of parity requires conservation of orbital angular momentum, L, as well. Also within the quantum nature of the angular momentum, one of its three components is conserved; this is analogous to charge conservation since charge may be considered a component of the internal spin, isotopic spin. The conservation of isospin also seems to be well established. We shall hereafter refer to total angular momentum as spin. Finally, the initial and final state baryons may have either of two spin orientations, so that there are four possible interactions to consider. However, space reflection and time reversal invariance restrict these to two forces, the non-flip and the spin-flip amplitudes.

We shall now use the conservation of spin, isospin, and parity (orbital angular momentum) to analyze our observations of the two body final states. Since the strong interaction seems to conform to the postulates of quantum mechanics, the physical states may be represented by vectors in a real Hilbert space; observables, such as angular distributions and polarizations, may be represented by Hermitian operators. The eigenvectors must correspond to states with definite spin, isospin, and parity, since these are conserved. When the vector (wave function) for the final state is expanded in these eigenvectors, the individual amplitudes, stripped of standard (reducible) functional dependence, are commonly called partial waves. Given these partial waves, the distribution of observations may be calculated by finding the expectation value of the corresponding operator. Conversely, given a set of observations we may try to find, through the use of a chi-squared minimization technique, a set of partial waves to account for them. This latter process is called partial wave analysis.

The initial state, $|i\rangle$, can be specified by a plane wave and the spinor for the baryon. The final state, $|f\rangle$, is related to the initial state by the scattering matrix, S, which may be written in a way that explicitly indicates the transitions:

$$|f\rangle = S\,|i\rangle = |i\rangle + 2i\,T\,|i\rangle$$

Since our reactions concern the part of $|f\rangle$ with different particles, we may restrict our attention to the transition matrix, T. As pointed out in Section III-B, it may depend on only two independent variables, which we choose to be E and cos θ of that section. T must be scalar in space and

isospace. For each isospin-spin-parity eigenstate, T is a two by two matrix; but as pointed out above, there are only two independent amplitudes. We may write the transition matrix and obtain expressions for observables as follows.[20, 26]

Since the transition must be scalar, it must take the form

$$T = f(E, \cos\theta) + g(E, \cos\theta)\ \vec{\sigma}\cdot\hat{n}$$

where $\vec{\sigma}$ is the Pauli spin matrix and $\hat{n}$ is the normal to the production plane used in Section III-B

$$\hat{n} = \frac{\vec{k} \times \vec{k}_\pi}{|\vec{k} \times \vec{k}_\pi|}$$

Here $\vec{k}$, $\vec{k}_\pi$ are the center of mass momenta for the beam (omitting subscript hereafter) and the pion respectively. Since $\vec{\sigma}$ transforms as a pseudovector, it must be contracted with another pseudovector; $\hat{n}$ is the only one available. (This is why the Σ's can be polarized only perpendicular to their line of flight.) With spin projection taken onto the beam direction, $\vec{\sigma}\cdot\hat{n}$ has no diagonal elements; thus g is the spin-flip amplitude, f is the non-flip amplitude.

$$f(E, \cos\theta) = \frac{1}{\sqrt{k\cdot k_\pi}} \sum_{I,L} \left[(L+1)\ T^+_{IL} + L\ T^-_{IL}\right] P_L(\cos\theta)$$

$$g(E, \cos\ ) = \frac{i}{\sqrt{k\cdot k_\pi}} \sum_{I,L} \left[T^+_{IL} - T^-_{IL}\right] P^1_L\ (\cos\theta)$$

All of the angular dependence (because of rotational invariance) can be described by the Legendre and first associated Legendre polynomials,

P_L and P_L^1 respectively. Here the parity is determined by the orbital angular momentum quantum number, L, $P = -(-1)^L$; and the states affected by $T_{IL}^{\pm}$ have spin $J = L \pm 1/2$. The $T_{IL}^{\pm}$ are in fact the partial waves we have tried to obtain.

Since the angular distribution simply counts events (into a given direction), the representative operator is just the identity matrix; the $\vec{\sigma}$ matrix counts events by spin configuration and hence represents the product distribution of Section III-B. Taking the expectation values of these operators for that part of the final state with $\pi\Sigma$, we find in terms of the functions f and g above:

$$\frac{d\sigma}{d\Omega} = \frac{k_\pi}{k} \left(|f|^2 + |g|^2\right)$$

$$\vec{P} \frac{d\sigma}{d\Omega} = \frac{2\, k_\pi}{k} \operatorname{Re}\,(f^* g)\, \hat{n}$$

We have used the fact that the target proton was unpolarized. Since the Legendre and first associated Legendre series are complete and orthonormal, we can also express these distributions

$$\frac{d\sigma}{d\Omega} = \lambda\!\!\!^{-2} \sum_n A_n P_n (\cos\theta)$$

$$\vec{P} \frac{d\sigma}{d\Omega} = \hat{n}\, \lambda\!\!\!^{-2} \sum_n B_n P_n^1 (\cos\theta)$$

where $\lambda\!\!\!^{-}$ is inversely proportional to k and explicit dependence on k_π is cancelled. For a given charge configuration the coefficients of the polynomials in the latter expressions are related to those of the former

by a binomial operator which projects products of two polynomials onto the complete series. This binomial operator has been tabulated in the literature;[26] the parts of it relevant to this experiment are given in Table XI, where the partial waves are designated by L_{2J} (S, P, D, F, G, being L = 0, 1, 2, 3, 4) with the isospace index not applicable. The charge states for the reactions considered here are related only to eigenstates with I=0 or 1.

$$T_L^{\pm}\,(K^- p \to \pi^+ \Sigma^-) = \sqrt{\tfrac{1}{2}}\; T_{0L}^{\pm} \sqrt{\tfrac{1}{3}} + \sqrt{\tfrac{1}{2}}\; T_{1L}^{\pm}\,(-\sqrt{\tfrac{1}{2}})$$

$$T_L^{\pm}\,(K^- p \to \pi^- \Sigma^+) = \sqrt{\tfrac{1}{2}}\; T_{0L}^{\pm} \sqrt{\tfrac{1}{3}} + \sqrt{\tfrac{1}{2}}\; T_{1L}^{\pm} \sqrt{\tfrac{1}{2}}$$

Here we have followed the current convention of writing the baryon first in the isostate product, for example $\pi^+\Sigma^-$ is $|1,-1;\ 1,1\rangle$.[25] These projection coefficients are tabulated in reference . We shall hereafter refer to the partial waves by the notation

$$L_{2J} \quad \text{or} \quad L_{I,2J}$$

commonly used for these reactions.

There are two further properties that are commonly assumed to hold for the strong interaction. These are causality, the notion that effects cannot precede causes, and conservation of probability, that the sum of the probabilities into all outgoing states is unity. The latter simply requires that the scattering matrix, S, be unitary. The implied restriction on the transition matrix is such that in inelastic reactions, such as the ones being studied, the partial waves cannot be greater in

magnitude than one-half. Causality places a restriction on the energy dependence of the phase, δ.[26] The Wigner condition can be expressed

$$\frac{d\delta}{dk} \geq - R$$

where k is the magnitude of the beam center of mass momentum and R is a characteristic radius of interaction. Using the Heisenberg uncertainty principle, R can be related to the inverse of the mass of a field particle; using an inverse pion mass, the restriction on the phase is that it cannot move clockwise more than about a radian per pion mass. Causality can also be related to the analyticity of the S-matrix.[20] These two properties seem imminently reasonable and afford powerful theoretical tools; however, we have not imposed them in any way in the following analysis.

B. Procedure

The partial wave analysis of the two body final states was done on a CDC 6600 using a system of programs described in a technical note.[21] Only the basic concepts will be mentioned here. The fitting program used a modified version of the code VARMIT, which minimizes a function using a variable metric in the parameter space.[27] The user must supply VARMIT with the function, F, and its gradient, G, at points, X, supplied by VARMIT; the program proceeds by iteration, and in the process builds up the metric matrix, H, which is essentially an error matrix

$$H^{\mu\nu} = \left\| \frac{\partial^2 F}{\partial X^\mu \partial X^\nu} \right\|^{-1}$$

For a chi-squared minimization the function and gradient are

$$F = \sum_i (t_i - x_i)(t_i - x_i)\, c_i$$

$$G^\mu = \frac{\partial F}{\partial X^\mu} = \sum_i 2 . \frac{\partial t_i}{\partial X^\mu} (t_i - x_i)\, c_i$$

The similarity in structure shown facilitiates both the coding and execution of the program. The subscript, i, may range over different types of data, different energies, and different bins of $\cos\theta$; x_i is an experimental datum, with c_i the inverse square of its error; t_i is the corresponding value calculated from the parameters. We may determine the last, and its derivatives, from the partial waves as follows

$$t_{dt,e,b} = w_{dt,e,b} \sum_{\ell,\ell'} \mathcal{B}_{dt}^{\ell\ell'} W_\ell^e W_{\ell'}^e$$

$$\frac{\partial t_{dt,e,b}}{\partial X^\mu} = w_{dt,e,b} \sum_{\ell,\ell'} \mathcal{B}_{dt}^{\ell\ell'} \left(W_\ell^e \frac{\partial W_{\ell'}^e}{\partial X^\mu} + \frac{\partial W_\ell^e}{\partial X^\mu} W_{\ell'}^e \right)$$

$$+ \frac{\partial w_{dt,e,b}}{\partial X^\mu} \sum_{\ell,\ell'} \mathcal{B}_{dt}^{\ell\ell'} W_\ell^e W_{\ell'}^e$$

The subscript, ℓ, is taken to range over the real and imaginary parts of the partial waves for a given reaction at the given energy; these W_ℓ^e are therefore simple real numbers. The binomial operator, $\mathcal{B}_{dt}$, carries the waves into either the A_n or the B_n. Hence if the x_i are the coefficients, the weights, $w_{dt,e,b}$, are all unity. For angular

distributions the weight is proportional to integrals of Legendre polynomials (another summation implied) over the given bin and to the ratio of experimental to calculated cross section. For polarizations the weight is proportional to integrals of associated Legendre polynomials and inversely related to the calculated angular distribution over the given bin. Not only are these time consuming calculations, but also in both of these cases the weight is inversely dependent on the parameters.

While it would be preferable to determine the partial waves at each energy separately, and thus not presuppose the energy dependence of the partial waves, this was not considered feasible in this experiment. The information content is essentially represented by the expansion coefficients, so that Table IX indicates twenty three pieces of information at each energy; since the seventh order coefficients become significant in our energy range, Table XI indicates need of eight two-component waves for two isospin states, or thirty-two independent W_ℓ^e. Thus we have given the waves a variety of general energy dependences:

$$\text{B:} \quad (q_1 + q_2\, k + q_3\, k^2) + i\, (q_4 + q_5\, k + q_6\, k^2)$$

$$\text{P:} \quad (q_1 + q_2\, k + q_3\, k^2)\, e^{i\, (q_4 + q_5\, k + q_6\, k^2)}$$

$$\text{V:} \quad q_1\, (k - q_2)\, e^{i\, (q_3 + q_4\, k + q_5\, k^2)}$$

$$\text{R:} \quad \frac{q_1\, q_3\, d_1(E)\, e^{i\, q_4}}{(q_2 - E) - i\, d_2(E)\, q_3}$$

The last is just the Breit-Wigner resonant parametrization, and is discussed in greater detail in Section V-A. The functions, d_i, depend only on the energy and appear only as constants in the fitting. The energy dependence of the other parameterizations is through the center of mass beam momentum, k. The only reason for this was to facilitate checking the causality restriction mentioned above. We emphasize that no constraints were placed upon any parameters. In particular the magnitude of P was allowed to go negative and the various zeroeth order phase parameters, which are redundant modulo 2π, were allowed to take on any value.

Frequently both a resonant and a non-resonant parameterization were included in a partial wave. In this case they were simply added, with the intention of keeping the gradient structure as simple as possible. Since the resonant parameterization contains an arbitrary phase, this is consistent with unitarity.[20] However, in the fits we shall describe we have not needed this parameter. Again we point out that we have not tried to impose unitarity.

In picking starting values for a fit, one could either do so randomly or attempt to use knowledge already available. The former is more important for energy independent fits; we have chosen the latter approach. First, some of the partial waves have well established resonances just below, within, or just above our energy range.[25] These resonances are often seen in more than one reaction, which confirms their interpretation (see below). We have consistently included the well established resonances in D05, D15, F05, F17 and G07 among the starting values; other resonances were introduced as seemed appropriate.

The first three resonate at energies below the range of this experiment; we have reported elsewhere an analysis of data from another experiment which encompassed these energies.[2b] We have included those data in the fits to be described here, in order to better determine the J = 5/2 waves; and we have started from the resonance parameters obtained in that analysis. For the resonances in the J = 7/2 waves, we have started from the generally accepted values.[25] The G07 resonates at the upper end of our energy range; this limits the reliability of the parameters we obtain for it. Secondly, because of the observed nature of the Legendre coefficients and the structure of Table XI, it is clear that the higher order waves emerge only at higher energies. For this we have made use of the V parameterization, starting its q_2 slightly below our energy range. Otherwise we have consistently started all other parameters from zero.

The analysis was carried out in three stages. The first might be termed a prefit: all resonance parameters were fixed, as were the q_2's for any V terms. This fit supplied a set of "background" waves consistent with the presumed resonant structure. In the second stage all parameters were left free to vary. The reasoning behind this procedure is as follows. The resonances first established are usually in the highest order waves open at the energies in question. This can probably be understood from Table XI, which shows that the highest order expansion coefficients with any significance can depend only on a limited number of partial waves, the highest order ones; hence any structure in these coefficients can most readily be interpreted.[28] These high order waves do not by themselves account for the structure in

all the coefficients; but it seems appropriate to start all other waves from zero and let the fitting program extract them from the data, using the fixed waves through means of the binomial operator to analyze the coefficients. This must be done in two stages, since given the choice of varying either zero or non-zero parameters, the program initially chooses the latter. The third stage, after studying the resulting energy dependence of individual waves, involves changing appropriate waves to a simpler parameterization, with estimated starting values. This may be done several times, starting with the stage two results in most waves. Thus the fits come in series, distinguished not so much by starting values as by starting structure. The structure of the fits is given in Table XII; in each wave the letters indicate the type of parameterization, the numbers indicate how many parameters were free to vary. For P(4) the quadratic coefficients were fixed at zero, for V(4) the q_2 parameter was fixed. The phases for all resonances were fixed to either 0 or π, and in the last fit some masses were fixed. The table indicates the grouping by series.

C. Results

The results of the partial wave analysis are depicted in Fig. 14. These plots in the complex plane, called Argand diagrams, show the variation with energy of each partial wave, $L_{I,2J}$. The results are also listed in Table XIII for the three fits with highest probability; the Legendre coefficients predicted by these three are plotted in Fig. 15, superimposed on all data presently available for the two reactions in the energy range covered by the analysis. Since the parameters obtained

in the fits specify the energy dependence, both Fig. 14 and Table XIII present the partial waves at equally spaced energies, not at the energies of the data. The statistical parameters describing the goodness of fit are given in Table XII; these include the number of degrees of freedom, the χ^2, and the probability of fit. For second stage fits the χ^2 and number of degrees of freedom for the corresponding prefit are also given. This table only describes fits to the Legendre coefficients; for fits with probabilities of at least 1% the χ^2 was calculated both from the original data--the cross sections, angular distributions, and polarizations--and from all the Legendre coefficients plotted in Fig. 15. The average contribution in each case is given in Table XII.

All attempts made after the use of the V parameterization was instituted have been included in Table XII. All of these are not represented in Fig. 14, however, since within a given series the Argand diagrams look essentially the same in most waves. The results of two fits to the original data are shown for comparison with the corresponding fits to the coefficients. These fits, as well as two fits to all the data in Fig. 15, will be discussed at the end of the section. First we shall report some observations that apply generally to all fits and then comment on the individual attempts.

The first general observation is that the fits are remarkably good, following smoothly not only the coefficients used in the fit but also on the average all available data. The second is that the coefficients predicted by different fits are very similar where data is available. Both may be seen in Fig. 15 for the three fits with highest probability; and decent fits within a given series show even less variation from the

parent solution, the additional χ^2 contribution from individual points being small. One can see that increased statistics, giving smaller errors, would not distinguish these solutions at most energies. Only in the B_n for the Σ^- final state, where polarization data is unavailable, do the solutions show marked differences. This means that a unique solution cannot be obtained without supporting data from other reactions. There is some information available in the literature for the reaction $K^- n \rightarrow \pi^0 \Sigma^0$ in the lower half of our energy range.[29] We have calculated the χ^2 from these data within the range of our fits: for just the cross sections (22 data points) the average contribution was 1.60 for fit A1, 2.10 for fit B2, and 1.61 for fit C1; for the angular distributions (151 data points, where we have combined bins to eliminate those with zero contents and errors) the respective averages are 1.09, 0.88, and 1.06. Since the neutron is not free but in a deuterium nucleus, the individual reactions are difficult to disentangle; also with limited statistics it is difficult to place definitive errors on the results obtained. The interference between non-flip and spin-flip forces could also be resolved by studying our reactions using a polarized target, although this may not be possible with available experimental techniques.

The next observations refer to the general properties of the partial waves. There is certainly no violation of unitarity, none of the waves approach the unitary limit of .5. The situation with causality is not quite so clear; reports on the earlier fits over the limited energy range described rather large violations of the Wigner condition.[30] With a wider energy range, however, the waves cannot vary rapidly at some energies without getting into trouble at others (except at the end

of the range); also the use of quadratic terms in the general parameterizations adds more flexibility to the minimization. The fits over the broader energy range do not seem to show significant violation of causality. To look for violations in Fig. 14, consider the Wigner limit of one radian per pion mass clockwise as roughly 60° per 140 MeV. Since the symbols in Fig. 14 are spaced by 25 MeV, a clockwise movement of more than about 10° between symbols constitutes a local violation. Most waves actually move counter-clockwise, especially for $J \geq 5/2$. Some of the low order waves do have rapid clockwise motions but usually close to the origin or near the end of the energy range; for these the significance is obscure since non-violating waves are within errors. Other violations, such as the D03 in several fits, could be related to the unappealing complexity of some other waves; such a situation may reproduce the results of a simpler structure unavailable to the parameterization. In the final series we imposed initially all structure that we felt could be taken seriously from the earlier fits, then removed the quadratic dependence in the P terms; the results plotted in Fig. 14-G1, show no violation of causality.

A final general observation might be made about the use of the parameterizations with quadratic phase dependence to look for structure in the waves. The contrast with the B parameterization, where the real and imaginary components are parameterized independently, is described below. Apparently the redundancy modulo 2π in the zeroeth order phase parameter can be put to very good use. The problem is that a minimization program, such as VARMIT, can only find local minima; it goes to the minimum nearest the starting point. Thus the choice of initial

values is usually crucial; if the program starts from poor position, it may be trapped in a high valley on the χ^2 surface. In our fits we have observed that whenever the second order phase parameter is large, which is needed for marked structure within a narrow energy range, the zeroeth order phase parameter is numerically of the same order of magnitude. It appears that the program can use the redundancy in this dimension to move along the direction of the corresponding second order parameter. Since this is usually occurring in several waves, one can imagine a very striking picture: there are so many acceptable minima nearby, 2π away in several variables, that the χ^2 surface is extremely "slippery"; the program cannot stop in high valleys, but is only satisfied in some rather deep depression. This is not guaranteed to be an absolute minimum; however, this picture suggests how we have been able to get relatively low χ^2. Also it encouraged us to ignore the problem of starting values. This is not really justified; however, since the solutions starting from zero non-resonant waves are good, the problem would be one of uniqueness, a problem we have found just by varying initial structure.

We shall now comment on the individual fits listed in Table XII.

A-series. A first fit to the entire energy range with only resonances in the J = 5/2 waves indicated that the upper portion of the energy range could not be reproduced without continued contribution from these waves. In the second fit, A1, P type backgrounds were added to the three resonating low in the range; the result was one of the fits with highest probability. However, the D5·F5 interference continued into lower energies is unacceptable, since the A_5 coefficients are known to vanish.

Several long series of fits were then attempted to remedy this, varying resonant structures and searching for new parameterizations. All had higher χ^2, all had the same problem at lower energies. A1 is presented as representative of the whole set.

B-series. The V parameterization proved to be the key and the first fit using it, B1, was quite successful. Even though the F15 resonance of A1 was replaced by a V term, the wave passes through the imaginary axis at roughly the same energy with about the same magnitude. The F05 and F15 waves were suggestive of the double resonance structure reported elsewhere.[4] The fit B2 made this variation and reached the lowest χ^2 we have obtained, although the complex variation in S01 suggests that this may be fortuitous. There are well established resonances in the D13 and D03 waves below the energy range we are fitting.[25] In this series the D03 was included and allowed to vary; it was shifted away from the accepted values. The significance of this is minimal since our range did not include the resonant energies. Similarly we would minimize the significance of our results for higher resonances in the F5 waves. If they do resonate, our energy range does not span their widths; and the V parameterization is fairly successful at reproducing them where we have data.

C-series. Both of the above series have a D13 which passes through the imaginary axis, counter-clockwise, at about the same energy. In fit C1 we parameterized this wave with the suggested resonance, with good results. A resonance in this wave had previously been reported for the $\pi\Sigma$ final state, with a slightly lower mass.[3] This fit retained the double

resonances in F05 and F15; in this case the two in F15 were moved to approximately the same mass with amplitudes greater than 1. Since they had opposite phase, the resulting wave did not violate unitarity, but the meaning was obscure. Notice that with entirely different parameters, the F15 wave is almost the same as in the B-series. In fit C2 the higher resonances in F05 and F15 were replaced by V terms with essentially no change. In fit C3, we tried to introduce the resonant structure suggested by the P11 and P13 of fit C1; also we added the well established resonances in D03 and D13, with fixed parameters, to look at the effect on the D13 resonance of C1. Probably too much structure was introduced simultaneously, the χ^2 is relatively high. Therefore, in fit C4 all of the structure of C1 was retained except in the P11 wave, which was given resonance parameters compatible with a resonance reported in the $\pi\Lambda$ final state.[31,3] The fit, although good, moved the resonance to a much lower mass.

D-series. In this case, the prefit was not followed up since it was in such great disagreement with the data. All of the structure of C3 was included, but the background waves could not adjust to it since the resonances in P11 and P13 were fixed. In particular the P11, with mass fixed to the value reported in $\pi\Lambda$, induced large departures from the data at nearby energies.

E-series. In order to study the effect of the resonances below our energy range, the fit E1 was tried with a very general parameterization. Only the well established resonances were included and V terms were added to all but the two highest. In the second stage the parameters for the D03 and D13 resonances were kept fixed. The waves with $J \geq 5/2$ were similar to

earlier fits, except for a significantly larger G07 and a non-zero G17. The waves with $L \leq 1$ remained similar to the prefit results contrasted with the B parameterizations below. Finally, the fixed resonances in D03 and D13 did not significantly distort these waves from the results of the C-series: the D03 lost the causality violating clockwise loop; and the D13, although no longer following the perfect resonance circle, still followed a counter-clockwise loop going through the imaginary axis at about the same mass.

F-series. Again this series was stopped after the prefit. The structure in F0 was exactly the same as in E0, except that B terms replaced the P terms in the waves with $L \leq 1$. The resulting waves for both prefits are shown in Fig. 16. Although E0 proceeded for some time and reached a minimum with rather detailed structure, the F0 fit reached a minimum after several iterations.[32] The waves parameterized with B terms have somewhat similar position and direction, but show no detailed structure.

G-series. In this final series, resonant parameterizations were introduced wherever consistent structure had been seen in earlier fits and the quadratic dependence of the P terms was removed. In particular the P11 was started with the resonance parameters seen for the $\pi\Lambda$ final state and a P term was added; added to the resonance in P13 was a V term set to vanish above the energy range. The fit was good although the resonance in P13 was rejected, moved far from the energy range. The resonance in P11 was made very broad so that the displaced spiral of the P term provided the structure of that wave. The V term of the D03 added a counter-clockwise loop onto the tail of the fixed resonance, and the

second resonance in D13 reached parameters similar to those in the C-series. Finally, all waves with $J \geq 5/2$ are similar to earlier fits. The wave in G17 is not significant, since it differs from zero at only one data energy. In G2 the suggested resonance was added to D03, and double resonances with fixed masses replaced the parameterizations in both P11 and F15. The fit was rather poor, the new resonance in D03 was rejected.

At this point searching for new solutions was terminated. Clearly as more explicit structure is imposed the X^2 increases; this was observed both starting from A1, and in the series we have described. This is consistent with the statistical meaning of the X^2, since a set of observations are more likely expressable with a good set of general parameterizations than with quite explicit parameterizations. The P and V parameterizations seem to constitute such a good set; and only theoretical prejudice, based on the causality principle and the resonance model, encourages going to the more explicit resonant parameterization. The only experimentally valid reason for replacing V and P terms with R terms would be achieving a similarly successful representation with fewer parameters; and the probability of the χ^2 for the number of degrees of freedom is the test for this. On this basis most of the fits described above, excepting the prefits and probably C3 and G2, cannot be distinguished; the data do not constitute a large enough population. Inclusion of data available from other experiments is indicated; also since new resonant structures are suggested near both limits of our energy range, and since some waves can be reduced to essentially structureless energy dependences, going to a broader energy range is

recommended. We consider this beyond the scope of this experiment.

However, we have taken some of the solutions found above and allowed the fitting to proceed with larger populations of data. This was facilitated by having the metric matrix, H, punched onto binary cards at the end of a fit. A subsequent fit with a different set of data, but the same parameters, could use this as a starting matrix. This eliminated the large number of iterations needed to build up a useful metric matrix. Since the execution time per iteration is roughly proportional to the number of data points, these extra iterations ought to be done with the smallest reasonable population of data. We searched for solutions with 368 data points (the coefficients in Table IX plus those from reference 2b); the times per iteration averaged about four seconds when all parameters were free to vary (time was also proportional to the number of terms in the gradient), and on the average about 700 iterations were required to reach the minimum. For prefits these numbers were about 2.5 seconds and about 1000 iterations, respectively.

As pointed out in Section III-B above, the statistical significance of the fits to the Legendre coefficients is obscured by the procedure used to obtain them. Fitting the original data with two early solutions, including A1, showed that the results from the fit to the coefficients were not misleading, either the waves or the probabilities of fit. Therefore subsequent fits were not carried over to and continued with the original data except for C1. The resulting waves from continuing A1 and C1 with the original data are shown in Fig. 14 as fits AD and CD, respectively; the statistical indicators are listed in Table XIV along with iteration times and numbers. In AD the data from our two energies, 1.952 and 1.970 GeV, were left combined; in CD and in the χ^2 calculated

for the $(\chi^2/DP)_d$ listing in Table XII, these two energies were separated. In the latter case the number of data points was 644; the large increase in the time per iteration is indicative of the extra time in calculating the distributions from the coefficients and in evaluating the more complex gradients. We point out that, quite aside from the time factor, this complex dependence of the gradient upon the parameters discouraged us from attempting prefits to the cross sections, angular distributions and polarizations.

We also continued two fits with all the available coefficients; these data, which are shown in Fig. 15, extend slightly beyond the energy range of the original fits. We chose the fits that we considered the most flexible and the most specific: the fit E1 contained only the well established resonances, with V terms added to the ones at lower energies; the fit C4, although it excluded the two well established resonances below our range, included or implied (through C2) three additional resonances with masses in our energy range. The latter was tightly restricted in its parameter space and reached minimum after very few iterations. The former, although initially having the highest χ^2 with respect to this population (see Table XII), was able to proceed to a much lower χ^2. The waves resulting from this latter fit, EA, are quite similar to those of E1, perhaps surprisingly considering the number of iterations; in fact, the waves with J = 5/2 tend to be closer even than those of E1 to corresponding waves of B2, C1, and G1 (all of these fits are shown in Fig. 14). This suggests that the fit improved the χ^2 by small variations in all waves, a point supported by the following. The fitting program was stopped by a time limit after 263 iterations, having reached

a χ^2 of 1374; the remaining small drop in χ^2 required another 260 iterations, and a minimum was still not reached. Since the program seemed to be working on minor details the fitting was not continued. This population of data contained 1048 points and resulted in an almost exactly proportional increase in time per iteration. Future fitting of the entire data sample might best follow a procedure of first fitting a set of points which average all the data in narrow energy bands. That all the data does not come from the same general population, but presumably are derived from the real population by slightly different experimental techniques, is indicated by the larger χ^2 contributions. For these two fits, CA and EA, the mean χ^2 contribution at each energy is plotted in Fig. 17; the error is the standard deviation of the mean. Since major discrepancies in the data occur in the Σ^- coefficients around 1.8 GeV, more data in this region is desirable. We point out that the worst of our sets of data is at 1.644 GeV/c; in Section III-B we questioned the statistical significance of this one, but altered the statistical requirement rather than combine energies. This choice was made because the set was near the end of the energy range; in general we consider our results near both extremes to have limited significance.

V. INTERPRETATION OF PARTIAL WAVES

A. The Resonance Model

The Breit-Wigner resonance parameterization for partial waves may be derived either by the Fourier transform of the wave function for a decaying state or from the linear expansion, near the lowest channel threshold, of the effective range of the force.[33] It takes the general form

$$\frac{\frac{1}{2}\sqrt{\Gamma_e \Gamma_r}}{E_R - E - i\,\frac{\Gamma}{2}}$$

Here E_R is the resonant energy; Γ_e is a measure of the coupling to the elastic, or initial state, channel; and Γ_r is a measure of the coupling to the reaction, or final state, channel. The quantity Γ determines the width of the resonance and is required by unitarity to have the form

$$\Gamma = \sum_i \Gamma_i$$

where the sum is taken over all communicating channels. In the interpretation of the resonance as the formation and rapid decay of an intermediate particle, the Fourier transform associates E_R with its rest mass and Γ with the inverse of its lifetime (the more channels open or more strongly coupled, the more quickly it decays). The properties of a resonance are:

a) well defined quantum numbers (it must be in a specific partial wave);

b) mass and width independent of the reaction in which it is seen;

c) factorization of couplings (decay independent of formation).

We have explicitly indicated the last, using the product $\Gamma_e \Gamma_r$. The Γ_i are called partial widths.

The coupling to a given channel is not independent of energy. First, it is proportional to the number of states, the phase space, available. Second, the decay of a state with given spin-parity into a channel with different spin-parity proceeds with orbital angular momentum between the particles in the channel; the angular momentum barrier affects the coupling. A formula widely used for this energy dependence was derived by Blatt and Weiskopf (BW) using a square-well potential in the non-relativistic limit.[34] Other authors have questioned the use of this in relativistic regions, such as ours, where momenta are comparable to rest masses; they use rather complex formulae derived from field theoretical models.[35] Glashow and Rosenfeld (GR), in an empirical fit to observed decays of resonances, used a simple form factor dependence.[36] We have chosen the last, primarily because of its simplicity. The energy dependence of a partial width is given by

$$v_i\ (E) = \frac{k_i}{E} \left(\frac{k_i^2}{k_i^2 + X^2} \right)^{\ell}$$

where k_i is the center of mass momentum for the channel and ℓ is its orbital angular momentum quantum number. For channels with spin ½, ℓ is uniquely determined; for others the decay mode with lowest ℓ dominates. The term k_i/E gives the phase space energy dependence; the remainder is the GR dependence for the angular momentum barrier penetration factor. We have used their value--X = .35 GeV/c -- while fitting. The partial widths and the full width may now be expressed

$$\Gamma_i = \gamma_i v_i(E) = \alpha_i \gamma v_i(E)$$
$$\Gamma = \sum_i \gamma_i v_i(E) = \gamma \sum_i \alpha_i v_i(E)$$

The quantity γ_i is called the reduced partial width and will be considered in more detail below; it is conveniently defined as

$$\gamma_i = \frac{\Gamma_i(E_R)}{v_i(E_R)}$$

The quantities γ and α_i are introduced merely to facilitate the partial wave fitting. The parameters in Section IV B are

$$q_1 = \sqrt{\alpha_e \alpha_r}$$
$$q_2 = E_R$$
$$q_3 = \gamma/2$$

Since our fits have used a phase, q_4, equal either to 0, or π, it may be given as the sign of q_1. All of the energy dependence is contained in the functions

$$d_1(E) = \sqrt{v_e(E) \; v_r(E)}$$
$$d_2(E) = \sum_i \alpha_i \; v_i(E)$$

The formulation of the full width depends of course upon the branching fractions into all channels; however, since the energy dependence is not well understood, we use $d_2(E)$ merely to get an approximate energy dependence. We have estimated the "reduced branching fractions," α_i, into just six channels; these channels and the values of α_i used for the resonances in our fits are given in Table XV. Note that the fitting parameter, q_1, is not related to these α_i. We have required

$$\Sigma \ \alpha_i = 1$$

although this is not necessary.[37] The resonances may or may not decay into the quasi-two body channels (see Section III-C). These channels are introduced since the resonances do not decay only into two-particle final states; these channels represent higher thresholds and different values of ℓ of multiparticle final states.

The energy independent parameters derived from our fits are given in Tables XVI and XVII, where

$$\tau = \pm\sqrt{\alpha_e \alpha_r}$$

combines q_1 and q_4. This should be distinguished from the quantity often found in the literature

$$t = \pm\sqrt{x_e(E_R)\,x_r(E_R)}$$

$$x_i(E) = \frac{\Gamma_i(E)}{\Gamma(E)}$$

The x_i are the true branching fractions; they are not necessarily independent of energy. The quantity t gives the resonant amplitude, which may be seen by expressing the Breit-Wigner form as

$$\frac{t}{\varepsilon - i}$$

$$\varepsilon = \frac{E_R - E}{\frac{\Gamma}{2}}$$

The resonant amplitude and the half width, evaluated at E_R, are also given in Tables XVI and XVII. These two quantities and the mass are clearly the experimentally significant quantities (Γ is constrained by

the rapidity with which the wave passes through resonance). However, to fit Γ or t directly requires a very complicated dependence on E_R.

$$x_e(E)x_r(E) = t\sqrt{\frac{Ve(E)}{V_e(E_R)}\frac{V_r(E)}{V_r(E_R)}}$$

We have avoided this by introducing the artificial parameters γ and τ.

The values of all quantities listed in Tables XVI and XVII are not those of individual fits, but rather "average" values. Because of the complex interrelation between mass, width and amplitude, it seemed inadvisable to average each parameter independently. We have rather calculated the partial wave at each energy for which we had data, from the parameters for each independent fit (we excluded fits C3, G2, and the prefits but included fits AD, CD, CA, and EA), and then made a least squares fit to these complex numbers. We first got a fit for each series: parameters remained similar within a series, and we did not want the overall fit affected by different numbers of modifications pursued. These are given in Tables XVI and XVII along with the overall fits, which used the series fitted values as input. The fitted values of τ and E_R differed negligibly from averages; the fitted values of $\gamma/2$, and hence $\Gamma/2$, did vary from averages--in most, but not all, cases larger. The error assigned to the overall fitted averages are one-third the spread in the series fitted values, a necessarily imprecise definition because of the non-uniqueness of the partial wave analysis.

This fitting procedure to find the final resonance parameters allowed us to check easily whether the energy dependence was critical. Once the complex numbers had been calculated using the GR dependence with X = .35, the least squares fit to these numbers could be made

using some other energy dependence. We tried fits using GR with $x = .2$ and $x = .5$, and we also tried one using the BW dependence with an interaction radius of 1 Fermi. Although the "reduced" parameters varied drastically, the resonant amplitude, mass, and half-width evaluated at resonance varied, if at all, well within the errors we have assigned to them (the only exception was for the G07 using the BW form, where we did not have available the complete barrier penetration function for $\ell = 4$).

B. SU(3) Symmetry Classifications

The resonances in Table XVI are distinguished from those in Table XVII because they have been previously assigned to multiplets of particles based on the symmetry of the SU(3) group. Group assignment of particles dates from the observation of charge invariance of the strong interaction: the proton and neutron are simply two states of the nucleon; the π^-, π^0, π^+ form an isospin triplet. Particles within the isospin multiplets may have slightly different masses; but the strong interaction conserves isospin, specific reactions are related to the isospin amplitudes by the projection coefficients of the SU(2) group. We used this in Section IV-A. All of the particles in an SU(3) multiplet have the same external quantum numbers; for baryons these are spin and parity so that the nucleon, Σ, Λ and Ξ with spin-parity $1/2^+$ have been so associated. In SU(2) different charged particles are distinguished by the spin component I_z of the isospin I; in SU(3) another label, Y, called hypercharge, is required

$$Y = 2\bar{Q}$$

where $\bar{Q}$ is the average charge in the isospin multiplet. In the tables and figures that follow, we use the baryon particle symbols as generic types for the Y, I states: N for 1, 1/2; Σ for 0, 1; Λ for 0, 0; Ξ for

-1, 1/2; Δ for 1, 3/2; and Ω for -2, 0. These are the only types that have been definitely observed at this time. The particles in the spin-parity $1/2^+$ multiplet have quite different masses; however, this has been successfully explained by a theory which predicted the subsequently observed Ω particle.[38] This theory assumes that the strong force, to first order, includes a part invariant under transformations of the SU(3) group and a symmetry breaking part which transforms like the Λ(Y=0, I=0) member of an octet representation. Note that the set of particles with spin-parity $1/2^+$ includes eight particles: Λ singlet, N and Ξ doublets, and Σ triplet. That they are assigned to an octet representation of SU(3) depends on the observation that reactions in which they are involved are related by the projection coefficients for this group. In particular, the pseudoscalar mesons (π, η, K, $\bar{K}$) also form an octet; the product of two octet representations may be reduced to a series of representations

$$8 \otimes 8 = 1 \oplus 8 \oplus 8 \oplus 10 \oplus \bar{1}0 \oplus 27$$

where the number stands for a representation of that multiplicity. The $1/2^+$ baryon - 0^- meson channels should communicate only with resonances (baryons) in these representations, and the reactions with different particles should be related by coefficients based solely on the systematics of the group. These SU(3) coefficients have been presented in the literature;[39] we have adopted the convention and used the coefficients given in Ref. 25. The coefficients relevant to the following discussion are given in Table XVIII. There are two octets in the above expansion; these are generally taken to be 8_d and 8_f, which are symmetric and antisymmetric in the channel and resonance baryon type, respectively.[39]

The multiplets in which the resonances of Table XVI fall are

incomplete, information on the Ξ states being hard to obtain; therefore we will not look at the mass relationships. However, it has been assumed in the past that the couplings are not affected by the SU(3) symmetry breaking force, except for the different kinematic factors due to different masses.[40,41] Thus the reduced partial widths, γ_i, should be related simply by the SU(3) projection coefficients. We have tested this for the multiplets in which the resonances of Table XVI fall: the D5 octet, the F5 octet, the F7 decuplet, and the G7 singlet. We have made these fits using the actually observed quantities

$$\pm\sqrt{\Gamma_e\Gamma_r} = t\Gamma$$

rather than to the derived Γ_i, as was done in Ref. 40. This agrees with the procedure in Ref. 41, and eliminates dependence on sometimes poorly known elastic amplitudes. It has the added advantage of introducing explicitly the relative signs of couplings; the importance of these for making SU(3) multiplet assignments has been pointed out.[42] Actually, it is the reduced partial widths that we must compare

$$\pm\sqrt{\gamma_e\gamma_r} = t\Gamma \;/\; v_e^{\frac{1}{2}}(E_R)\,v_r^{\frac{1}{2}}(E_R)$$

If SU(3) symmetry holds for the couplings, these should take the form

$$t = g_e v_e^{\frac{1}{2}}(E_R)\; g_r v_r^{\frac{1}{2}}(E_R)\; m_N$$

$$g_i = C_i^d\, g_d + C_i^f\, g_f$$

$$\text{or} \qquad g_i = C_i\, g$$

where we use the mass of the nucleon, m_N, as the arbitrary scale factor. The first expression for g_i holds for octet-octet coupled to octet, the other for coupling to decumplet of singlet. The coefficients, C, are

just the SU(3) projection coefficients of Table XVIII. We have obtained values for g_d and g_f for the D5, g_d and g_f for the F5, g_{10}^2 for the F7, and g_1^2 for the G7 using the data listed in Table XIX. These data include all the values in Table XVI plus recent data on the decay of the Δ(F7) into Σ^+K^+.[43] All of the other values are taken from the compilation in Ref. 25; where these authors have not given means and errors, we have estimated them from the spread of values found in different experiments. This procedure is not sound statistically, but is in keeping with the general uncertainties of partial wave analysis. The significance of the χ^2 for the fits to these data is limited. We have tried a variety of energy dependences, including GR with different values of X and BW with an interaction radius of 1. Fermi. We find, as did the authors of Ref. 41, that the best fits are obtained for the energy dependence, ND, with no denominator in the barrier penetration factor

$$V_i\ (E) = \frac{k_i^{\ 2\ell+1}}{E}$$

The variations in χ^2 for the different forms of energy dependence are shown in Fig. 18 for all multiplets.

This last energy dependence is quite different from that used in the original partial wave analysis; the growth of the partial and full widths is not moderated as in the GR and BW dependences. Therefore we felt it necessary to check whether this form of energy dependence is compatible with experimental data. We tried both fitting the partial waves calculated from the series averages shown in Table XVI and continuing an individual fit (C2 of Table XII because it contains all the resonances in Table XVI with at most the flexible V-parameterization added) using this energy dependence. In the results of fitting the

partial waves, all masses were shifted to lower masses than the average; the half-widths, $\Gamma/2$, varied significantly outside the quoted errors from the fitted values quoted in Table XVI, again at lower values. The exception to this was the G07, which was moved to a higher mass and significantly larger width; this obtained because all our data lie below its resonant energy. In the fit to the data, the χ^2 increased from 306. to 326. Although this test alone is not conclusive, we feel that the ND energy dependence is probably not related to the data; to prefer it because it gives a better fit to unbroken SU(3) symmetry is not experimentally valid. This procedure of letting the radius of interaction go to zero (equivalently letting the constant X dominate the denominator) was first suggested for fitting the decay rates of the $3/2^+$ decuplet, based mainly on the distinction between widths observed in production processes (as a resonance in an invariant mass-squared plot, Fig. 13) and in partial wave analyses.[44] These authors suggest that if relativistic corrections are introduced, as in the GR energy dependence, then symmetry breaking must be considered. That the various decay rates for the $3/2^+$ decuplet can be related by the same symmetry breaking that gives the mass relationships has been shown.[45] In particular it has been shown using the GR energy dependence with X = .35.[45b] The relations based on octet dominated symmetry breaking for decays into octet-octet channels are available both for decuplet resonances,[45a] and for octet resonances.[46] We cannot check these relationships for the multiplets we are testing because the Ξ resonances and many decay channels are not definitely known. However, because the ND energy dependence is probably

experimentally inadequate, we shall assume that fitting to unbroken SU(3) is deceptive and present the results from the fit using the energy dependence originally used in the partial wave analysis--the GR form with X = .35.

The values for g_d, g_f and g^2 for the various reactions, obtained assuming this energy dependence, are plotted in Fig. 19. The fitted values for the multiplets are given in Table XX. For the octets the plots are curves in the g_d - g_f plane. Since there is an overall sign ambiguity we restricted g_d to positive values. For elastic reactions there is a square root sign ambiguity. In most cases this sign is determined by the relative sign for the reaction with a final state for which C^f is zero, since the slope for the elastic line is fixed and we assume $g_d > 0$. For the cases $N \to N\pi$, we have chosen the g_f intercept giving a line most consistent with the others. Probably the worst disagreement is for the two reactions involving the G7. We should point out that the amplitude we obtained for this resonance is significantly less than the values obtained by the authors of Ref. 4, who had data extending above this resonance. For the F5 multiplet, the three lines representing reactions involving the N and Λ resonances closely intersect at a point far from our fitted point; before the decay amplitudes of the F15 were well established, this point was assumed to give the coupling constants for the F5 multiplet.[40] This point disagrees with the <u>sign</u> of the amplitudes for the inelastic reactions involving the F15; and the sign is not subject to error. This intersection is close to the line, $g_f = 1.34g_d$ shown in the figure, for which the Σ decouples from the $N\bar{K}$ channel (see Table XVIII). If this

is taken to give the correct coupling constants and unbroken SU(3) is assumed, the amplitude for the reaction

$$N\bar{K} \to \Sigma\ (F5) \to \Sigma\pi$$

should be quite small but positive. In several of our fits, even with quite different parameterizations (for example B2, C1, and E1 in Fig. 16) the F15 first makes a small counter-clockwise loop in the positive half-plane. Could this indicate the F15 resonance that should be associated with the N(1688) and Λ(1823)? The reaction with $\Lambda\pi$ substituted in the final state should have a quite similar amplitude; and Argand diagrams plotted for various analyses available in the literature show this possibility in some cases,[3] but not in others.[31,47] Such a possibility would also be in better agreement with models requiring a lower mass for the Σ member of the F5 multiplet.[48] However, this would leave the F15 resonating around 1.925 GeV unaccounted for; since it is seen in both $\Lambda\pi$ and $\Sigma\pi$ final states with the same sign of the amplitude, it cannot be a member of a decuplet representation. We feel it is more likely that symmetry breaking does affect the couplings and that the Σ(1925) is associated with the N(1688) and Λ(1823) in an octet representation.

C. Comments on New Resonant States

For the resonances we have listed in Table XVII, those without previous multiplet assignments, little can be definitely said. The D13 resonance strongly emerged in our analysis. It has been seen previously, both for the $\Sigma\pi$ final state,[3] and for the $\Lambda\pi$ final state.[47,3] We feel that its existence is fairly well established. Since the amplitudes into the two final states have the same sign, it cannot belong to a decuplet representation. We have mentioned earlier that

we do not feel our analysis can confirm or reject the F05 or F15 near the upper end of our energy range, seen in Ref. 4. Similarly, the possibility of a resonance in the P11 wave near the lower end of our energy range cannot be fully supported by our data alone. However, it is unlikely to be associated with the P11 resonance seen in the $\Lambda\pi$ final state at an energy near the center of our range.[31, 47, 3]

What is most interesting to us is that, seemingly, a process of iteration has revealed resonant structures, or at least counter-clockwise loops, in most partial waves. This is in agreement with the contention that there can be no "background" in a reaction such as ours.[5] Of course the probability of fit dropped, although perhaps not significantly, as we introduced more resonant parameterizations; and the existence of a resonance depends on a very definite variation of the partial wave with energy (even considering the uncertainties in the energy dependence of the partial and full widths, the phase of the wave must move most rapidly at the resonant energy). Possibly the presence of counterclockwise loops only indicates that causality is obeyed. Still we feel we have developed a procedure for looking for resonances: starting with previously established resonances fixed and other amplitudes zero, the program analyses the Legendre expansion coefficients by means of the binomial operator in Table XI; if the general parameterizations indicate a resonant looking loop, the appropriate parameters may be estimated from the Argand diagram and such a fit tried. This eliminates the temptation to try certain resonances required by unfilled SU(3) multiplets; the appropriate resonances are suggested by the data.

VI. ACKNOWLEDGEMENTS

This experiment could not have been done without the help and support of many people. I would like to express my heartfelt thanks to the crews of the Bevatron and the 25" Bubble Chamber, to the scanners and measurers of the Powell-Birge Group, and to the staffs of the Data Handling Group and Computer Operations. I have especially benefitted from very helpful discussions with Drs. Robert Tripp, Robert Ely, George Kalmus, and Robert Birge, Finally, my warmest appreciation to Mrs. Jane Kennedy, both for her skill and dedication in typing this thesis and for her sympathetic support during the final stages of this experiment.

This work was done under the auspices of the U. S. Atomic Energy Commission.

VII. FOOTNOTES AND REFERENCES

1. (a) R. Armenteros, M. Ferro-Luzzi, D. W. G. Leith, R. Levi-Setti, A. Minten, R. D. Tripp, H. Filthuth, V. Hepp, E. Kluge, H. Schneider, R. Barloutaud, P. Granet, J. Meyer, and J. P. Porte, Physics Letters 24, B198 (1967). (First presentation of partial wave analysis for this data.)

   (b) R. Armenteros, M. Ferro-Luzzi, D. W. G. S. Leith, R. Levi-Setti, A. Minten, R. D. Tripp, H. Filthuth, V. Hepp, E. Kluge, H. Schneider, R. Barloutaud, P. Granet, J. Meyer, and J. P. Porte, Nuclear Physics B8, 233 (1968). (The data was presented in this report. We have obtained the Legendre coefficients, shown in Fig. 15, from the author of Ref. 3).

   (c) R. Armenteros, P. Baillon, C. Bricman, M. Ferro-Luzzi, E. Pagiola, J. O. Petersen, D. E. Plane, E. Burkhardt, H. Filthuth, E. Kluge, and H. Oberlack, The $\bar{K}N$ Interaction Between 400 and 1200 MeV/c: First Attempt to an Energy Independent Partial Wave Analysis in the $\bar{K}N$, $\Sigma\pi$ and $\Lambda\pi$ Channels, in Proceedings of the Duke Conference on Hyperon Resonances, (Moore Publishing Company, Durham, North Carolina, 1970), p. 123. (Most recently published partial wave analysis by the authors of this data.)

2. (a) R. Bell, Physical Review Letters 19, 936 (1967). (First presentation of partial wave analysis for this data.)

   (b) Daniel F. Kane, Jr., A Study of the Reactions $K^-p \to \Sigma^{\pm}\pi^{\mp}(\pi^0)$ at Laboratory Momenta Between .85 and 1.15 GeV/c, UCRL-20676, April 1971.

3. Angela Barbaro-Galtieri, Review of Partial-Wave Analyses of the $\bar{K}N$ System Above 1.1-GeV/c K^- Beam Momentum, in Ref. 1c, p. 173. (This review presented partial wave analysis of several reactions; the analysis of $\Sigma\pi$ final state made use of data from Refs. 1b and 4 as well. We thank the author for giving us the Legendre coefficients in advance of publication.)

4. A. Berthon, J. Vrana, I. Butterworth, P. J. Litchfield, J. R. Smith, J. Meyer, E. Pauli, and B. Tallini, Nuclear Physics B24, 417 (1970).

5. H. Harari, Resonances-Theoretical, in Proceedings of the 14th International Conference on High Energy Physics, (CERN, Scientific Information Service, Geneva, 1968), p. 195.

6. Phillippe Eberhard, Myron L. Good, and Harold K. Ticho, The Review of Scientific Instruments 31, 1054 (1960).

7. (a) John A. Kadyk, K67 Beam, Phase I, Trilling-Goldhaber Group (LRL) Technical Note 122, November 1966.

   (b) John A. Kadyk, K67 Beam, All Phases, Trilling-Goldhaber Group (LRL) Technical Note 124, January 1967.

   (c) D. Kane, Modification of K67 Beam for Momenta Between 1.0 and 2.0 BeV/c, Powell Birge Group (LRL) Physics Note 123, February 1968.

8. D. Kane, Beam Normalization for Experiments 50-52, Powell-Birge Group (LRL) Physics Note 172, April 1971.

9. Emilio Segre, Nuclei and Particles (W. A. Benjamin, Inc., New York, 1964), p. 32.

10. Herbert C. Albrecht, Eugene P. Binnall, Robert W. Birge, Myron H. Myers, and P. Wes Weber, The Cobweb Data Reduction System,

UCRL-18528 Rev., October 1968.

11. H. S. White, S. S. Buckman, D. E. Hall, E. Hurwitz, L. B. Meissner, J. C. Smith, and F. R. Stannard, The FOG, CLOUDY, and FAIR Programs for Bubble Chamber Data Reduction, UCRL-9457, August 1960 (unpublished).

12. John Visser, Supplement to Bookie Write-up, Powell-Birge Group (LRL) Technical Note 138, January 1969.

13. This was determined by comparing the results of visual determination with results of logical selection in FAIR. The level for acceptable FAIR selection was chosen so that incorrect determinations were made in less than 3% of cases. Since this determination was necessary in less than one-fourth of the events, this gave a negligible contamination.

14. (a) M. S. Bartlett, Statistical Estimation of Mean Lifetimes, Philosophy Magazine 44, 249 (1953).

    (b) J. Louie, Lambda Lifetime and Bartlett S-Function Technique, Powell-Birge Group (LRL) Technical Note 104, December 1966.

15. Roger Bangerter (LRL), private communication, October 1970.

16. For a two body final state the spin may be aligned along the production normal, as described in Section IV-A. In a multiparticle final state, the Σ may be one of the decay products of an unstable resonance, the spin could be preferentially aligned along the normal to the decay plane--but again the Σ momentum lies in the plane.

17. This was suggested by the following observation which held approximately for all of the four batches in which the data were processed and for both event types: if the proportion of events giving good fits for each successive measurement is projected to

a hypothetical third measurement, the accumulative total of good fits is approximately the number of fits after two measurements.

18. We have used the values 1.0 for $\Sigma^- \to \pi^- n$, .528 for $\Sigma^+ \to \pi^0 p$, and .472 for $\Sigma^+ \to \pi^+ n$. These were taken from Naomi Barash-Schmidt, Angela Barbaro-Galtieri, Leroy R. Price, Arthur H. Rosenfeld, Paul Soding, Charles G. Wohl, Matts Roos, and Gianni Conforto, Reviews of Modern Physics 41, 109 (1969). The values for Σ^+ decays are slightly different in more recent compilations, but the difference is well within our experimental error.

19. In combining subsets of data, the means of the efficiency and the momentum were determined based on unweighted numbers of events in all final states.

20. C. Michael, S-Matrix, in Methods of Subnuclear Physics, Vol. II, (Gordon and Breach, New York, 1968), p. 31.

21. D. Kane, A System of Programs for Analysis of Two Body Final States With Limited Statistics, Powell-Birge Group (LRL) Technical Note 173, April 1971.

22. Emilio Segre, Nuclei and Particles (W. A. Benjamin, Inc., New York, 1964), P. 676.

23. (a) Frank T. Solmitz, Annual Review of Nuclear Science 14, 375 (1964).

(b) These formulae for P and ΔP are not correct when cuts are made in the data (or events are missed due to imperceptible kinks). The correct formulae were given in Roger Odell Bangerter, Nonleptonic Decay of Sigma Hyperons, (Ph.D. Thesis) UCRL-19244, July 1969. We thank Professor R. D. Tripp for pointing this out. We have compared the results of these formulae with our previous results: because of limited

statistics the differences are neither significant nor systematic.

24. R. Hagedorn, Relativistic Kinematics, (W. A. Benjamin, Inc., New York, 1964), Chapter 7.

25. For particle properties determined from many observations, we refer to the Review of Particle Properties for the averaging or compatibility studies. Complete references to the original literation are given in this compilation. The most recently published edition is: Matts Roos, Claude Bricman, Angela Barbaro-Galtieri, Leroy R. Price, Alan Rittenberg, Arthur H. Rosenfeld, Naomi Barash-Schmidt, Paul Soding, Chih Yung Chien, Charles G. Wohl, and Thomas Lasinski, Physics Letters 33, B1 (1970).

26. R. D. Tripp, Baryon Resonances, in Proceedings of the International School of Physics "Enrico Fermi," (Academic Press, Inc., New York, 1966), Course XXXIII.

27. (a) W. C. Davidon, "Variable Metric Minimization," Argonne National Laboratory Report ANL-5990, Rev. 1959 (unpublished).

    (b) E. R. Beals, "Program VARMIT Writeup," LRL Computer Library Note (unpublished).

28. A classic example of this can be found in Charles G. Wohl, Frank T. Solmitz, and M. Lynn Stevenson, Physical Review Letters 17, 107 (1966).

29. R. Armenteros, P. Baillon, P. Lexa, A. Minten, K. H. Nguyen, E. Pagiola, V. Pelosi, R. Barloutaud, F. Bigata, M. Crozon, C. Louedec, J. L. Narjoux, and F. Pierre, Nuclear Physics B18, 425 (1970).

30. D. Kane, R. W. Birge, R. P. Ely, Jr., J. Hoven, G. E. Kalmus, and A. Van Horn, $K^- p \to \Sigma^{\pm} \pi^{\mp}$ Between 1730 MeV and 2150 MeV, UCRL-19790, August 1970 (unpublished).

31. Wesley M. Smart, Physical Review 169, 1330 (1968).

32. This we would call "stopping in a high valley on the χ^2 surface," discussed in Section IV-B.

33. M. Ferro-Luzzi, Three Lectures on Baryon Resonances, in Proceedings of the 1968 CERN School of Physics, CERN 68-23, Vol. II, p. 433.

34. John M. Blatt and Victor F. Weisskopf, Theoretical Nuclear Physics, (John Wiley and Sons, Inc., New York, 1952), p. 358.

35. (a) J. G. Rushbrook, Physical Review 143, 1345 (1966).
(b) E. Golowich, Physical Review 177, 2295 (1969).

36. Sheldon L. Glashow and Arthur H. Rosenfeld, Physical Review Letters 10, 192 (1963).

37. If we knew the partial widths into all channels, this would follow from the definition $\gamma = \sum_i \gamma_i$. We do not know all of them, so the procedure is arbitrary.

38. M. Gell-Mann and Y. Ne'eman, The Eightfold Way (W. A. Benjamin, Inc., New York, 1964), Parts I and II. Although this is a reprint volume, the editors are also the authors of the original papers referred to in Parts I and II.

39. J. J. DeSwart, Review of Modern Physics 35, 916 (1963).

40. (a) R. D. Tripp, D. W. G. Leith, A. Minten, R. Armenteros, M. Ferro-Luzzi, R. Levi-Setti, H. Filthuth, V. Hepp, E. Kluge, H. Schneider, R. Barloutaud, P. Granet, J. Meyer and J. P. Porte, Nuclear Physics B3, 10 (1967).
(b) R. D. Tripp, Resonances-Experimental 3 ($B = 1$, $S \neq 0$), in Ref. 5, p. 173.
(c) R. Levi-Setti, Baryon Strange Resonances (exp), in Proceedings of the Lund International Conference on Elementary Particles,

(Berlingska Boktryckeriet, Lund, Sweden, 1969), p. 341.

41. D. E. Plane, P. Baillon, C. Bricman, M. Ferro-Luzzi, J. Meyer, E. Pagiola, N. Schmitz, E. Burkhardt, H. Filthuth, E. Kluge, H. Oberlack, R. Barloutaud, P. Granet, J. P. Porte, and J. Prevost, Nuclear Physics B22, 93 (1970).

42. Anne Kernan and Wesley M. Smart, Physical Review Letters 17, 832 (1966).

43. G. E. Kalmus, G. Borreani, and J. Louie, New Data in the Reaction $\pi^+p \rightarrow \Sigma^+K^+$ at 1.28 and 1.41 GeV/c and a Test of Charge Independence in the c.m. Energy Range 1.820 to 2.090 GeV, UCRL-19777, July 1970 (to be published).

44. H. Pilkuhn and A. Swoboda, Lettere al Nuovo Cimento I, 854 (1969).

45. (a) Virendra Gupta and Virendra Singh, Physical Review 135, B1442 (1964).

    (b) C. Becchi, E. Eberle, and G. Morpurgo, Physical Review 136, B808 (1964).

46. Virendra Gupta and Virendra Singh, Physical Review 136, B782 (1964).

47. P. J. Litchfield, Nuclear Physics B22, 269 (1970).

48. R. P. Feynman, S. Pakvasa, and S. F. Tuan, Physical Review D2, 1267 (1970).

Table I. Beam Normalization

XVTX 28.0->62.0 YEND 39.0->59.0

MOMENTUM*	FIDUCIAL VOLUME CUTS++		PATH LENGTH+	MICROBARN+
	ZEND	BETE	(KM)	EQUIVALENTS
1.262 ± .014	37.37 ± 1.90	345.86 ± 2.05	133.6 ± 6.0	2.08 ± .09
1.190 ± .011	37.34 ± 1.72	346.76 ± 2.04	117.8 ± 5.2	2.36 ± .10
1.384 ± .018	37.40 ± 1.30	345.23 ± 2.02	136.2 ± 6.2	2.04 ± .09
1.311 ± .015	37.36 ± 1.26	345.76 ± 2.06	82.3 ± 4.6	3.38 ± .19
1.311 ± .016	38.05 ± 1.53	346.23 ± 2.17	77.8 ± 4.3	3.58 ± .20
1.500 ± .020	38.14 ± 1.54	344.61 ± 2.21	171.8 ± 7.2	1.82 ± .07
1.567 ± .019	38.04 ± 1.54	344.17 ± 1.89	149.5 ± 6.6	1.86 ± .08
1.153 ± .011	38.00 ± 1.80	347.73 ± 2.20	121.0 ± 5.0	2.30 ± .10
1.308 ± .016	38.05 ± 1.83	346.21 ± 2.28	81.2 ± 4.3	3.43 ± .18
1.278 ± .017	38.01 ± 1.76	346.10 ± 2.08	183.8 ± 6.6	1.70 ± .07
1.345 ± .020	38.03 ± 1.48	345.40 ± 2.11	143.3 ± 6.3	1.94 ± .08
1.454 ± .023	38.01 ± 1.51	344.92 ± 2.18	260.0 ± 9.4	1.07 ± .04
1.644 ± .017	37.67 ± 1.13	345.01 ± 1.86	153.1 ± 6.9	1.82 ± .08
1.694 ± .019	37.68 ± 1.15	344.92 ± 1.80	223.6 ± 8.8	1.24 ± .05
1.208 ± .016	37.71 ± 1.20	349.32 ± 2.26	189.2 ± 7.2	1.47 ± .06
	ALFE 90.02 ± 1.56			

* WITH ONE STANDARD DEVIATION ++ ACCEPTED SPREAD IS THREE STANDARD DEVIATIONS (AS USED FOR CROSS SECTIONS)
\+ ERROR COMBINES STATISTICAL UNCERTAINTY, UNCERTAINTY IN MOMENTUM, AND UNCERTAINTIES IN TAU EFFICIENCY CORRECTIONS

XBL 713-486

Table II. Bookkeeping Summary.

Category	No. Events	Sub-totals
A. Original Good Fits	18,776	
B. Measure Reject Sustained	1,217	
C. Kinked track not		4,353
1. Good Fit Ξ^-	1,415	
2. Negative Kink > .6 nsec.	2,468	
3. Positive Kink > .6 nsec.	470	
D. Events Remeasured		8,641
1. Good Fits	4,351	
2. Fits	1,134	
3. No Fit	1,340	
4. CLOUDY Reject	392	
5. FOG Reject	926	
6. Remeasure Reject	498	
TOTAL Good Fits (A + D1)		23,127
TOTAL Good Candidates (A + D)		27,417
TOTAL Scanned	32,987	

Table III. Mean Lifetimes.

Mean Life (nsec.)	$K^- p \to \pi\Sigma$	$K^- p \to \pi\ \Sigma\ \pi^0$
$\Sigma^- \to \pi^- n$	.154 ± .004	.160 ± .003
$\Sigma^+ \to \pi^0 p$	.092 ± .003	.089 ± .002
$\Sigma^+ \to \pi^+ n$	.085 ± .002	.082 ± .002

Table IV. Cuts Used.

	L_{MIN} (cm)	L_{MAX} (cm)	τ_k (nsec.)	δ (deg.)	ϕ (deg.)
Cross Sections					
$\Sigma^- \to \pi^- n$	.4	15.	.5	5.	20.
$\Sigma^+ \to \pi^o p$	.5	15.	.3	6.	40.
$\Sigma^+ \to \pi^+ n$	.5	15.	.3	5.	20.
Distributions					
$\Sigma^- \to \pi^- n$	.3	15.	.5	5.	0.
$\Sigma^+ \to \pi^o p$	.3	15.	.3	3.	0.
$\Sigma^+ \to \pi^+ n$	.3	15.	.3	5.	0.

Table V. Effects of Cuts.

	Fail Phase Space or Chamber Volume Cuts	Fail Length or Angle Cuts	Pass All Cuts
Cross Sections			
$\Sigma^- \to \pi^- n$	1,645	1,197	6,329
$\Sigma^+ \to \pi^o p$	756	2,164	2,775
$\Sigma^+ \to \pi^+ n$	1,125	2,007	4,329
Distributions			
$\Sigma^- \to \pi^- n$	1,186	441	8,344
$\Sigma^+ \to \pi^o p$	525	348	4,822
$\Sigma^+ \to \pi^+ n$	770	458	6,233

Table VI. Efficiency Percentages

Momentum	Scanning Efficiency	Thru-put Efficiency
1.262	99.1 ± 0.3	96.0 ± 3.0
1.190	99.7 ± 0.2	96.0 ± 3.0
1.384	99.4 ± 0.3	96.0 ± 3.0
1.311	99.7 ± 0.2	96.0 ± 3.0
1.311	99.7 ± 0.2	94.0 ± 3.0
1.500	96.7 ± 1.0	94.5 ± 2.0
1.567	99.6 ± 0.1	94.0 ± 3.0
1.153	99.9 ± 0.1	94.0 ± 3.0
1.308	99.8 ± 0.2	94.0 ± 3.0
1.278	97.1 ± 1.0	94.5 ± 3.0
1.345	96.6 ± 1.0	94.5 ± 2.0
1.454	99.6 ± 0.2	94.0 ± 3.0
1.644	96.4 ± 1.0	92.5 ± 2.5
1.694	96.7 ± 1.0	92.5 ± 2.5
1.208	97.2 ± 1.0	92.5 ± 2.5

Table VII. Cross Sections

A. $K^-p \to \pi^+\Sigma^-$

P_{LAB} GEV/C	UNWEIGHTED NUMBER	AVERAGE WEIGHT	E_{CM} GEV	$\sigma \pm \Delta\sigma$ (mb)
1.153	274	1.62	1.865	1.084 ± .087
1.190	213	1.65	1.887	.833 ± .050
1.208	304	1.63		
1.262	163	1.64	1.919	.536 ± .037
1.278	162	1.65		
1.308	70	1.65		
1.311	79	1.66	1.937	.458 ± .037
1.311	77	1.67		
1.345	101	1.67	1.952	.358 ± .040
1.384	95	1.72	1.970	.350 ± .041
1.454	208	1.70	2.001	.405 ± .034
1.500	118	1.70	2.022	.356 ± .037
1.567	97	1.74	2.051	.336 ± .039
1.644	94	1.73	2.084	.331 ± .038
1.694	121	1.74	2.106	.293 ± .030

B. $K^-p \to \pi^-\Sigma^+$

P_{LAB} GEV/C	UNWEIGHTED NUMBER	AVERAGE WEIGHT	E_{CM} GEV	$\sigma \pm \Delta\sigma$ (mb)
1.153	119	2.21	1.865	1.364 ± .144
1.190	129	2.11	1.887	1.415 ± .098
1.208	195	2.09		
1.262	128	2.17	1.919	1.421 ± .099
1.278	182	2.15		
1.308	69	2.02		
1.311	93	2.07	1.937	1.277 ± .099
1.311	84	1.92		
1.345	137	2.09	1.952	1.288 ± .127
1.384	139	2.05	1.970	1.293 ± .131
1.454	237	2.08	2.001	1.196 ± .097
1.500	147	2.14	2.022	1.184 ± .113
1.567	128	2.22	2.051	1.199 ± .124
1.644	137	2.21	2.084	1.305 ± .131
1.694	168	2.09	2.106	1.036 ± .095

XBL 713-485

Table VII. Cross Sections (cont.)

C. $K^-p \rightarrow \pi^+\Sigma^-\pi^0$

P_{LAB} GEV/C	UNWEIGHTED NUMBER	AVERAGE WEIGHT	E_{CM} GEV	$\sigma \pm \Delta\sigma$ (mb)
1.153	226	1.55	1.865	.859 ± .073
1.190	209	1.58	1.887	.871 ± .051
1.208	341	1.57		
1.262	208	1.58	1.919	.806 ± .049
1.278	293	1.56		
1.308	166	1.56		
1.311	168	1.57	1.937	.913 ± .058
1.311	143	1.56		
1.345	266	1.58	1.952	.892 ± .070
1.384	246	1.57	1.970	.827 ± .070
1.454	474	1.57	2.001	.852 ± .058
1.500	321	1.57	2.022	.893 ± .066
1.567	278	1.58	2.051	.872 ± .071
1.644	337	1.60	2.084	1.097 ± .084
1.694	481	1.60	2.106	1.068 ± .071

D. $K^-p \rightarrow \pi^-\Sigma^+\pi^0$

P_{LAB} GEV/C	UNWEIGHTED NUMBER	AVERAGE WEIGHT	E_{CM} GEV	$\sigma \pm \Delta\sigma$ (mb)
1.153	104	1.90	1.865	1.023 ± .114
1.190	125	1.87	1.887	1.211 ± .085
1.208	189	1.85		
1.262	131	1.84	1.919	1.122 ± .082
1.278	148	1.85		
1.308	97	1.89		
1.311	83	1.87	1.937	1.414 ± .104
1.311	112	1.85		
1.345	138	1.85	1.952	1.150 ± .113
1.384	123	1.82	1.970	1.016 ± .108
1.454	263	1.82	2.001	1.159 ± .091
1.500	174	1.81	2.022	1.186 ± .106
1.567	145	1.82	2.051	1.112 ± .110
1.644	159	1.82	2.084	1.247 ± .119
1.694	247	1.79	2.106	1.306 ± .105

XBL 713-484

Table VIII. Raw Data in Twenty Equal Bins of the Production Cosine, cos θ.

A. $K^- p \rightarrow \pi^+ \Sigma^-$

NUMBER WEIGHTED / NUMBER UNWEIGHTED

CENTER	1.865 GEV	1.887 GEV	1.919 GEV	1.937 GEV	1.952 GEV	1.970 GEV
-.95	32.7/ 28	60.0/ 51	37.9/ 32	53.3/ 45	14.6/ 12	23.8/ 20
-.85	32.7/ 28	48.9/ 42	26.7/ 23	19.3/ 16	7.0/ 6	14.3/ 12
-.75	41.7/ 36	32.6/ 28	14.1/ 12	12.9/ 11	3.5/ 3	4.7/ 4
-.65	32.2/ 28	38.4/ 33	17.6/ 15	9.2/ 8	4.6/ 4	3.5/ 3
-.55	18.5/ 16	26.6/ 23	15.2/ 13	5.7/ 5	4.6/ 4	3.6/ 3
-.45	19.3/ 17	20.7/ 18	21.8/ 19	5.7/ 5	3.4/ 3	4.6/ 4
-.35	6.8/ 6	10.3/ 9	5.8/ 5	11.4/ 10	3.4/ 3	4.6/ 4
-.25	2.3/ 2	7.9/ 7	7.9/ 7	9.0/ 8	4.5/ 4	0. / 0
-.15	4.6/ 4	6.8/ 6	9.0/ 8	9.1/ 8	3.4/ 3	1.2/ 1
-.05	9.1/ 8	14.9/ 13	14.8/ 13	4.6/ 4	3.4/ 3	1.1/ 1
+.05	10.3/ 9	21.8/ 19	17.3/ 15	12.5/ 11	2.3/ 2	2.3/ 2
+.15	12.6/ 11	37.8/ 33	27.6/ 24	13.7/ 12	6.8/ 6	1.1/ 1
+.25	25.4/ 22	57.8/ 50	27.6/ 24	9.2/ 8	4.6/ 4	0. / 0
+.35	30.3/ 26	46.7/ 40	33.5/ 29	18.4/ 16	4.6/ 4	10.4/ 9
+.45	19.9/ 17	55.1/ 47	31.4/ 27	17.4/ 15	7.0/ 6	2.4/ 2
+.55	19.0/ 16	44.9/ 38	30.6/ 26	16.4/ 14	5.9/ 5	1.2/ 1
+.65	18.1/ 15	49.3/ 41	13.2/ 11	10.7/ 9	3.6/ 3	3.5/ 3
+.75	11.2/ 9	37.0/ 30	24.4/ 20	9.7/ 8	11.0/ 9	6.1/ 5
+.85	36.3/ 28	75.6/ 59	31.9/ 25	35.5/ 28	18.9/ 15	15.1/ 12
+.95	63.3/ 44	139.4/ 96	101.9/ 72	89.0/ 63	45.1/ 32	63.6/ 45
TOTAL	446.5/370	832.5/683	510.3/420	372.6/304	162.2/131	166.9/132

CENTER	2.001 GEV	2.022 GEV	2.051 GEV	2.084 GEV	2.106 GEV
-.95	58.0/ 47	29.7/ 24	27.5/ 22	30.1/ 24	35.8/ 28
-.85	24.3/ 19	26.8/ 21	18.3/ 14	9.7/ 8	19.1/ 15
-.75	15.6/ 13	10.7/ 9	10.8/ 9	12.4/ 10	8.8/ 7
-.65	11.3/ 9	11.1/ 9	9.0/ 7	3.7/ 3	4.0/ 3
-.55	6.9/ 6	3.5/ 3	2.4/ 2	0. / 0	0. / 0
-.45	9.4/ 8	3.5/ 3	3.5/ 3	4.7/ 4	3.9/ 3
-.35	10.4/ 9	8.4/ 7	1.2/ 1	1.2/ 1	6.1/ 5
-.25	8.1/ 7	6.0/ 5	1.1/ 1	1.2/ 1	4.6/ 4
-.15	4.5/ 4	11.6/ 10	2.3/ 2	0. / 0	2.4/ 2
-.05	2.3/ 2	2.3/ 2	1.2/ 1	1.2/ 1	2.3/ 2
+.05	2.3/ 2	0. / 0	0. / 0	1.1/ 1	0. / 0
+.15	2.5/ 2	0. / 0	1.1/ 1	2.3/ 2	3.4/ 3
+.25	4.6/ 4	2.3/ 2	1.1/ 1	0. / 0	0. / 0
+.35	5.7/ 5	5.8/ 5	1.2/ 1	2.3/ 2	1.1/ 1
+.45	8.1/ 7	9.4/ 8	11.1/ 9	2.3/ 2	1.1/ 1
+.55	3.5/ 3	3.5/ 3	2.3/ 2	4.6/ 4	5.8/ 5
+.65	8.3/ 7	2.3/ 2	4.7/ 4	1.2/ 1	2.4/ 2
+.75	8.5/ 7	4.8/ 4	3.6/ 3	3.6/ 3	4.7/ 4
+.85	37.5/ 30	13.8/ 11	17.5/ 14	21.2/ 17	22.3/ 18
+.95	98.5/ 70	63.5/ 45	64.6/ 46	52.2/ 38	67.5/ 49
TOTAL	330.4/261	219.0/173	184.5/143	154.9/122	195.4/152

XBL 713-483

Table VIII. Raw Data in Twenty Equal Bins of the Production Cosine, cos θ (cont.).

B. $K^- p \rightarrow \pi^- \Sigma^+$

(Data From $\Sigma^+ \rightarrow \pi^+ n$ Only)

NUMBER WEIGHTED / NUMBER UNWEIGHTED

CENTER	1.865 GEV	1.887 GEV	1.919 GEV	1.937 GEV	1.952 GEV	1.970 GEV
-.95	11.6/ 10	45.3/ 39	41.2/ 35	46.3/ 40	21.0/ 18	17.3/ 15
-.85	19.8/ 17	48.9/ 42	39.4/ 34	33.6/ 29	10.4/ 9	9.2/ 8
-.75	9.3/ 8	18.7/ 16	30.3/ 26	29.0/ 25	12.7/ 11	19.8/ 17
-.65	8.2/ 7	25.7/ 22	22.2/ 19	18.6/ 16	4.7/ 4	8.1/ 7
-.55	4.7/ 4	2.3/ 2	10.5/ 9	8.2/ 7	2.3/ 2	3.5/ 3
-.45	2.4/ 2	3.5/ 3	2.3/ 2	7.0/ 6	3.5/ 3	3.5/ 3
-.35	2.4/ 2	2.4/ 2	4.7/ 4	4.7/ 4	2.4/ 2	2.4/ 2
-.25	2.4/ 2	4.8/ 4	0. / 0	2.4/ 2	8.2/ 7	8.3/ 7
-.15	6.0/ 5	1.2/ 1	8.3/ 7	8.3/ 7	7.1/ 6	5.9/ 5
-.05	3.6/ 3	7.2/ 6	15.5/ 13	20.2/ 17	6.0/ 5	2.4/ 2
+.05	7.3/ 6	15.7/ 13	13.2/ 11	15.6/ 13	13.1/ 11	14.4/ 12
+.15	7.4/ 6	14.6/ 12	23.1/ 19	23.0/ 19	10.8/ 9	16.8/ 14
+.25	8.7/ 7	28.4/ 23	20.9/ 17	23.2/ 19	12.4/ 10	15.7/ 13
+.35	13.8/ 11	30.0/ 24	18.6/ 15	18.5/ 15	13.6/ 11	12.3/ 10
+.45	15.4/ 12	30.5/ 24	17.6/ 14	15.0/ 12	6.2/ 5	8.7/ 7
+.55	9.2/ 7	24.7/ 19	19.3/ 15	12.8/ 10	1.3/ 1	2.6/ 2
+.65	14.8/ 11	40.0/ 30	21.2/ 16	7.9/ 6	5.3/ 4	3.9/ 3
+.75	32.5/ 23	64.2/ 46	52.7/ 38	37.0/ 27	16.4/ 12	10.9/ 8
+.85	28.9/ 19	86.7/ 57	61.5/ 41	63.8/ 43	31.3/ 21	29.5/ 20
+.95	58.5/ 30	160.6/ 86	204.8/111	107.2/ 60	80.6/ 45	74.2/ 43
TOTAL	266.8/192	655.6/471	627.3/446	502.2/377	269.2/196	269.2/201

CENTER	2.001 GEV	2.022 GEV	2.051 GEV	2.084 GEV	2.106 GEV
-.95	11.6/ 10	8.2/ 7	12.6/ 11	7.4/ 6	7.7/ 6
-.85	19.6/ 17	8.2/ 7	5.7/ 5	2.3/ 2	8.0/ 7
-.75	16.1/ 14	8.0/ 7	4.6/ 4	4.6/ 4	11.6/ 10
-.65	18.5/ 16	11.6/ 10	7.0/ 6	3.5/ 3	5.8/ 5
-.55	7.0/ 6	5.8/ 5	4.6/ 4	3.9/ 3	4.6/ 4
-.45	5.8/ 5	8.2/ 7	2.3/ 2	4.9/ 4	9.3/ 8
-.35	7.0/ 6	7.0/ 6	5.8/ 5	5.9/ 5	5.8/ 5
-.25	9.5/ 8	8.2/ 7	4.9/ 4	5.8/ 5	2.3/ 2
-.15	16.4/ 14	7.0/ 6	3.8/ 3	5.8/ 5	5.8/ 5
-.05	16.5/ 14	8.3/ 7	10.7/ 9	2.3/ 2	5.8/ 5
+.05	26.1/ 22	14.2/ 12	11.8/ 10	4.8/ 4	11.7/ 10
+.15	32.3/ 27	10.7/ 9	3.6/ 3	17.7/ 15	26.2/ 22
+.25	22.9/ 19	21.6/ 18	18.1/ 15	12.0/ 10	17.8/ 15
+.35	15.8/ 13	9.7/ 8	13.3/ 11	13.4/ 11	16.8/ 14
+.45	12.5/ 10	6.1/ 5	7.4/ 6	12.2/ 10	3.6/ 3
+.55	1.3/ 1	6.3/ 5	2.5/ 2	9.9/ 8	9.9/ 8
+.65	1.3/ 1	1.3/ 1	2.6/ 2	2.6/ 2	8.9/ 7
+.75	14.9/ 11	12.2/ 9	18.7/ 14	9.3/ 7	7.9/ 6
+.85	62.4/ 43	40.4/ 28	38.9/ 27	35.2/ 25	42.4/ 30
+.95	141.3/ 81	102.4/ 58	101.3/ 58	107.2/ 63	125.0/ 75
TOTAL	458.8/338	305.3/222	280.2/201	270.8/194	336.9/247

XBL 713-482

Table VIII. Raw Data in Twenty Equal Bins of the Production Cosine, cos θ (cont.).

C. $K^-p \to \pi^-\Sigma^+$

(Data From $\Sigma^+ \to \pi^0 p$ Only)

SUM OF POLAR COSINE / NUMBER UNWEIGHTED

CENTER	1.865 GEV	1.887 GEV	1.919 GEV	1.937 GEV	1.952 GEV	1.970 GEV
-.95	-1.2/ 9	.0/ 24	1.4/ 31	-2.1/ 29	-2.3/ 11	-1.1/ 6
-.85	-.2/ 10	-1.4/ 26	-.5/ 13	2.6/ 21	.7/ 12	.1/ 3
-.75	-.5/ 8	3.7/ 21	.8/ 16	-.2/ 18	-1.9/ 4	-2.4/ 7
-.65	-.4/ 3	-3.6/ 9	.4/ 7	-4.1/ 11	-.6/ 4	-.6/ 2
-.55	.4/ 2	1.5/ 8	-1.2/ 5	-1.8/ 5	-2.2/ 3	-.6/ 1
-.45	-.9/ 2	-2.2/ 6	.5/ 2	-2.0/ 4	0. / 0	.5/ 1
-.35	-.3/ 1	-.9/ 2	-.4/ 1	-.4/ 1	0. / 0	0. / 0
-.25	0. / 0	-.8/ 1	-.3/ 3	0. / 0	1.5/ 2	.7/ 1
-.15	-2.0/ 3	-.1/ 3	-.8/ 4	-.2/ 10	.4/ 2	.5/ 3
-.05	-.5/ 5	.6/ 5	-3.6/ 10	.8/ 8	.6/ 3	-2.1/ 5
+.05	-1.0/ 2	-2.6/ 5	-2.5/ 17	-.1/ 11	-1.1/ 3	1.3/ 5
+.15	-1.1/ 4	-2.0/ 12	-3.4/ 9	-9.7/ 14	-3.1/ 7	-.6/ 9
+.25	-1.8/ 5	-2.4/ 16	-3.4/ 18	-1.8/ 10	-.2/ 7	-1.5/ 8
+.35	-1.2/ 5	-4.6/ 20	-4.0/ 17	-4.8/ 11	-1.9/ 3	-3.6/ 11
+.45	-.3/ 10	-2.8/ 28	-3.0/ 17	-5.5/ 13	-.7/ 2	-2.5/ 5
+.55	1.8/ 8	-.7/ 17	-4.2/ 8	-2.1/ 12	.1/ 1	0. / 0
+.65	6.3/ 13	7.7/ 20	4.0/ 15	2.7/ 9	1.8/ 4	.7/ 1
+.75	6.4/ 16	10.2/ 34	6.8/ 23	5.9/ 13	3.2/ 6	1.3/ 4
+.85	11.0/ 30	15.1/ 60	3.6/ 37	11.2/ 48	1.1/ 27	.9/ 6
+.95	6.3/ 36	7.0/ 70	14.2/ 71	6.9/ 91	8.2/ 45	7.7/ 25
TOTAL	0. /172	0. /387	0. /324	0. /339	0. /146	0. /103

CENTER	2.001 GEV	2.022 GEV	2.051 GEV	2.084 GEV	2.106 GEV
-.95	-4.0/ 9	.0/ 2	.5/ 8	-.5/ 3	-1.4/ 2
-.85	-1.3/ 10	-1.5/ 3	1.3/ 3	1.0/ 1	.6/ 3
-.75	-1.4/ 8	-2.0/ 6	.7/ 3	.0/ 3	-.8/ 3
-.65	-.8/ 8	-1.4/ 5	.7/ 5	.8/ 4	.8/ 2
-.55	-.7/ 8	-.7/ 6	-3.1/ 10	-.4/ 3	-.7/ 4
-.45	1.5/ 10	-1.9/ 7	-.5/ 4	.1/ 2	.1/ 2
-.35	2.2/ 7	1.3/ 3	.5/ 1	0. / 0	-.3/ 1
-.25	3.2/ 8	.5/ 2	.3/ 1	.9/ 5	1.2/ 2
-.15	.9/ 10	1.3/ 5	-.0/ 3	1.1/ 3	2.0/ 4
-.05	3.0/ 13	-.5/ 10	.4/ 3	-1.3/ 4	.2/ 3
+.05	.6/ 13	-.7/ 11	-.5/ 10	-.6/ 2	-1.3/ 6
+.15	-.4/ 10	-3.4/ 8	1.6/ 9	-1.5/ 8	-2.7/ 11
+.25	-.7/ 18	-6.4/ 14	-.8/ 7	-1.3/ 8	-.3/ 7
+.35	-1.6/ 15	1.4/ 11	-3.9/ 8	-.7/ 5	.1/ 8
+.45	-1.2/ 7	.9/ 3	-.3/ 1	-2.1/ 3	-2.8/ 7
+.55	.3/ 1	0. / 0	.7/ 1	.5/ 6	1.6/ 2
+.65	.9/ 3	.6/ 1	-1.5/ 4	.5/ 1	1.2/ 6
+.75	-.1/ 16	-.3/ 9	-.2/ 10	-.7/ 6	2.3/ 11
+.85	-7.9/ 33	-2.2/ 31	-3.1/ 25	-2.2/ 15	-6.2/ 21
+.95	-2.8/ 82	-2.1/ 43	-9.2/ 58	-.8/ 46	-5.0/ 45
TOTAL	0. /289	0. /180	0. /174	0. /128	0. /150

XBL 713-481

Table IX. Legendre Coefficients

A. From $K^-p \to \pi^+\Sigma^-$ Angular Distributions

E_{CM}	$A_0 \times 10^{+3}$	$A_1 \times 10^{+3}$	$A_2 \times 10^{+3}$	$A_3 \times 10^{+3}$	$A_4 \times 10^{+3}$	$A_5 \times 10^{+3}$	$A_6 \times 10^{+3}$	$A_7 \times 10^{+3}$
1.865	72 ± 3	7 ± 8	83 ± 10	16 ± 12	20 ± 14	97 ± 15	35 ± 16	-8 ± 18
1.887	60 ± 2	35 ± 4	66 ± 6	2 ± 7	36 ± 8	58 ± 9	41 ± 9	-8 ± 10
1.919	41 ± 2	24 ± 4	42 ± 5	9 ± 7	46 ± 7	46 ± 8	41 ± 8	-3 ± 9
1.937	37 ± 2	18 ± 4	64 ± 6	15 ± 8	69 ± 8	27 ± 9	48 ± 9	11 ± 10
1.961	30 ± 1	24 ± 4	68 ± 6	34 ± 7	63 ± 8	30 ± 8	38 ± 7	11 ± 9
2.001	38 ± 2	13 ± 5	97 ± 8	36 ± 10	83 ± 10	25 ± 11	50 ± 9	11 ± 12
2.022	35 ± 2	6 ± 6	76 ± 8	32 ± 11	73 ± 11	49 ± 13	53 ± 13	47 ± 16
2.051	35 ± 2	16 ± 7	96 ± 10	39 ± 14	77 ± 12	56 ± 15	55 ± 26	30 ± 25
2.084	35 ± 3	19 ± 8	108 ± 12	39 ± 14	94 ± 14	40 ± 16	59 ± 18	19 ± 15
2.106	34 ± 2	14 ± 7	97 ± 9	38 ± 12	93 ± 12	30 ± 13	46 ± 11	34 ± 17

B. From $K^-p \to \pi^-\Sigma^+$ Angular Distributions

E_{CM}	$A_0 \times 10^{+3}$	$A_1 \times 10^{+3}$	$A_2 \times 10^{+3}$	$A_3 \times 10^{+3}$	$A_4 \times 10^{+3}$	$A_5 \times 10^{+3}$	$A_6 \times 10^{+3}$	$A_7 \times 10^{+3}$
1.865	90 ± 6	90 ± 15	140 ± 20	54 ± 24	66 ± 28	81 ± 32	2 ± 30	41 ± 41
1.887	100 ± 4	108 ± 11	194 ± 15	54 ± 17	92 ± 20	79 ± 22	19 ± 19	-7 ± 26
1.919	108 ± 5	107 ± 12	220 ± 17	116 ± 20	158 ± 22	151 ± 25	26 ± 22	31 ± 21
1.937	104 ± 5	63 ± 12	172 ± 17	55 ± 19	136 ± 21	87 ± 25	-22 ± 24	-43 ± 24
1.961	109 ± 5	102 ± 13	179 ± 18	120 ± 21	218 ± 22	151 ± 25	49 ± 23	-21 ± 25
2.001	112 ± 6	118 ± 14	160 ± 20	181 ± 23	227 ± 25	200 ± 27	11 ± 26	-2 ± 25
2.022	115 ± 7	136 ± 18	188 ± 26	216 ± 32	223 ± 32	187 ± 43	64 ± 37	-3 ± 53
2.051	122 ± 8	170 ± 21	240 ± 30	226 ± 35	271 ± 39	178 ± 44	101 ± 41	-26 ± 39
2.084	146 ± 10	224 ± 25	259 ± 36	293 ± 45	335 ± 43	310 ± 61	211 ± 51	98 ± 78
2.106	116 ± 7	166 ± 18	211 ± 26	214 ± 32	263 ± 32	229 ± 39	109 ± 35	-15 ± 42

C. From $K^-p \to \pi^-\Sigma^+$ (Polarization) × (Angular Distribution)

E_{CM}	$B_0 \times 10^{+3}$	$B_1 \times 10^{+3}$	$B_2 \times 10^{+3}$	$B_3 \times 10^{+3}$	$B_4 \times 10^{+3}$	$B_5 \times 10^{+3}$	$B_6 \times 10^{+3}$	$B_7 \times 10^{+3}$
1.865	0 ± 0	-12 ± 8	-47 ± 8	-47 ± 8	-32 ± 7	-4 ± 6	-0 ± 6	4 ± 5
1.887	0 ± 0	-13 ± 7	-29 ± 7	-41 ± 7	-29 ± 6	-10 ± 6	1 ± 5	7 ± 4
1.919	0 ± 0	4 ± 7	-16 ± 8	-32 ± 8	-25 ± 7	-14 ± 6	-2 ± 4	-2 ± 4
1.937	0 ± 0	23 ± 7	-21 ± 7	-33 ± 8	-29 ± 7	-16 ± 6	10 ± 4	5 ± 4
1.961	0 ± 0	8 ± 8	-25 ± 8	-22 ± 8	-33 ± 7	-14 ± 6	2 ± 5	-0 ± 4
2.001	0 ± 0	5 ± 9	9 ± 7	30 ± 7	-0 ± 7	15 ± 6	13 ± 5	10 ± 5
2.022	0 ± 0	30 ± 11	-0 ± 11	21 ± 12	3 ± 12	21 ± 11	24 ± 8	0 ± 7
2.051	0 ± 0	25 ± 11	35 ± 11	27 ± 13	21 ± 11	14 ± 10	24 ± 8	20 ± 9
2.084	0 ± 0	22 ± 14	30 ± 14	3 ± 15	0 ± 15	10 ± 14	16 ± 11	7 ± 9
2.106	0 ± 0	20 ± 11	21 ± 10	23 ± 10	11 ± 10	31 ± 10	28 ± 8	15 ± 7

XBL 713-480

Table X. Average Weights in Regions of Dalitz Plots $K^-p \to \pi^{\pm}\Sigma^{\mp}\pi^0$

A. Data From $\Sigma^- \to \pi^- n$ Decays

(m_0^2 across, m_-^2 up in GeV^2)

	1.8 ±.1	2.0 ±.1	2.2 ±.1	2.4 ±.1	2.6 ±.1	2.8 ±.1	3.0 ±.1	3.2 ±.1	3.4 ±.1	3.6 ±.1
3.6 ±.1	1.22 ±.13	1.21 ±.10	1.21 ±.09							
3.4 ±.1	1.20 ±.07	1.20 ±.08	1.24 ±.17	1.26 ±.17						
3.2 ±.1	1.18 ±.06	1.18 ±.06	1.20 ±.10	1.23 ±.14	1.25 ±.14					
3.0 ±.1	1.19 ±.06	1.19 ±.07	1.19 ±.08	1.20 ±.09	1.22 ±.08	1.21 ±.04				
2.8 ±.1	1.17 ±.05	1.17 ±.05	1.17 ±.05	1.18 ±.07	1.19 ±.08	1.19 ±.06	1.25 ±.10			
2.6 ±.1		1.17 ±.03	1.17 ±.05	1.18 ±.07	1.19 ±.13	1.19 ±.07	1.23 ±.12	1.18 ±.06		
2.4 ±.1		1.18 ±.03	1.17 ±.04	1.17 ±.06	1.17 ±.06	1.18 ±.07	1.22 ±.19	1.24 ±.16	1.19 ±.04	
2.2 ±.1			1.17 ±.02	1.17 ±.05	1.16 ±.07	1.17 ±.07	1.18 ±.07	1.25 ±.46	1.21 ±.06	1.21 ±.04
2.0 ±.1					1.17 ±.06	1.17 ±.05	1.18 ±.06	1.21 ±.13	1.19 ±.06	1.18 ±.05
1.8 ±.1						1.17 ±.04	1.19 ±.07	1.17 ±.06	1.21 ±.07	1.20 ±.05

XBL 713-474

Table X. Average Weights in Regions of Dalitz Plots $K^-p \to \pi^{\pm}\Sigma^{\mp}\pi^0$ (cont).

B. Data From $\Sigma^+ \to \pi^+ n$ Decays

(m_o^2 across, m_+^2 up in GeV^2)

	1.8 ±.1	2.0 ±.1	2.2 ±.1	2.4 ±.1	2.6 ±.1	2.8 ±.1	3.0 ±.1	3.2 ±.1	3.4 ±.1	3.6 ±.1
3.6 ±.1	1.35 ±.17	1.32 ±.16								
3.4 ±.1	1.28 ±.13	1.26 ±.13	1.29 ±.22	1.24 ±.16						
3.2 ±.1	1.32 ±.15	1.28 ±.12	1.23 ±.10	1.25 ±.10	1.25 ±.11					
3.0 ±.1	1.29 ±.12	1.28 ±.13	1.21 ±.07	1.24 ±.14	1.35 ±.44	1.27 ±.17				
2.8 ±.1	1.30 ±.11	1.27 ±.09	1.25 ±.11	1.26 ±.14	1.23 ±.10	1.21 ±.07	1.19 ±.05			
2.6 ±.1		1.28 ±.09	1.27 ±.12	1.25 ±.12	1.22 ±.07	1.22 ±.09	1.22 ±.09	1.28 ±.15		
2.4 ±.1		1.29 ±.03	1.27 ±.06	1.25 ±.08	1.24 ±.08	1.23 ±.07	1.23 ±.16	1.23 ±.08	1.27 ±.12	
2.2 ±.1			1.27 ±.06	1.25 ±.04	1.26 ±.08	1.24 ±.07	1.22 ±.06	1.27 ±.14	1.21 ±.06	1.36 ±.19
2.0 ±.1					1.25 ±.07	1.26 ±.09	1.26 ±.09	1.27 ±.13	1.23 ±.08	1.24 ±.09
1.8 ±.1						1.25 ±.11	1.26 ±.10	1.26 ±.12	1.23 ±.08	1.29 ±.13

XBL 713-475

Table X. Average Weights in Regions of Dalitz Plots $K^-p \to \pi^{\pm}\Sigma^{\mp}\pi^0$ (cont).

C. Data From $\Sigma^+ \to \pi^0 p$ Decays)

(m_0^2 across, m_+^2 up in GeV^2)

	1.8 ±.1	2.0 ±.1	2.2 ±.1	2.4 ±.1	2.6 ±.1	2.8 ±.1	3.0 ±.1	3.2 ±.1	3.4 ±.1	3.6 ±.1
3.6 ±.1	1.27 ±.10	1.31 ±.14	1.44 ±.22							
3.4 ±.1	1.32 ±.13	1.33 ±.15	1.33 ±.12	1.38 ±.18						
3.2 ±.1	1.35 ±.17	1.30 ±.11	1.29 ±.13	1.26 ±.07						
3.0 ±.1	1.32 ±.12	1.30 ±.11	1.28 ±.10	1.26 ±.09	1.25 ±.05	1.21 ±.00				
2.8 ±.1	1.29 ±.08	1.28 ±.09	1.27 ±.10	1.27 ±.09	1.27 ±.09	1.28 ±.11				
2.6 ±.1		1.30 ±.09	1.28 ±.09	1.28 ±.11	1.25 ±.06	1.27 ±.08	1.27 ±.12			
2.4 ±.1		1.29 ±.06	1.28 ±.07	1.28 ±.08	1.26 ±.09	1.29 ±.13	1.26 ±.07	1.24 ±.05	1.30 ±.11	
2.2 ±.1			1.28 ±.02	1.28 ±.05	1.25 ±.05	1.26 ±.06	1.32 ±.22	1.30 ±.11	1.25 ±.03	1.23 ±.02
2.0 ±.1				1.29 ±.03	1.27 ±.05	1.28 ±.08	1.29 ±.08	1.28 ±.10	1.27 ±.10	1.25 ±.09
1.8 ±.1						1.33 ±.08	1.29 ±.07	1.26 ±.07	1.24 ±.04	1.29 ±.12

XBL 713-476

Table XI. Binomial Operator From Partial Waves to Distribution Coefficients, Values Approximate, see Ref. 26 for exact values.

$U \cdot V = R_e(U^* V)$	A_0	A_1	A_2	A_3	A_4	A_5	A_6	A_7	B_7	B_6	B_5	B_4	B_3	B_2	B_1	$U \times V = I_m(U^* V)$
$S_1 \cdot S_1 + P_1 \cdot P_1$	1.0															
$S_1 . P_1$		2.0													2.0	$S_1 \times P_1$
$S_1 \cdot P_3 + P_1 \cdot D_3$		4.0													-2.0	$S_1 \times P_3 - P_1 \times D_3$
$S_1 \cdot D_3 + P_1 \cdot P_3$			4.0											2.0		$S_1 \times D_3 - P_1 \times P_3$
$S_1 \cdot D_5 + P_1 \cdot F_5$			6.0											-2.0		$S_1 \times D_5 - P_1 \times F_5$
$S_1 \cdot F_5 + P_1 \cdot D_5$				6.0									2.0			$S_1 \times F_5 - P_1 \times D_5$
$S_1 \cdot F_7 + P_1 \cdot G_7$				8.0									-2.0			$S_1 \times F_7 - P_1 \times G_7$
$S_1 \cdot G_7 + P_1 \cdot F_7$					8.0							2.0				$S_1 \times G_7 - P_1 \times F_7$
$P_3 \cdot P_3 + D_3 \cdot D_3$	2.0		2.0													
$P_3 . D_3$		0.8		7.2									2.4		1.6	$P_3 \times D_3$
$P_3 \cdot D_3 + D_3 \cdot F_5$		7.2		4.8									-0.4		-3.6	$P_3 \times D_3 - D_3 \times F_5$
$P_3 \cdot F_5 + D_3 \cdot D_5$			1.7		10.3							2.6		1.4		$P_3 \times F_5 - D_3 \times D_5$
$P_3 \cdot F_7 + D_3 \cdot G_7$			10.3		5.7							-0.6		-3.4		$P_3 \times F_7 - D_3 \times G_7$
$P_3 \cdot G_7 + D_3 \cdot F_7$				2.7		13.3					2.7		1.3			$P_3 \times G_7 - D_3 \times F_7$
$D_5 \cdot D_5 + F_5 \cdot F_5$	3.0		3.4		2.6											
$D_5 . F_5$		0.5		3.2		14.3					2.9		1.6		1.5	$D_5 \times F_5$
$D_5 \cdot F_7 + F_5 \cdot G_7$		10.3		8.0		5.7					-0.2		-0.7		-5.1	$D_5 \times F_7 - F_5 \times G_7$
$D_5 \cdot G_7 + F_5 \cdot F_7$			1.1		4.7		10.2			3.0		1.6		1.3		$D_5 \times G_7 - F_5 \times F_7$
$F_7 \cdot F_7 + G_7 \cdot G_7$	4.0		4.8		4.2		3.0									
$F_7 . G_7$		0.4		2.2		6.6		22.8	3.3		1.8		1.5		1.5	$F_7 \times G_7$

XBL 713-600

Table XII. Summary of Partial Wave Fits to the Legendre Coefficients of Tables IX and Ref. 2b.

FIT	A1	B1	B2	C1	C2	C3	C4
S01	P(6)	P(6)	P(6)	P(6)	P(6)	P(6)	P(6)
S11							
P01							
P11						R(3)	R(3)
P03						P(6)	P(6)
P13						R(3)	
D03		R(3)+P(6)	R(3)+P(6)			R(0)+V(5)	
D13		P(6)	P(6)	R(3)	R(3)	R(0)+R(3)	R(3)
D05	R(3)+P(6)	R(3)+V(5)	R(3)+V(5)	R(3)+V(5)	R(3)+V(5)	R(3)+V(5)	R(3)+V(5)
D15							
F05			R(3)+R(3)	R(3)+R(3)			R(3)+R(3)
F15	R(3)	V(5)				V(5)	
F07	P(6)		V(5)	V(5)	V(5)		V(5)
F17	R(3)	R(3)	R(3)	R(3)	R(3)	R(3)	R(3)
G07							
G17	---	---	---	---	---	---	---
NV	90	91	90	84	89	78	81
$(\chi^2/DF)_i$	379./296	303./300	---	375./305	---	---	---
$(\chi^2/DF)_f$	296./279	300./277	288./278	303./284	306./280	353./290	320./287
PROB.	21%	17%	33%	21%	14%	1%	8%
$(\chi^2/DP)_d$	0.94	0.97	0.93	0.95	0.98	1.14	0.98
$(\chi^2/DP)_a$	1.57	1.59	1.56	1.54	1.54	1.56	1.56

FIT	D0	E1	F0	G1	G2
S01	P(6)	P(6)	B(6)	P(4)	P(4)
S11					
P01					
P11	R(0)			R(3)+P(4)	R(2)+R(2)
P03	P(6)			P(4)	P(4)
P13	R(0)			R(3)+V(5)	R(3)+V(5)
D03	R(0)+V(4)	R(0)+V(5)	R(0)+V(4)	R(0)+V(5)	R(0)+R(3)
D13	R(0)+R(0)			R(0)+R(3)	
D05	R(0)+V(4)	R(3)+V(5)		R(3)+V(5)	R(3)+V(5)
D15					
F05	R(0)+R(0)				
F15		V(5)	V(4)		R(2)+R(2)
F07	V(4)			R(3)	R(3)
F17	R(0)	R(3)	R(0)		
G07					
G17	---	V(5)	V(4)		---
NV	48	91	68	83	68
$(\chi^2/DF)_i$	1035./320	422./300	1015./300	584./318	---
$(\chi^2/DF)_f$	---	312./277	---	317./285	368./300
PROB.	---	7%	---	9%	.4%
$(\chi^2/DP)_d$	---	1.01	---	1.11	---
$(\chi^2/DP)_a$	---	1.01	---	1.62	---

NV NUM. OF VARIABLES (APPLIES TO f)

DP-NUM. OF DEGREES OF FREEDOM

DP-NUM. OF DATA POINTS

i -FOR PREFIT, WHERE APPROPRIATE

f -FOR ACTUAL FIT

d -FROM ANGULAR DISTRIBUTIONS AND POLARIZATIONS

a -FROM ALL COEFFICIENTS IN FIG. 15.

NO FIT INVOLVED FOR d OR a.

XBL 713-596

Table XIII. Partial Waves Calculated From Fitted Parameters

A. For Fit A1

ECM	S01	P01	P03	D03	D05	F05	F07	G07
1.725	.097, .092	.201, .080	.130, .167	.168,-.077	.012,-.070	-.068,-.146	.004, .002	.004, .000
1.750	.079, .076	.223,-.054	.138, .118	.139,-.036	-.003,-.074	-.144,-.100	.005, .002	.005, .000
1.775	.066, .061	.181,-.151	.136, .081	.105,-.016	-.021,-.087	-.165,-.095	.007, .003	.007, .001
1.800	.056, .047	.127,-.200	.129, .053	.073,-.008	-.030,-.120	-.126,-.180	.010, .004	.008, .001
1.825	.050, .034	.089,-.214	.122, .034	.044,-.006	.000,-.166	.034,-.249	.014, .004	.010, .001
1.850	.045, .024	.076,-.209	.116, .020	.018,-.004	.069,-.165	.140,-.193	.018, .005	.012, .002
1.875	.042, .015	.086,-.188	.113, .011	-.004, .001	.105,-.117	.154,-.149	.023, .006	.014, .003
1.900	.040, .007	.108,-.153	.113, .005	-.021, .011	.103,-.076	.147,-.133	.029, .007	.017, .004
1.925	.040,-.001	.129,-.099	.117, .002	-.031, .026	.088,-.052	.141,-.128	.035, .007	.020, .006
1.950	.041,-.010	.130,-.034	.124, .000	-.031, .045	.073,-.043	.141,-.124	.042, .007	.023, .008
1.975	.041,-.022	.099, .025	.135, .001	-.019, .063	.062,-.044	.148,-.117	.050, .007	.027, .012
2.000	.038,-.036	.043, .049	.150, .004	.004, .075	.061,-.051	.161,-.103	.058, .007	.031, .018
2.025	.031,-.054	.001, .025	.167, .011	.035, .074	.069,-.056	.174,-.078	.066, .006	.034, .026
2.050	.016,-.072	.013,-.014	.187, .023	.066, .056	.086,-.054	.182,-.042	.075, .004	.035, .037
2.075	-.010,-.086	.067, .003	.209, .041	.086, .021	.106,-.039	.177, .002	.084, .002	.031, .051
2.100	-.046,-.091	.065, .099	.231, .066	.086,-.023	.121,-.009	.152, .046	.094,-.000	.020, .063

ECM	S11	P11	P13	D13	D15	F15	F17	G17
1.725	.059, .181	-.059,-.062	-.004,-.009	.041,-.013	.007, .012	-.024,-.004	-.008,-.000	0. ,0.
1.750	.096, .166	-.045,-.076	.021, .020	.030,-.053	.001, .075	-.031,-.006	-.009,-.001	0. ,0.
1.775	.128, .142	-.035,-.083	.056, .025	-.005,-.075	-.006, .105	-.039,-.010	-.011,-.001	0. ,0.
1.800	.153, .111	-.030,-.084	.088, .010	-.043,-.074	-.007, .101	-.049,-.017	-.014,-.001	0. ,0.
1.825	.169, .075	-.031,-.081	.108,-.016	-.069,-.062	.001, .080	-.060,-.029	-.016,-.002	0. ,0.
1.850	.175, .038	-.038,-.073	.117,-.044	-.084,-.049	.013, .052	-.070,-.049	-.020,-.003	0. ,0.
1.875	.173, .001	-.046,-.061	.118,-.068	-.089,-.043	.025, .025	-.073,-.080	-.024,-.005	0. ,0.
1.900	.162,-.033	-.053,-.044	.114,-.086	-.086,-.046	.035, .001	-.057,-.117	-.029,-.007	0. ,0.
1.925	.143,-.062	-.056,-.022	.109,-.097	-.076,-.055	.045,-.019	-.017,-.141	-.036,-.011	0. ,0.
1.950	.119,-.084	-.050,-.001	.103,-.100	-.057,-.067	.054,-.035	.026,-.135	-.044,-.018	0. ,0.
1.975	.092,-.098	-.035, .015	.099,-.097	-.028,-.073	.064,-.046	.053,-.114	-.053,-.031	0. ,0.
2.000	.063,-.104	-.016, .020	.094,-.088	.004,-.068	.074,-.052	.064,-.092	-.060,-.052	0. ,0.
2.025	.036,-.103	-.002, .012	.089,-.073	.030,-.046	.085,-.053	.067,-.074	-.053,-.086	0. ,0.
2.050	.012,-.094	-.001,-.003	.082,-.055	.037,-.015	.096,-.049	.067,-.061	-.018,-.115	0. ,0.
2.075	-.006,-.079	-.017,-.009	.071,-.036	.021, .006	.107,-.038	.064,-.051	.028,-.109	0. ,0.
2.100	-.018,-.060	-.036, .007	.053,-.017	.001, .003	.116,-.023	.062,-.043	.052,-.082	0. ,0.

XBL 713-479

Table XIII. Partial Waves Calculated From Fitted Parameters (cont.)

B. For Fit B2

ECM	S01	P01	P03	D03	D05	F05	F07	G07
1.725	-.001, .002	.252,-.132	.125, .144	.092,-.101	-.019,-.030	-.068,-.033	-.001, .001	.005, .000
1.750	.047,-.020	.245,-.155	.117, .139	.087,-.008	-.025,-.035	-.092,-.069	-.000, .003	.006, .000
1.775	.089, .027	.238,-.167	.111, .135	.053,-.007	-.036,-.053	-.103,-.140	.002, .006	.007, .000
1.800	.095, .092	.233,-.168	.107, .132	.039,-.022	-.030,-.099	-.050,-.235	.007, .007	.009, .001
1.825	.055, .138	.230,-.160	.105, .130	.032,-.037	.043,-.133	.075,-.267	.012, .008	.011, .001
1.850	.026, .161	.228,-.144	.105, .130	.025,-.051	.105,-.085	.172,-.212	.019, .006	.014, .002
1.875	.014, .169	.225,-.120	.106, .131	.014,-.060	.113,-.034	.210,-.143	.026, .004	.017, .003
1.900	.023, .166	.219,-.090	.109, .133	-.002,-.064	.106,-.002	.220,-.088	.033, .000	.021, .004
1.925	.050, .151	.209,-.057	.113, .136	-.023,-.060	.097, .018	.220,-.046	.040,-.003	.025, .007
1.950	.083, .117	.192,-.023	.118, .139	-.043,-.044	.090, .033	.216,-.012	.049,-.005	.031, .010
1.975	.104, .063	.167, .008	.125, .144	-.055,-.016	.085, .044	.210, .018	.057,-.005	.038, .017
2.000	.093, .001	.134, .033	.133, .149	-.053, .017	.082, .052	.201, .045	.067,-.003	.046, .028
2.025	.048,-.034	.095, .046	.143, .155	-.032, .046	.081, .059	.189, .070	.077, .003	.051, .047
2.050	.004,-.018	.056, .045	.154, .161	.002, .059	.082, .065	.173, .092	.086, .015	.044, .076
2.075	.017, .023	.021, .028	.167, .167	.036, .048	.085, .069	.154, .110	.093, .032	.014, .099
2.100	.080, .001	-.002,-.004	.182, .173	.052, .019	.091, .071	.134, .124	.095, .056	-.023, .095

ECM	S11	P11	P13	D13	D15	F15	F17	G17
1.725	-.039, .164	.091,-.016	.074, .089	-.137,-.090	.033, .060	.015, .013	-.005,-.000	0. ,0.
1.750	.010, .167	.062,-.049	.098, .063	-.084,-.085	-.007, .095	.013, .017	-.006,-.000	0. ,0.
1.775	.053, .156	.032,-.062	.110, .038	-.040,-.071	-.037, .079	.008, .020	-.008,-.001	0. ,0.
1.800	.087, .137	.007,-.061	.115, .018	-.010,-.047	-.033, .058	-.002, .019	-.009,-.001	0. ,0.
1.825	.112, .114	-.011,-.054	.115, .004	.003,-.021	-.019, .044	-.014, .012	-.012,-.002	0. ,0.
1.850	.129, .090	-.023,-.045	.112,-.005	-.001, .002	-.005, .033	-.022,-.009	-.014,-.002	0. ,0.
1.875	.139, .065	-.030,-.038	.109,-.007	-.017, .011	.007, .022	-.014,-.040	-.018,-.004	0. ,0.
1.900	.144, .043	-.035,-.032	.106,-.005	-.034, .004	.017, .011	.022,-.062	-.023,-.006	0. ,0.
1.925	.146, .024	-.039,-.028	.102, .002	-.040,-.017	.025, .001	.063,-.052	-.029,-.011	0. ,0.
1.950	.144, .008	-.042,-.026	.097, .012	-.029,-.040	.033,-.007	.086,-.024	-.036,-.021	0. ,0.
1.975	.140,-.006	-.046,-.026	.089, .025	-.002,-.052	.041,-.014	.092, .003	-.041,-.041	0. ,0.
2.000	.136,-.016	-.051,-.028	.078, .038	.027,-.043	.049,-.018	.087, .025	-.027,-.071	0. ,0.
2.025	.130,-.023	-.055,-.033	.063, .050	.043,-.016	.059,-.019	.080, .040	.013,-.078	0. ,0.
2.050	.125,-.028	-.058,-.042	.045, .059	.056, .012	.070,-.015	.071, .050	.036,-.055	0. ,0.
2.075	.120,-.031	-.060,-.053	.023, .063	.014, .023	.082,-.005	.062, .057	.039,-.035	0. ,0.
2.100	.115,-.032	-.058,-.069	.002, .060	-.002, .012	.092, .012	.055, .061	.036,-.024	0. ,0.

XBL 713-477

Table XIII. Partial Waves Calculated From Fitted Parameters (cont.)

C. From Fit C1

ECM	S01	P01	P03	D03	D05	F05	F07	G07
1.725	.156, -.012	.093, -.070	.147, .119	.158, -.161	-.037, -.003	-.087, -.038	-.000, .000	.005, .000
1.750	.140, .028	.099, -.086	.140, .112	.156, -.096	-.048, -.011	-.115, -.076	-.000, .002	.006, .000
1.775	.119, .052	.103, -.098	.136, .106	.134, -.053	-.059, -.032	-.132, -.147	.002, .004	.008, .000
1.800	.101, .063	.104, -.107	.133, .102	.105, -.027	-.054, -.077	-.096, -.250	.006, .005	.009, .001
1.825	.088, .067	.104, -.111	.132, .099	.075, -.014	.005, -.115	.024, -.313	.011, .004	.011, .001
1.850	.079, .066	.103, -.112	.132, .097	.046, -.008	.067, -.088	.145, -.280	.017, -.000	.014, .002
1.875	.074, .062	.101, -.110	.134, .095	.019, -.004	.086, -.049	.206, -.208	.022, -.006	.017, .002
1.900	.074, .056	.099, -.104	.138, .095	-.004, .001	.089, -.023	.227, -.144	.026, -.012	.020, .004
1.925	.076, .047	.095, -.095	.143, .095	-.024, .011	.088, -.007	.230, -.094	.031, -.018	.025, .005
1.950	.079, .035	.091, -.083	.149, .096	-.039, .025	.087, .005	.227, -.055	.036, -.024	.031, .009
1.975	.083, .020	.084, -.070	.156, .097	-.045, .045	.087, .015	.220, -.022	.043, -.028	.038, .014
2.000	.086, .002	.074, -.055	.165, .099	-.041, .067	.088, .024	.210, .006	.053, -.030	.046, .023
2.025	.085, -.020	.062, -.040	.176, .101	-.024, .089	.088, .034	.197, .031	.065, -.026	.055, .038
2.050	.077, -.044	.046, -.025	.187, .103	.005, .103	.087, .044	.182, .053	.078, -.017	.057, .066
2.075	.061, -.069	.026, -.011	.200, .105	.044, .104	.085, .054	.164, .070	.090, .001	.039, .100
2.100	.035, -.090	.003, -.001	.215, .107	.086, .095	.082, .066	.144, .083	.097, .028	-.006, .115

ECM	S11	P11	P13	D13	D15	F15	F17	G17
1.725	.215, .168	-.151, .006	.017, .032	-.016, -.002	.017, .033	.009, .010	-.004, -.000	0. ,0.
1.750	.190, .165	-.091, -.109	.039, .033	-.019, -.003	.009, .070	.008, .015	-.005, -.000	0. ,0.
1.775	.174, .155	-.000, -.133	.059, .024	-.023, -.005	-.016, .066	.003, .021	-.007, -.001	0. ,0.
1.800	.164, .141	.058, -.109	.074, .010	-.027, -.008	-.009, .045	-.008, .025	-.008, -.001	0. ,0.
1.825	.159, .123	.081, -.079	.083, -.005	-.032, -.011	.005, .030	-.025, .023	-.010, -.001	0. ,0.
1.850	.156, .102	.083, -.061	.088, -.017	-.038, -.017	.017, .017	-.045, .006	-.012, -.002	0. ,0.
1.875	.155, .079	.073, -.057	.091, -.025	-.045, -.026	.025, .006	-.053, -.029	-.015, -.003	0. ,0.
1.900	.154, .055	.055, -.062	.094, -.028	-.050, -.040	.032, -.005	-.033, -.068	-.019, -.004	0. ,0.
1.925	.151, .028	.028, -.067	.096, -.027	-.050, -.060	.037, -.014	.011, -.087	-.024, -.008	0. ,0.
1.950	.145, .001	-.005, -.061	.098, -.020	-.038, -.083	.042, -.020	.055, -.075	-.030, -.013	0. ,0.
1.975	.135, -.027	-.032, -.040	.098, -.009	-.011, -.099	.049, -.025	.080, -.046	-.037, -.025	0. ,0.
2.000	.120, -.054	-.039, -.006	.095, .006	.019, -.096	.056, -.027	.087, -.015	-.039, -.048	0. ,0.
2.025	.099, -.078	-.022, .019	.089, .023	.038, -.081	.065, -.024	.082, .008	-.015, -.075	0. ,0.
2.050	.072, -.098	.002, .017	.076, .040	.047, -.064	.075, -.017	.073, .025	.023, -.069	0. ,0.
2.075	.041, -.111	.006, .002	.057, .055	.049, -.050	.085, -.004	.063, .035	.037, -.046	0. ,0.
2.100	.005, -.116	-.004, .004	.034, .063	.048, -.040	.092, .016	.053, .041	.037, -.030	0. ,0.

XBL 713-478

Table XIV. Summary of Fits to Other Data

Fit	Starting from	Data	Number of Data Points	Time Per Iteration	Number of Iterations	χ^2/DF	Probability
AD	A1	Original Distributions	625	14.3 sec.	189	558.2/503	4%
CD	C1	Original Distributions	644	9.2 sec.	317	560.9/526	14%
CA	C4	All Coefficients in Fig. 15	1048	29.5 sec.	7	1582.6/967	---
EA	E1	All Coefficients in Fig. 15	1048	10.9 sec.	5.23	1357.7/957	---

DF - Degrees of Freedom (Note that Fit AD(CD) required 32(34) normalizations.)

Table XV. Channel Descriptions and "Reduced Branching Fractions." The fractions listed are the artificial α_i described in the text. The first six resonances correspond to those in Table XIV.

J^P	$1/2^-$	$1/2^-$	$3/2^-$	$3/2^+$	$1/2^-$	$1/2^+$
Masses	.938, 494	1.192, .140	1.383, .140	1.518, .140	1.115, .140	1.405, .140
D05	.20	.30	.50			
D15	.44	.06	.13	.15	.14	.08
F05	.64	.11	.25			
F15	.10	.20	.20	.20	.10	.20
F17	.20	.05	.15	.15	.30	.15
G07	.25	.05	.70			
D13	.05	.20	.15	.20	.20	.20
F05	.10	.30	.60			
P11	.10	.25	.15	.20	.10	.20
F15	.10	.20	.20	.20	.10	.20

Table XVI. Parameters for Resonances Already Classified in SU(3) Multiplets. Listed are the fitted averages for each series in Table XII. These were then averaged, in the sense described in text, and errors assigned. The parameters τ and $\gamma/2$ are artificial parameters for convenience of fitting.

WAVE		τ	E_R GEV	$\gamma/2$	AMP (E_R)	$\Gamma/2$ GEV
	A	-.122	1.833	.481	-.174	.049
	B	-.105	1.825	.460	-.152	.045
	C	-.096	1.826	.391	-.124	.038
D05	E	-.084	1.829	.365	-.121	.036
	G	-.093	1.840	.451	-.133	.044
	AVG	-.096	1.832	.441	-.138	.044
	ERR	±.013	±.005	±.040	±.018	±.005
	A	-.262	1.824	.455	-.242	.048
	B	-.290	1.821	.519	-.266	.054
	C	-.345	1.829	.590	-.319	.063
F05	E	-.284	1.821	.374	-.262	.039
	G	-.283	1.821	.535	-.262	.055
	AVG	-.290	1.823	.500	-.268	.052
	ERR	±.029	±.003	±.075	±.027	±.008
	A	.060	2.116	.602	.058	.095
	B	.097	2.081	.396	.096	.058
	C	.095	2.093	.553	.093	.085
G07	E	.166	2.086	.463	.163	.069
	G	.091	2.099	.417	.079	.063
	AVG	.090	2.092	.480	.096	.072
	ERR	±.037	±.012	±.072	±.037	±.013

WAVE		τ	E_R GEV	$\gamma/2$	AMP (E_R)	$\Gamma/2$ GEV
	A	.082	1.777	.810	.105	.077
	B	.065	1.750	.462	.084	.040
	C	.043	1.760	.405	.055	.036
D15	E	.075	1.775	.875	.096	.083
	G	.045	1.763	.318	.059	.029
	AVG	.058	1.765	.656	.074	.060
	ERR	±.014	±.009	±.195	±.017	±.019
	A	-.119	1.932	.661	-.145	.072
	B	-.123	1.912	.738	-.153	.076
	C	-.123	1.936	.748	-.150	.083
F15						
	G	-.089	1.918	.491	-.110	.051
	AVG	-.111	1.925	.684	-.137	.073
	ERR	±.012	±.008	±.090	±.015	±.011
	A	-.095	2.058	.448	-.119	.062
	B	-.062	2.017	.351	-.079	.044
	C	-.064	2.034	.362	-.081	.047
F17	E	-.072	2.022	.444	-.092	.056
	G	-.068	2.031	.461	-.087	.060
	AVG	-.069	2.034	.453	-.086	.059
	ERR	±.012	±.014	±.038	±.014	±.006

XBL 713-599

Table XVII. Parameters for Resonances not classified in SU(3) multiplets. Listed are the fitted averages for each series in Table XII. These were then averaged, in the sense described in text, and errors assigned. The parameters τ and $\gamma/2$ are artificial parameters for convenience of fitting.

WAVE	FIT	τ	E_R GEV	$\gamma/2$	AMP (E_R)	$\Gamma/2$ GEV
D13	C	-.094	1.990	.504	-.102	.090
	G	-.079	1.993	.668	-.086	.122
	AVG	-.086	1.985	.577	-.093	.104
	ERR	±.005	±.005	±.057	±.006	±.011
F05	B	.178	2.148	1.175	.170	.244
	C	.140	2.130	1.274	.134	.258
	AVG	.159	2.141	1.226	.152	.252
	ERR	±.013	±.006	±.035	±.013	±.005
P11	C	-.078	1.772	.305	-.108	.040
	G	-.059	1.864	2.895	-.078	.466
F15	B2	.091	2.057	3.025	.104	.453

Table XVIII. SU(3) Isoscalar Coefficients For Coupling to Octet-Octet Channel. These values are approximate; for exact values see Ref. 25. Baryon symbols specify Y,I as described in text.

N	8_d	8_f
$N\pi$	.67	.50
ΣK	-.67	.50

Δ	10
$N\pi$	-.71
ΣK	.71

Σ	8_d	8_f	10
NR	-.55	.41	-.41
$\Sigma\pi$	0.	.82	.41
$\Lambda\pi$	.45	0.	-.50

Λ	8_d	8_f	1
$N\bar{K}$	.32	.71	.50
$\Sigma\pi$	-.78	0.	.61

Table XIX. Data Used for Fits to SU(3) Coupling Constants. Reactions are indicated by N_R: 1 $N\pi \to N\pi$, 2 $N\bar{K} \to N\bar{K}$, 3 $N\bar{K} \to \Sigma\pi$, 4 $N\bar{K} \to \Lambda\pi$, 5 $N\pi \to \Sigma K$.

Multiplet	Mass Mev	Γ Mev	N_R	$\pm\sqrt{x_e x_r}$
D5	N(1670)	140. ± 35.	1	.420 ± .030
OCTET	Σ(1765)	120. ± 38.	2	.436 ± .018
			3	.074 ± .017
			4	-.250 ± .025
	Λ(1832)	88. ± 10.	2	.090 ± .010
			3	-.138 ± .018
F5	N(1688)	142 ± 37.	1	.620 ± .060
OCTET	Σ(1925)	146 ± 22.	2	.100 ± .030
			3	-.137 ± .015
			4	-.090 ± .020
	Λ(1823)	104. ± 16.	2	.639 ± .006
			3	-.268 ± .027
F7	Δ(1950)	190 ± 30.	1	.450 ± .060
DECUPLET			5	-.090 ± .020
	Σ(2034)	118 ± 12.	2	.200 ± .080
			3	-.086 ± .014
			4	.200 ± .020
G7	Λ(2092)	144. ± 26.	2	.290 ± .040
SINGLET			3	.096 ± .037

Table XX. SU(3) Coupling Constants From Fits to Data in Table XIX, assuming Glashow and Rosenfeld energy dependence with X = .35 and the nucleon mass as scale factor.

	g_d	g_f	g^2
D5	.88	-.14	
F5	.87	.52	
F7			.49
G7			.51

FIGURE CAPTIONS

Fig. 1. Schematic of secondary beam used for this experiment.

Fig. 2. One view of a typical Σ^- event.

Fig. 3. Comparison of non-Gaussian distributed fiducial quantities for Σ events and τ decays. The cuts applied for these quantities are indicated.

Fig. 4. Decay vertex fiducial volume.

Fig. 5. Differential lifetime distributions--numbers of events weighted only for decay angle losses. The time intervals for Σ^- (Σ^+) decays are .05 (.03) nsec.

Fig. 6. Decay angular distributions.

a. Azimuthal angle, ϕ, as described in text.

b. Cosine of center of mass angle, $c = \cos \delta^*$, as defined in text.

Fig. 7. Illustration of Lorentz transformation of the decay angle. The momenta in the rest frame, represented by a unit sphere, are carried into the lab frame, represented by an ellipsoid (e.g. vector OS to vector AL). Perpendicular components are unaltered, but the angle δ^* is transformed to the lab angle δ. For the case $R > 1$ (symbols defined in text), a cut in δ corresponds to two cuts in the center of mass cosine, $c_\pm$.

Fig. 8. Distribution of fitted beam momenta for both the τ decays and the Σ events. Numbers of events passing all cuts are shown per bin of .005 GeV/c.

Fig. 9. Cross sections from all available data for the reactions studied. See Fig. 15 caption for references to other experiments.

a. $K^-p \to \pi^+\Sigma^-$

b. $K^-p \to \pi^-\Sigma^+$

c. $K^-p \to \pi^+\Sigma^-\pi^o$

d. $K^-p \to \pi^-\Sigma^+\pi^o$

Fig. 10. Production angular distributions, showing sums of weighted events in the bin combinations. Widths of combinations are multiples of 0.1 in the production cosine, $\cos\theta = \hat{k}_K \cdot \hat{k}_\pi$.

a. $K^-p \to \pi^+\Sigma^-$

b. $K^-p \to \pi^-\Sigma^+$

Fig. 11. Polarizations for $K^-p \to \pi^-\Sigma^+$ in intervals of the production cosine, $\cos\theta$. The dashed curves show the functional representation calculated from the Legendre series expansions.

Fig. 12. Functional representation of the production angular distributions. The dashed curves are the Legendre series expansions in the production cosine, $\cos\theta$; the shaded histograms give weighted numbers of events per bin of 0.1.

a. $K^-p \to \pi^+\Sigma^-$

b. $K^-p \to \pi^-\Sigma^+$

Fig. 13. Dalitz plots and invariant mass-squared distributions. Dashed curves in plots indicate kinematically imposed boundaries for each of the energies, E, included in the plot. Dashed curves over histograms indicate the average shape that would result from completely isotropic distribution of the final state momenta. The histograms are of weighted events per bin of

Fig. 13 (cont.)

0.04 GeV^2. The quantities m_o^2, $m_\pm^2$ are defined in text. Note that the histograms are not correctly aligned with the scatter plots: the tick marks should be one bin lower in mass-squared.

a. $K^-p \to \pi^+\Sigma^-\pi^o$

b. $K^-p \to \pi^-\Sigma^+\pi^o$. The Dalitz plots include events from both $\Sigma^+ \to \pi^o p$ and $\Sigma^+ \to \pi^+ n$; the invariant mass-squared distributions include only events from $\Sigma^+ \to \pi^+ n$.

Fig. 14. Argand diagrams for selected partial wave fits to $K^-p \to \pi^\pm\Sigma^\mp$ reactions. The labels for the fits correspond to those in Tables XII and XIV. The waves are labeled by L, I, 2J (where S, P, D, F, G stand for L = 0, 1, 2, 3, 4 respectively). For each separate value of J, the I = 0 waves have dotted curves, the I = 1 waves have solid curves. The symbols, plotted at energies starting from 1.725 GeV and separated by .025 GeV, distinguish parity states: the symbol + for P = -1 and the symbol X for P = +1.

Fig. 15. Legendre coefficients predicted by the three fits with highest probability--fits A, B, C are A1, B2, C1 of Table XII, respectively. All data available for these reactions are superimposed. The references to other experiments are: Ref. 2b for LRL 1 (these data were included in the analysis); Ref. 1b for CHS; Ref. 3 for LRL 2; and Ref. 4 for CRS.

a. $K^-p \to \pi^+\Sigma^-$ Legendre series coefficients.

b. $K^-p \to \pi^+\Sigma^-$ associated Legendre series coefficients. No data are available here since the Σ^- polarization is not observed.

Fig. 15 (cont.)

c. $K^-p \to \pi^-\Sigma^+$ Legendre series coefficients.

d. $K^-p \to \pi^-\Sigma^+$ associated Legendre series coefficients.

Fig. 16. Comparison of partial waves using P and B parameterizations.

a. Waves resulting from prefit E0 using the P parameterization.

b. Waves resulting from prefit F0 using the B parameterization.

Fig. 17. Average χ^2 contribution from all coefficients at each energy in the fits to all the data in Fig. 15. The fit CA varied little from C4; the fit EA better accommodated the data not included in the original fit. See Fig. 15 caption for references to other experiments.

Fig. 18. Values of χ^2 for fits to SU(3) coupling constants for each multiplet. Three types of energy dependence were tried: the Blatt and Weisskopf form (BW) and an interaction radius of 1. Fermi; the Glashow and Rosenfeld form (GR) with different values of the form factor parameter X; and the "no denominator" form (ND).

$$\frac{k^{2\ell+1}}{E}$$

Fig. 19. SU(3) coupling constants calculated from the amplitudes for individual reactions assuming the GR energy dependence with X = .35. The coupling constants are dimensionless; the scale factor was the nucleon mass. Elastic reactions are indicated only be the final state channel.

a. D5 Octet

Fig. 19 (cont.)

b. F5 Octet

c. F7 Decuplet

d. G7 Singlet

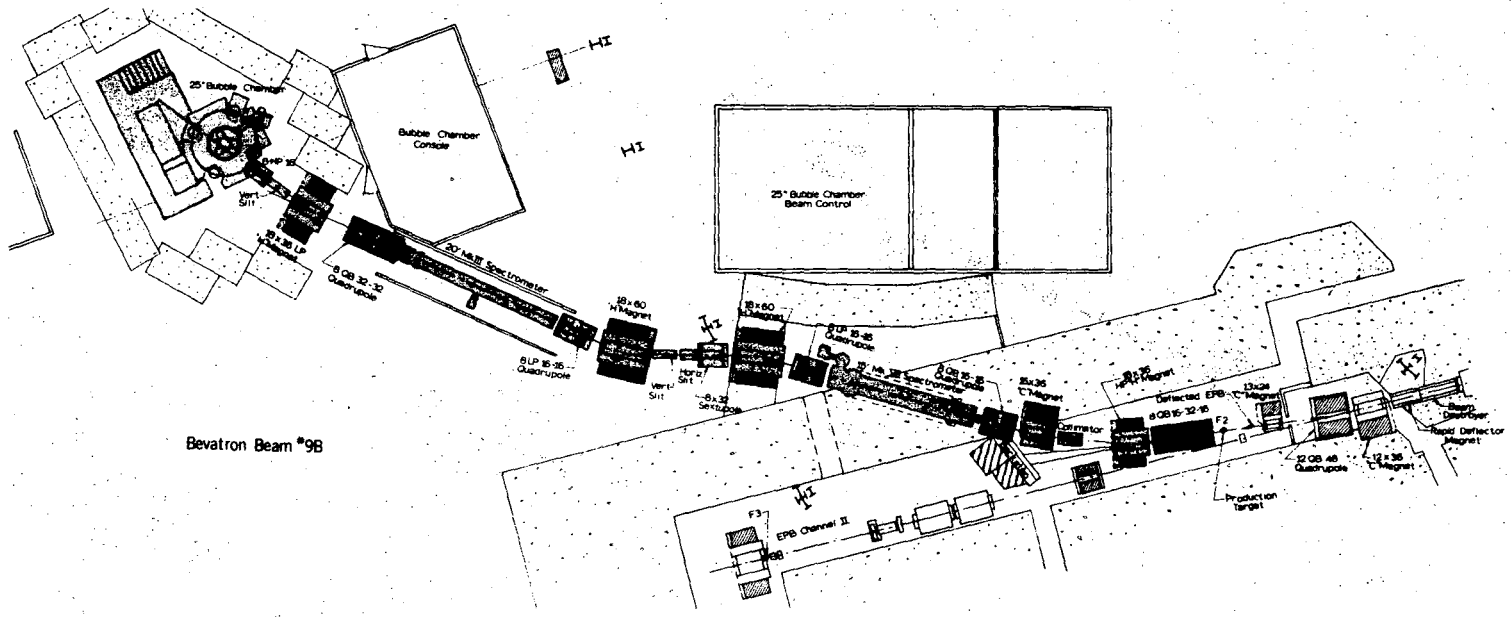
25" Bubble Chamber
Bubble Chamber Console
25" Bubble Chamber Beam Control
Vert Slit
Horiz Slit
Vert Slit
Horiz Slit
Collimator
Deflected EPB
Production Target
EPB Channel II
Beam Dump
Rapid Deflector Magnet
Bevatron Beam #9B
XBL 6712-6265

Fig. 1

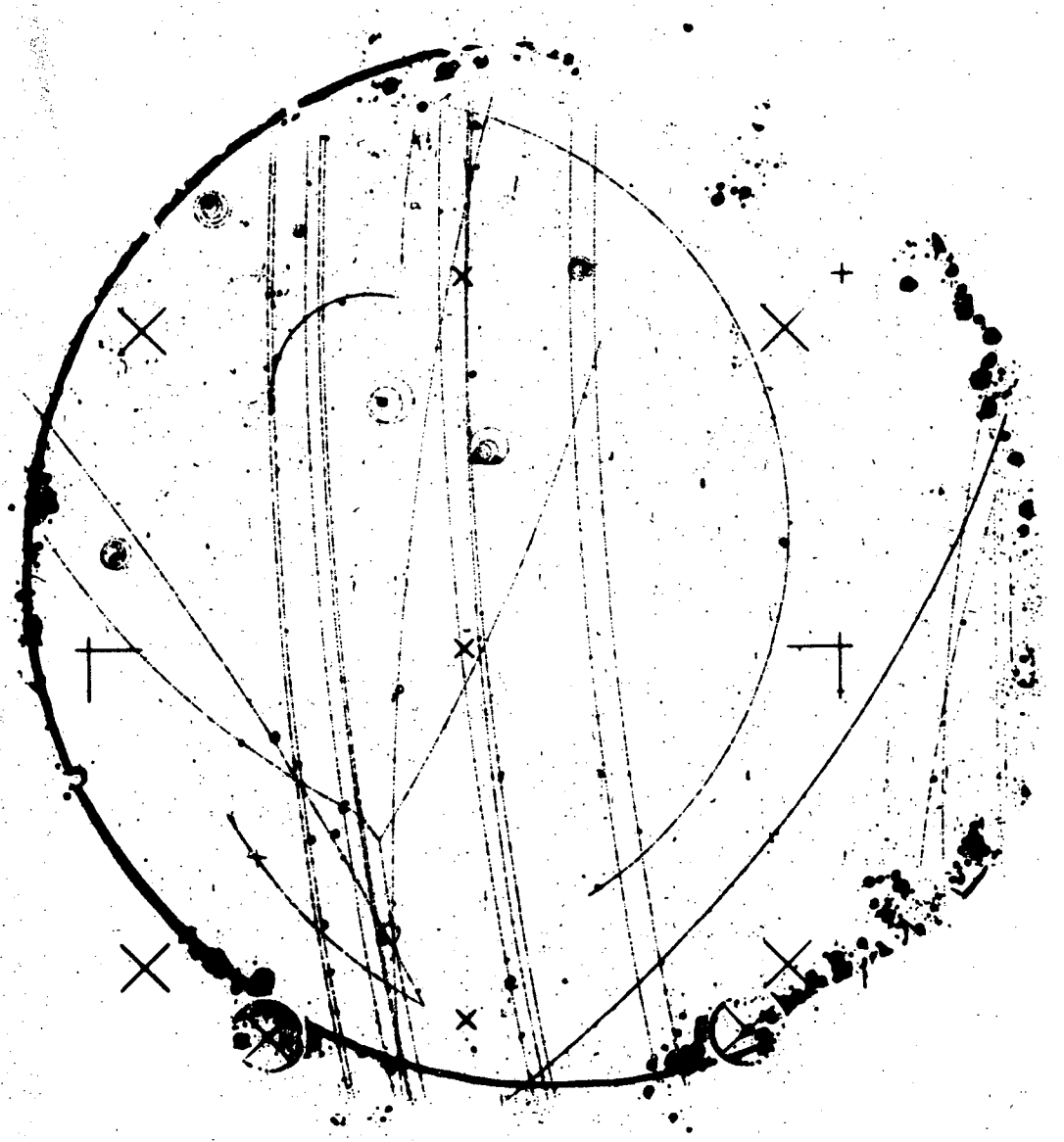

Fig. 2

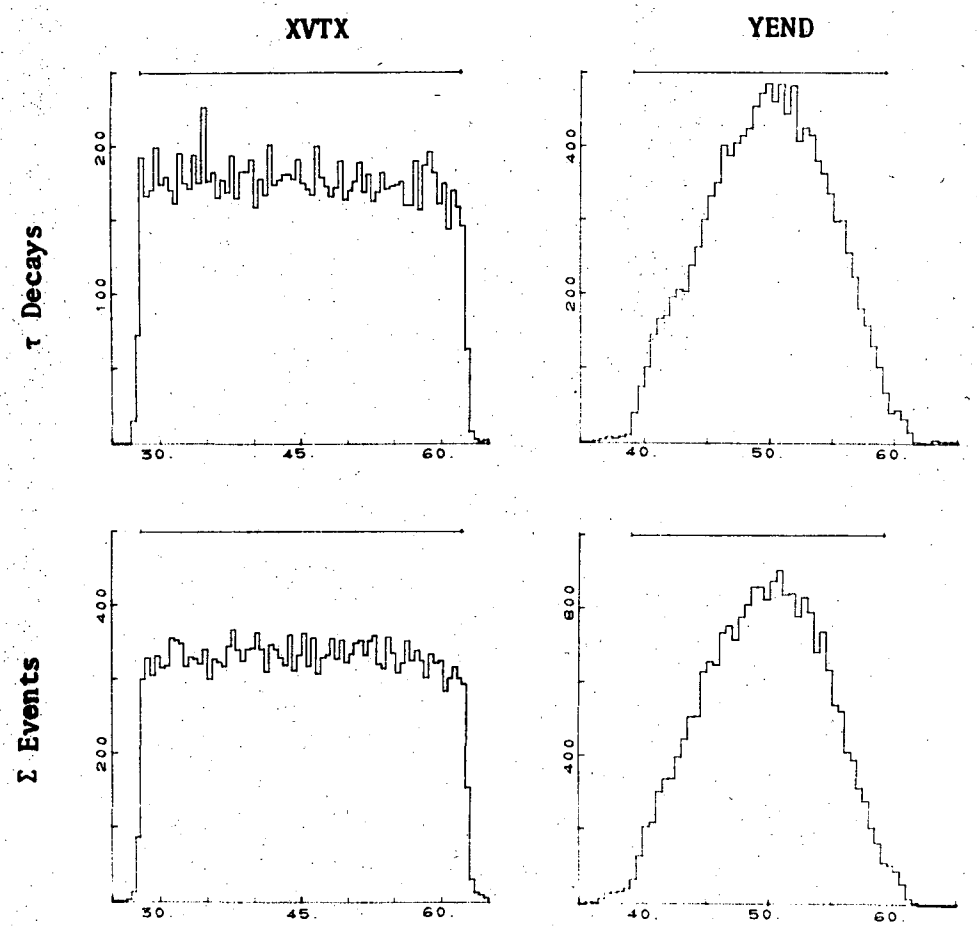

Fig. 3

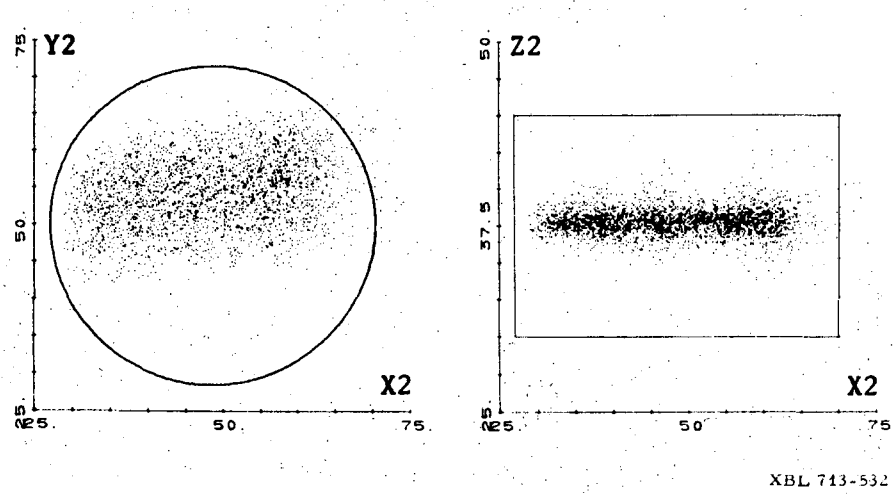

XBL 713-532

Fig. 4

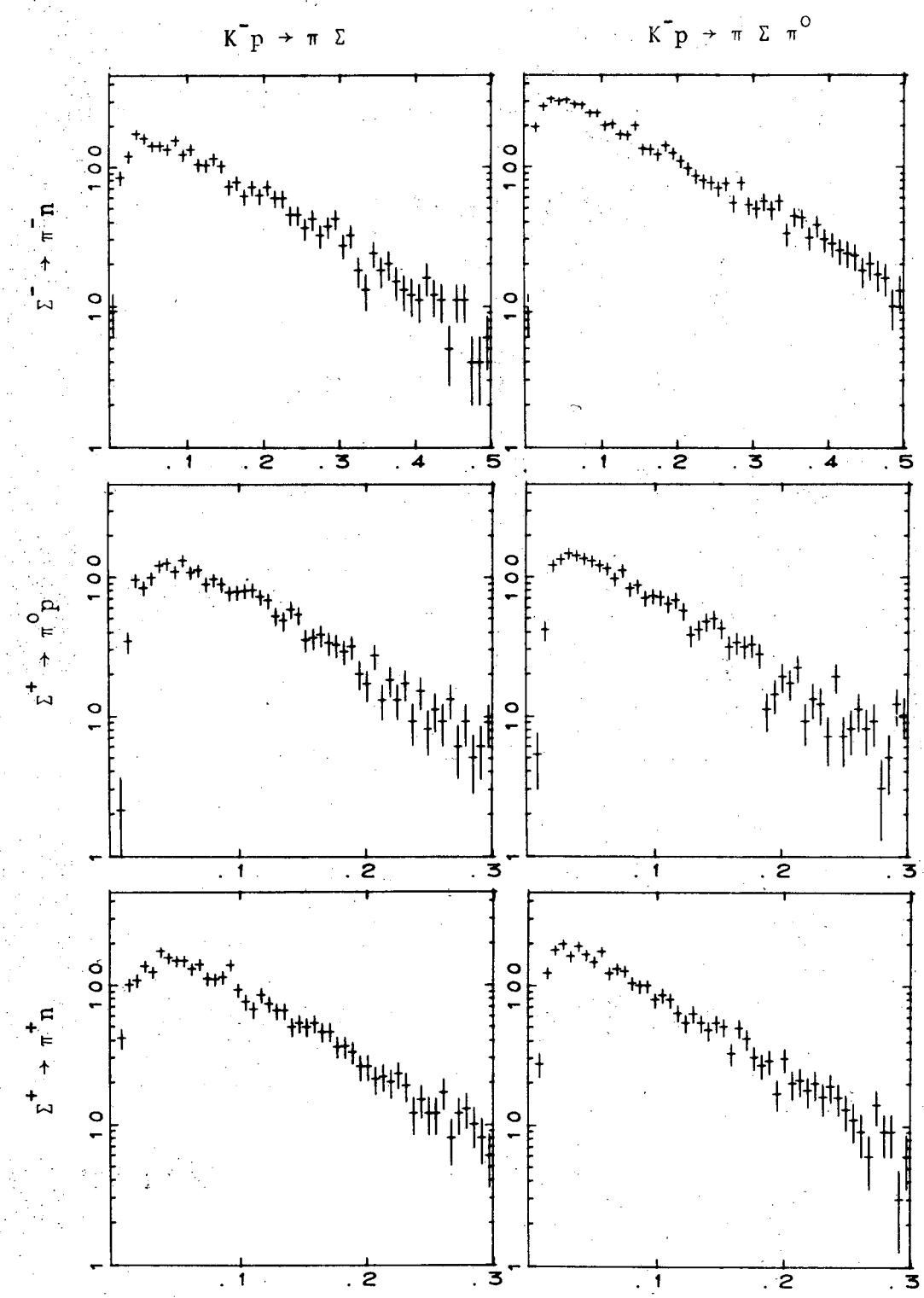

XBL 713-502

Fig. 5

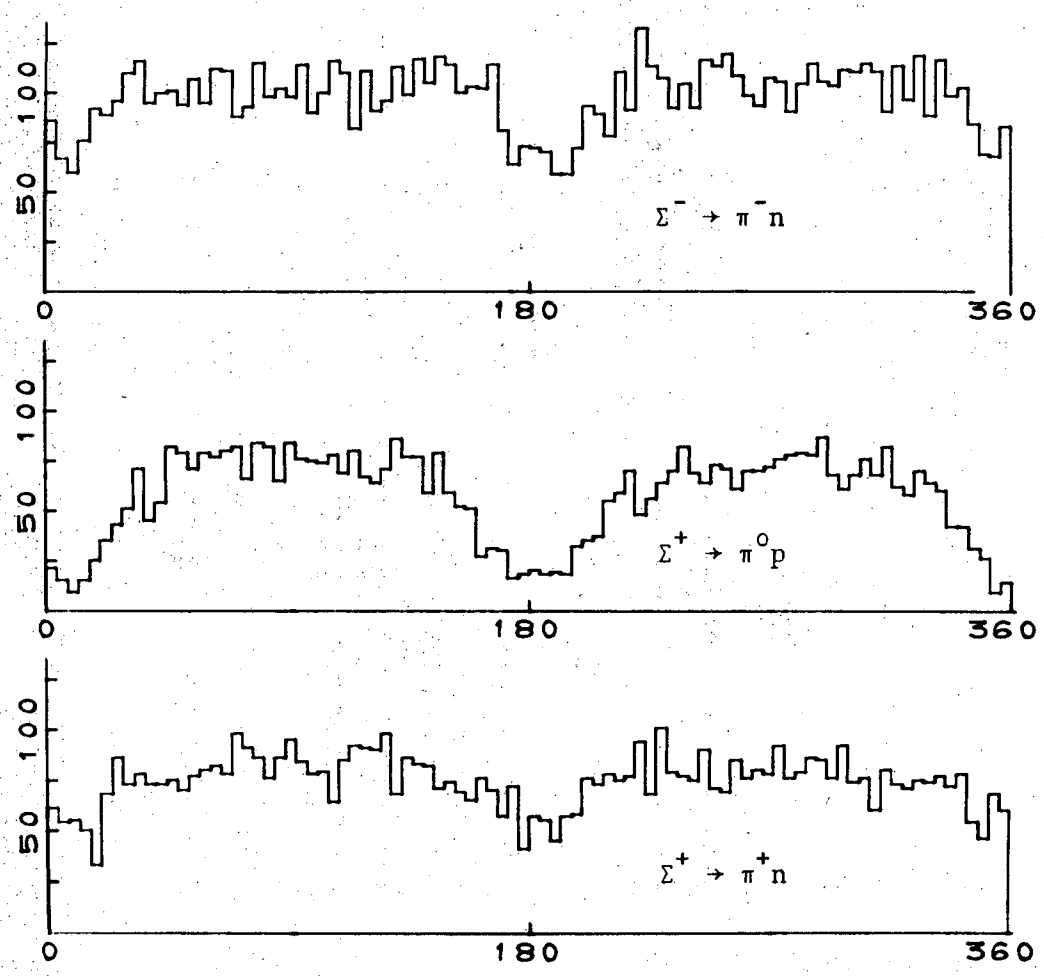

Fig. 6a

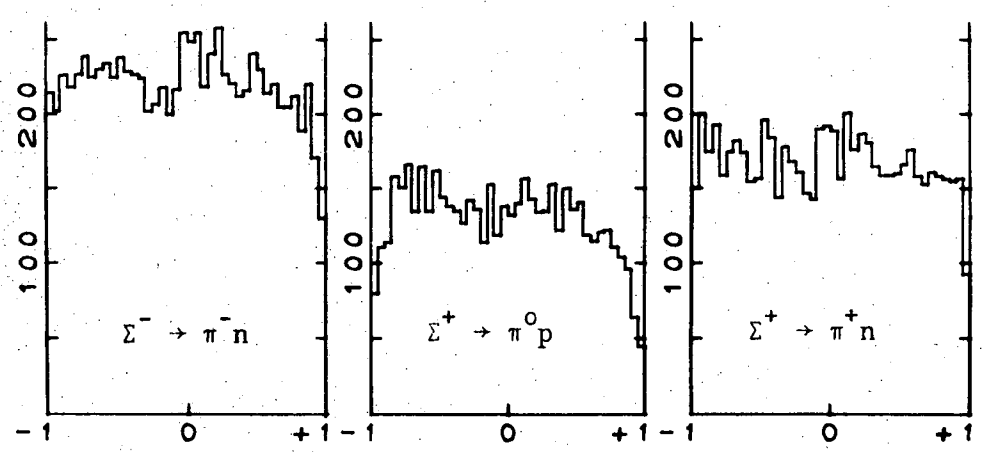

XBL 713-488

Fig. 6b

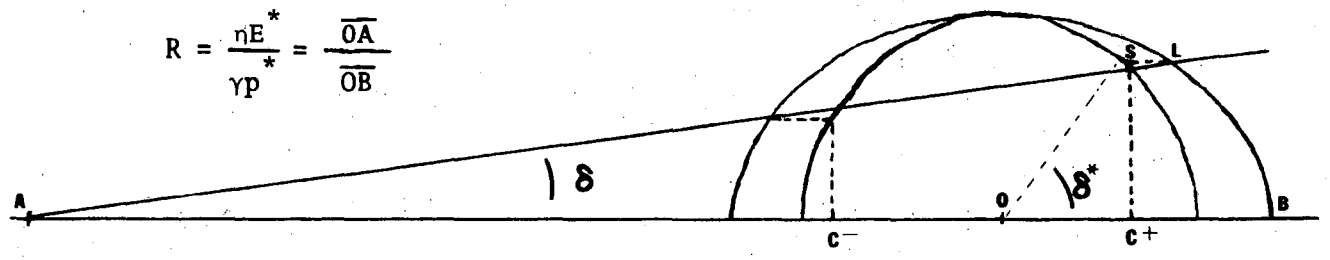

XBL 713-601

Fig. 7

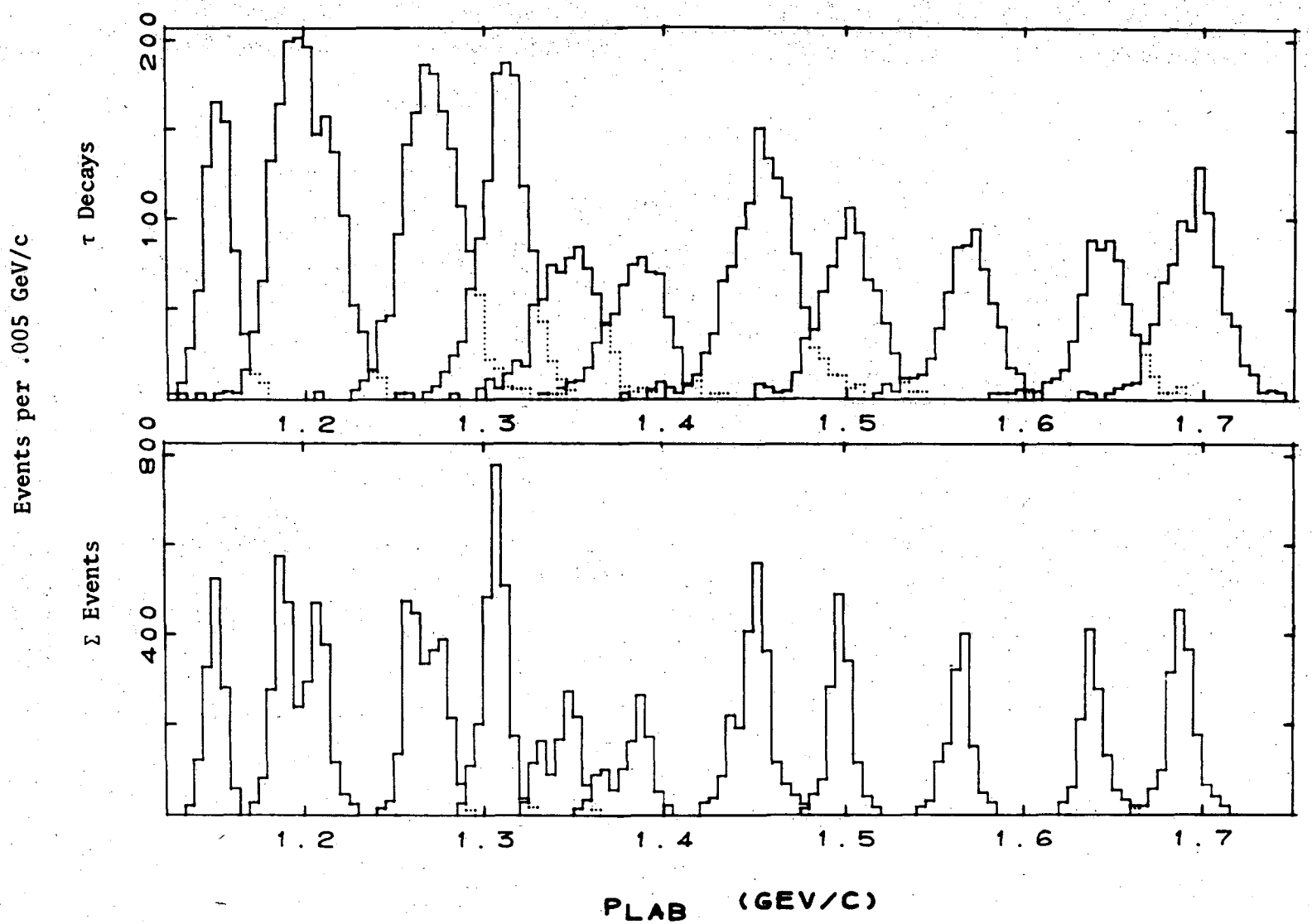

XBL 713-487

Fig. 8

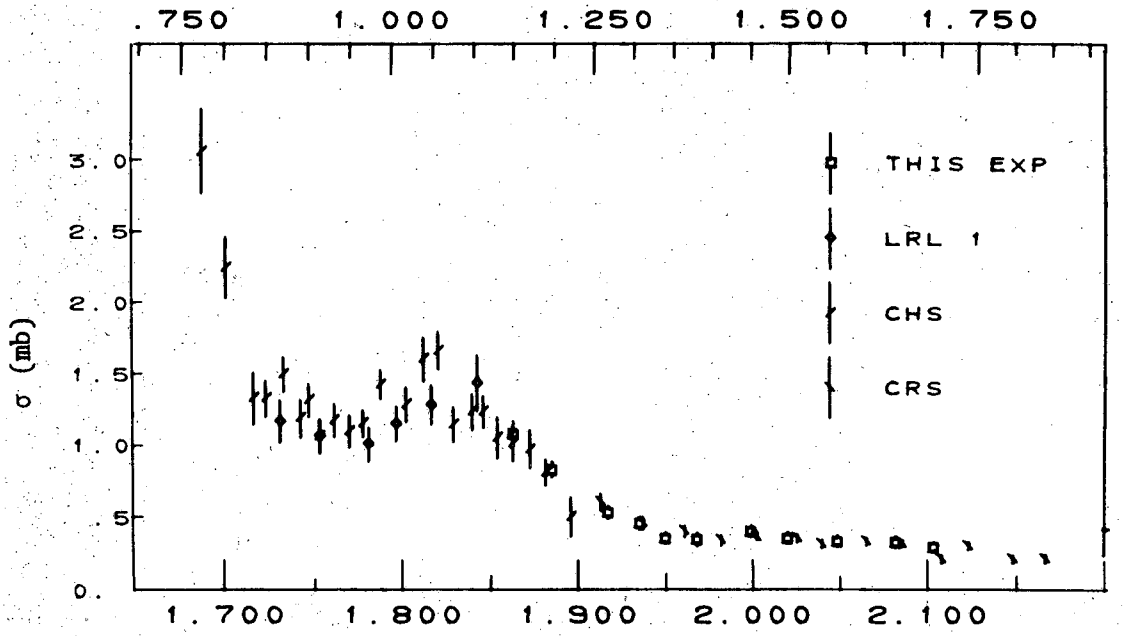

Fig. 9a. $K^-p \to \pi^+\Sigma^-$

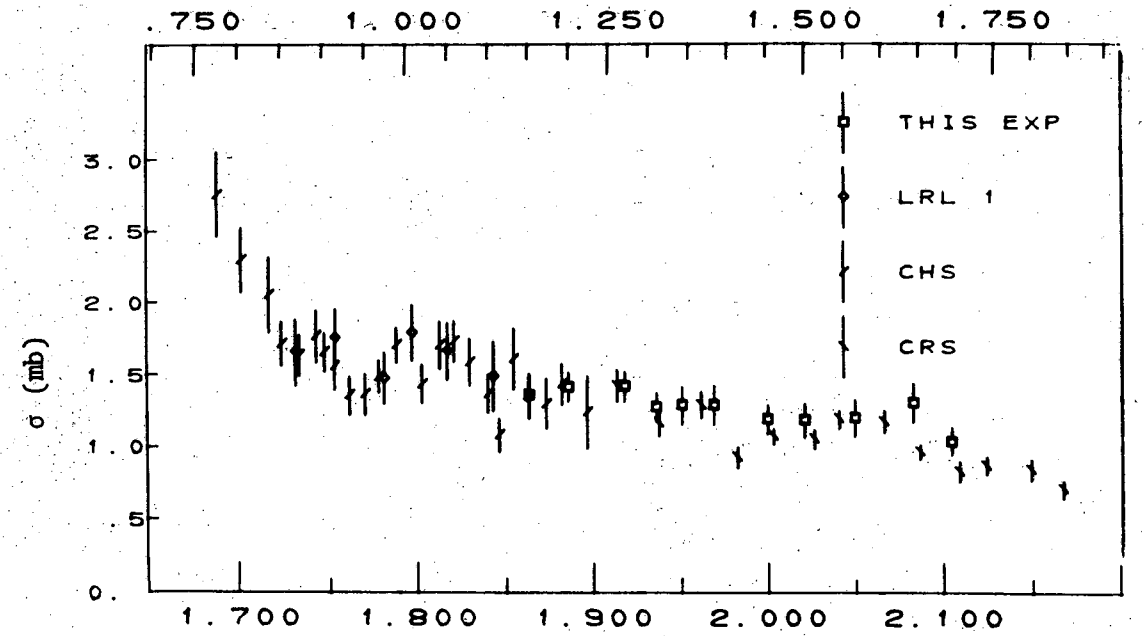

XBL 713-489

Fig. 9b. $K^-p \to \pi^-\Sigma^+$

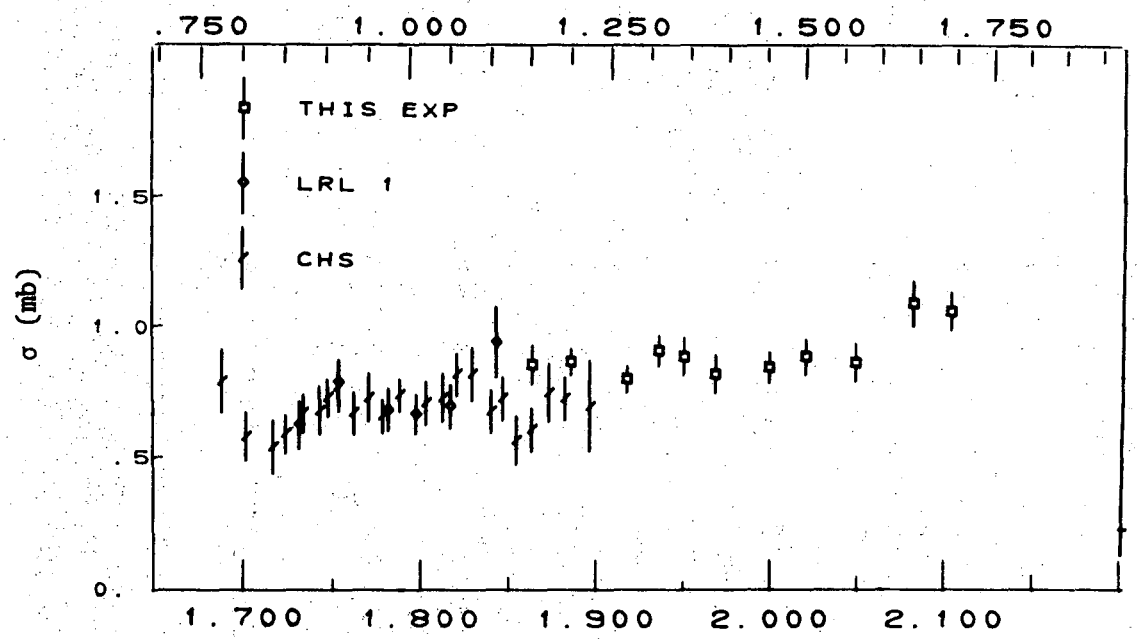

Fig. 9c. $K^-p \rightarrow \pi^+\Sigma^-\pi^0$

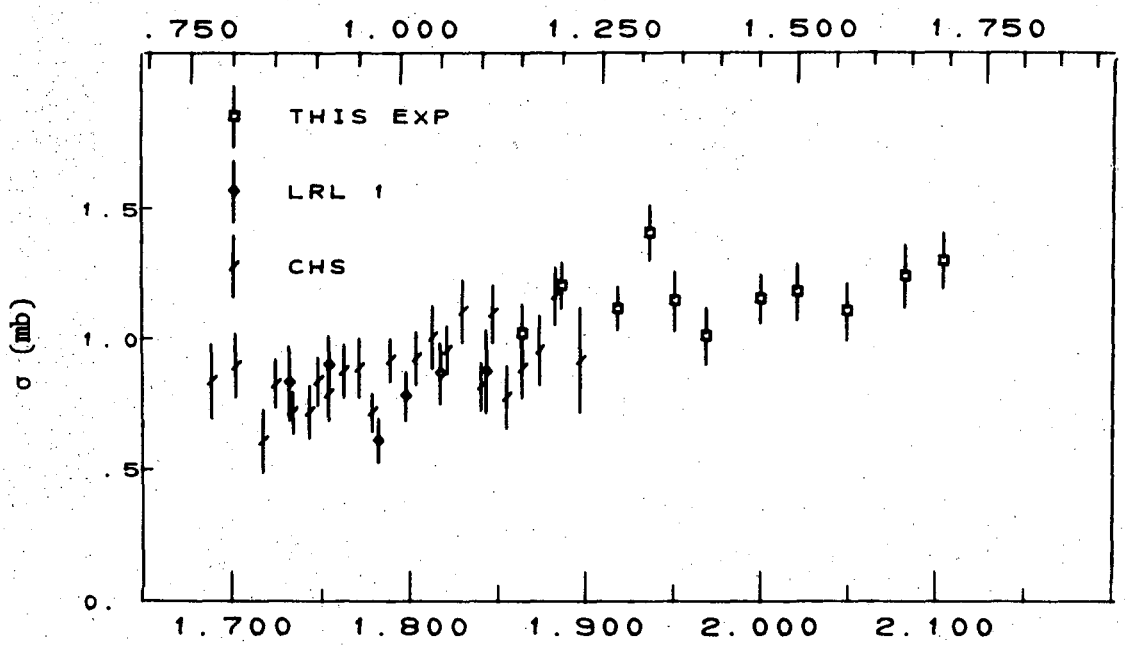

XBL 713-490

Fig. 9d. $K^-p \rightarrow \pi^-\Sigma^+\pi^0$

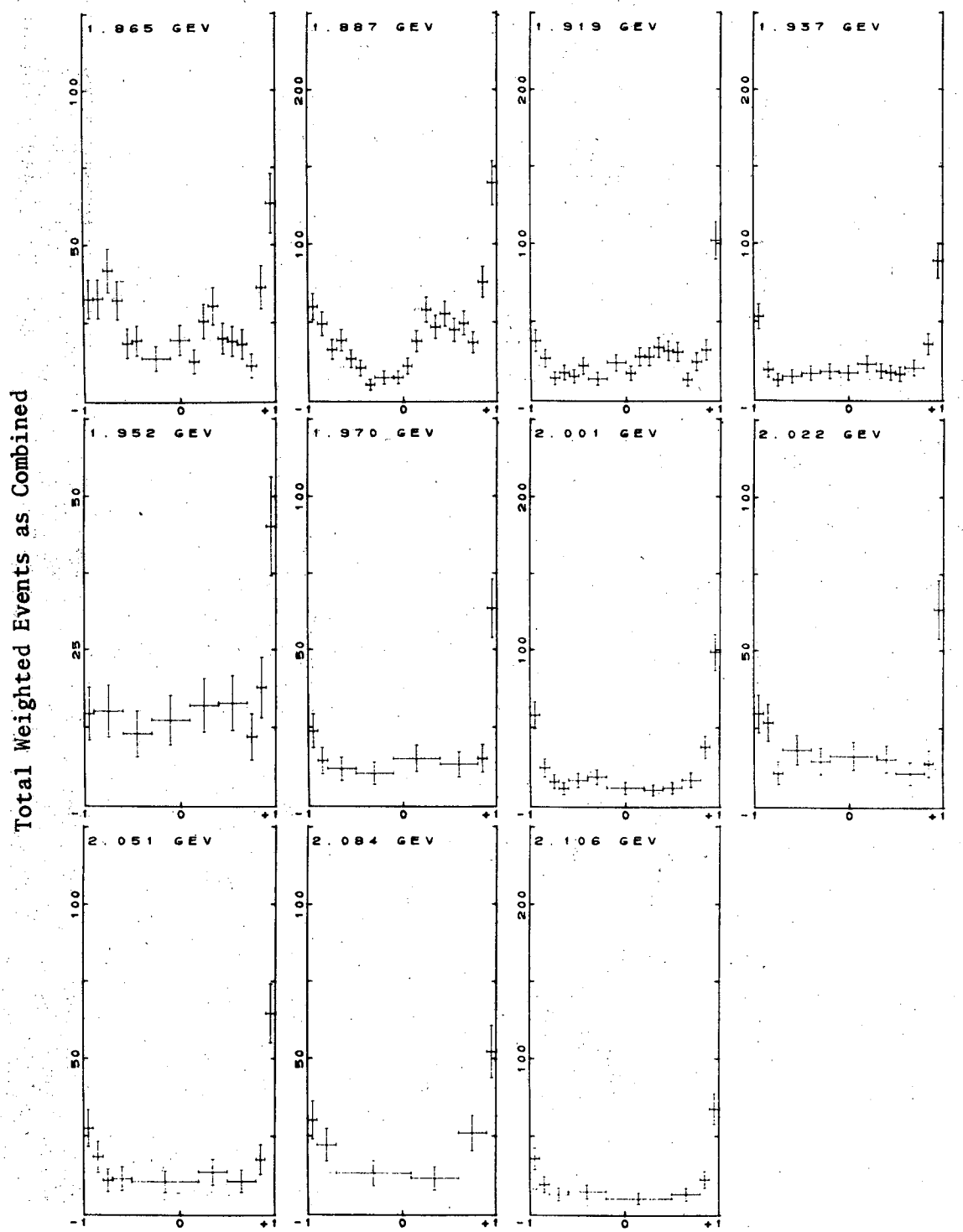

XBL 713-492

Fig. 10a. $K^-p \rightarrow \pi^+\Sigma^-$

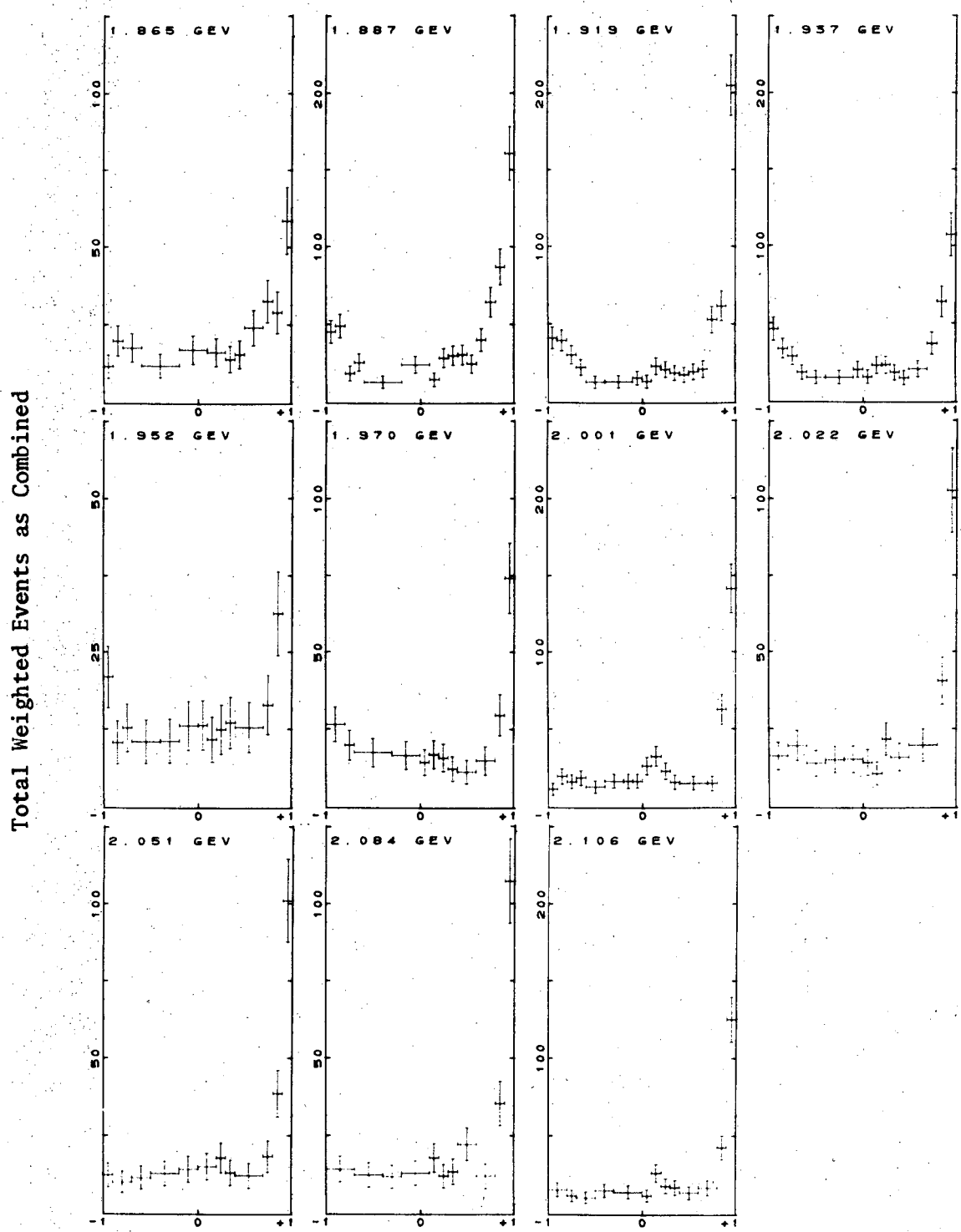

XBL 713-494

Fig. 10b. $K^-p \rightarrow \pi^-\Sigma^+$

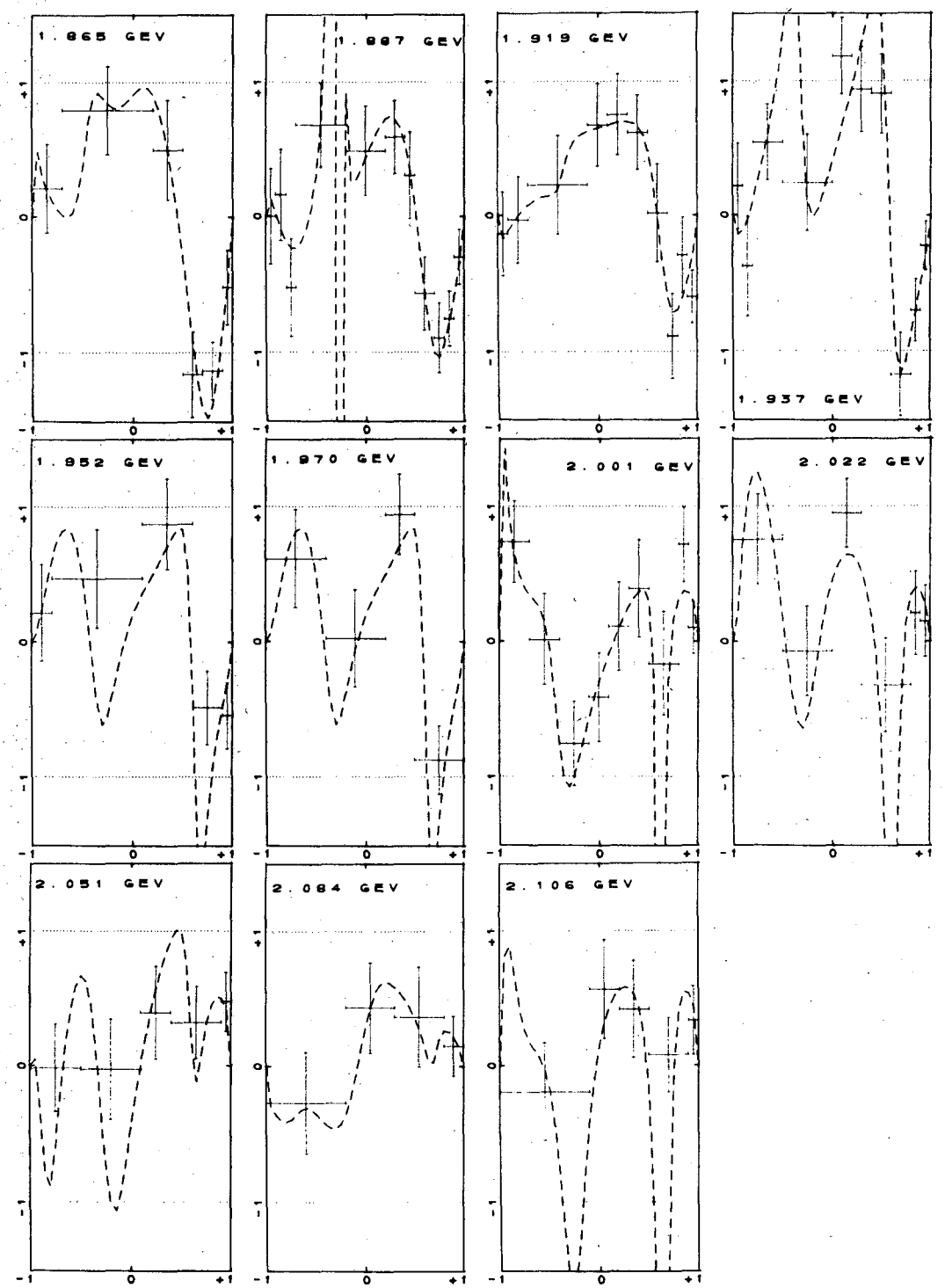

XBL 713-495

Fig. 11. $K^-p \rightarrow \pi^-\Sigma^+$

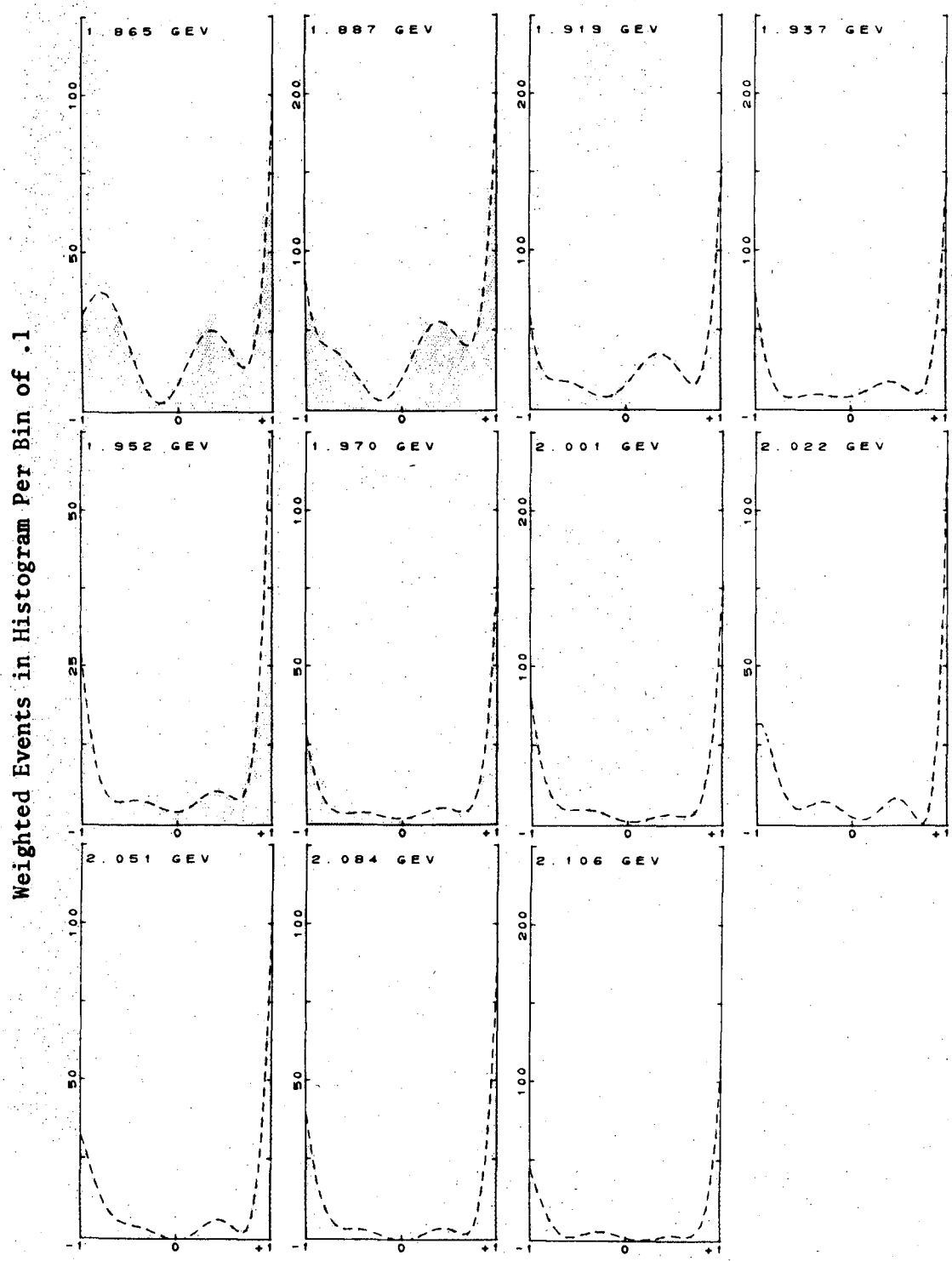

XBL 713-491

Fig. 12a. $K^-p \rightarrow \pi^+\Sigma^-$

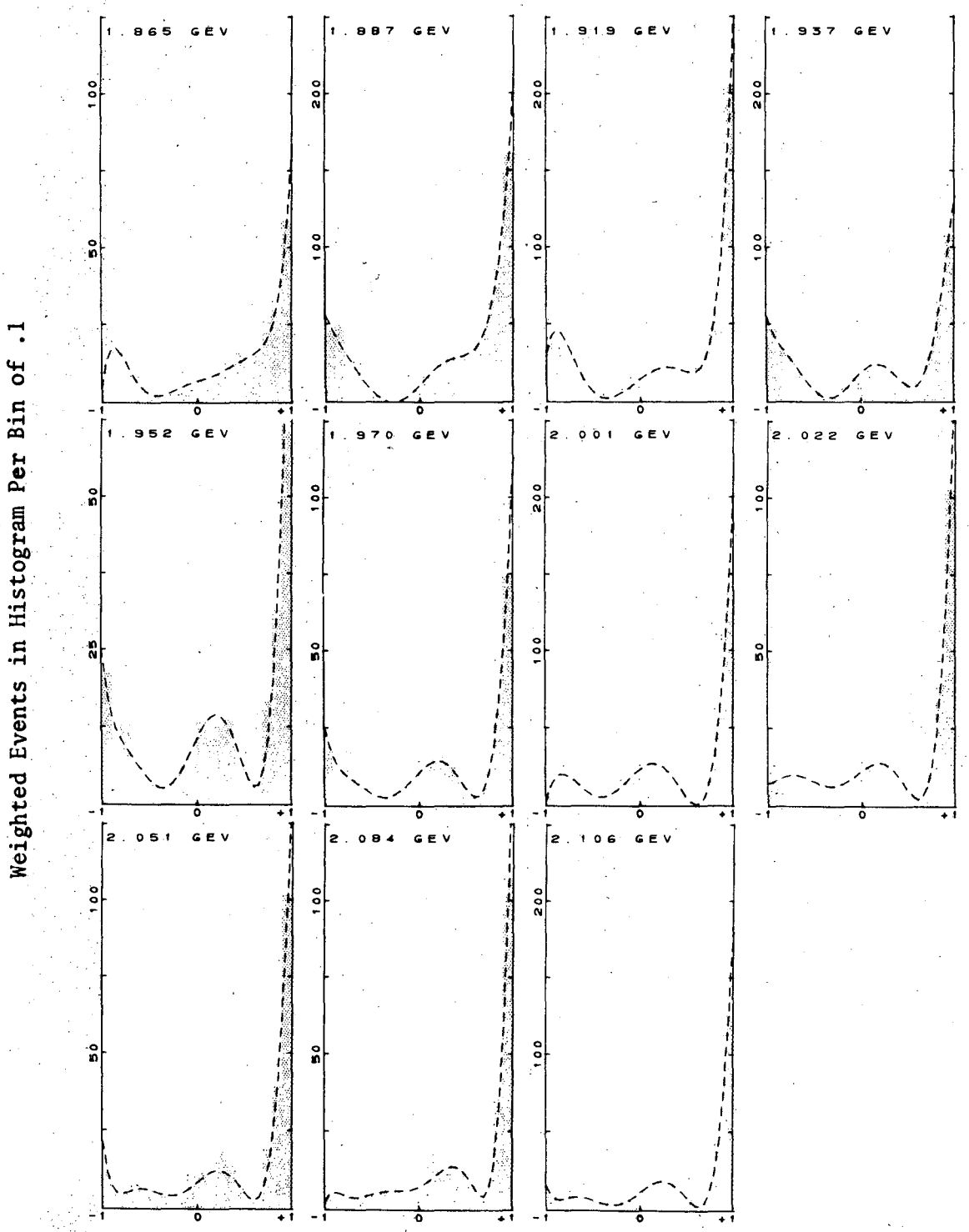

XBL 713-493

Fig. 12b. $K^-p \rightarrow \pi^-\Sigma^+$

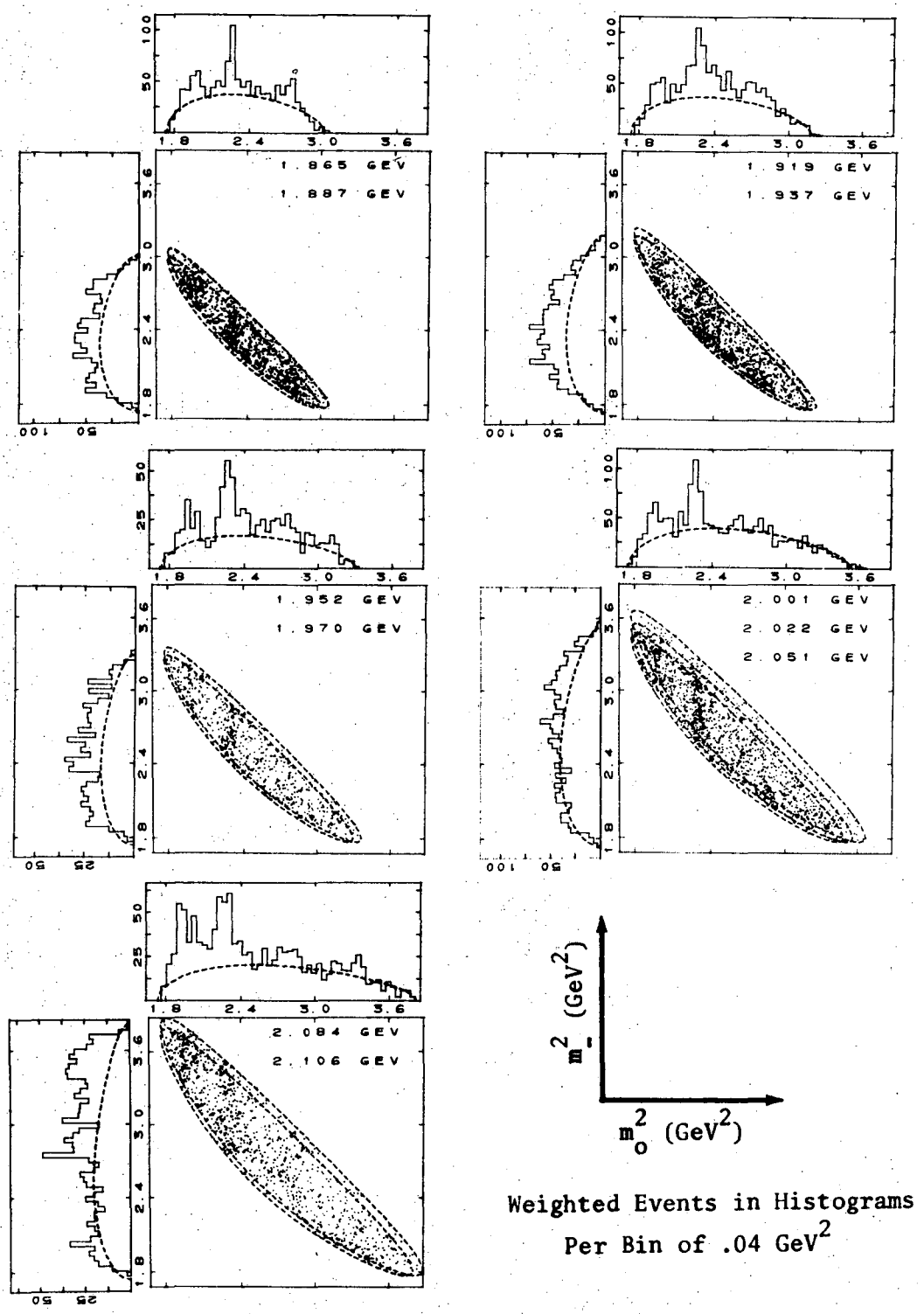

Fig. 13a. $K^-p \to \pi^+\Sigma^-\pi^0$

XBL 713-496

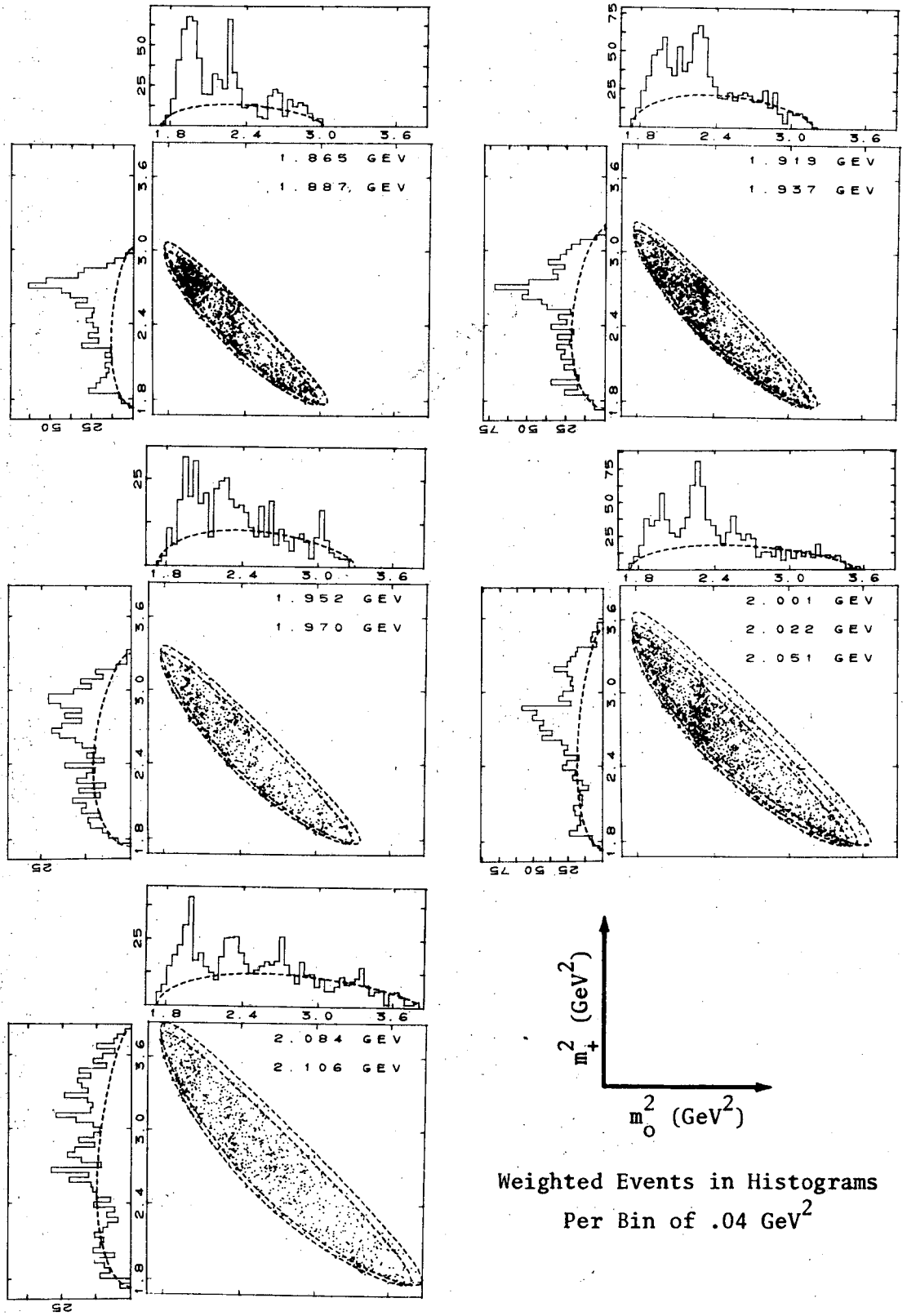

Fig. 13b. $K^- p \rightarrow \pi^- \Sigma^+ \pi^0$

XBL 713-497

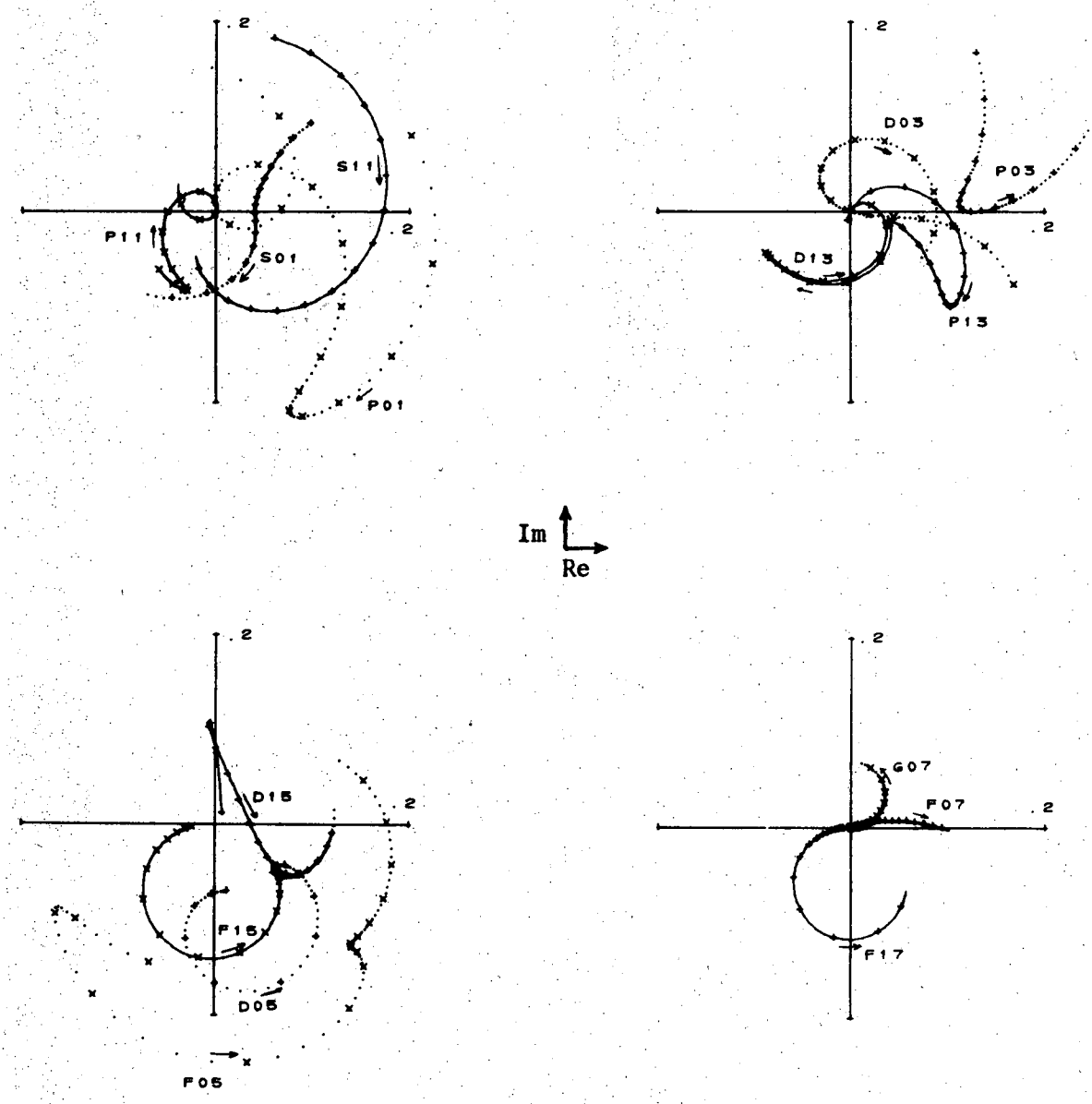

XBL 713-525

Fig. 14-A1

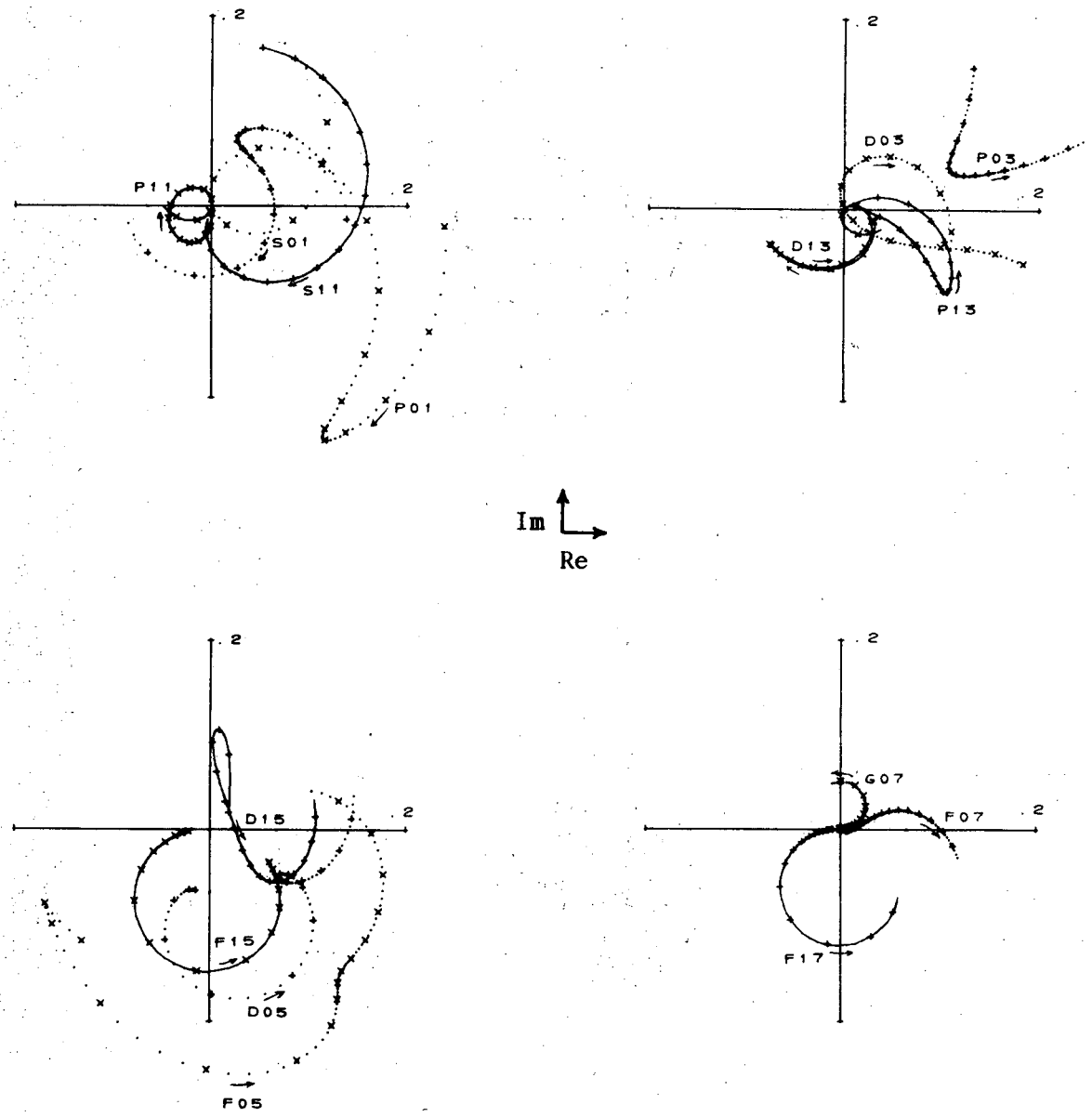

XBL 713-526

Fig. 14-AD

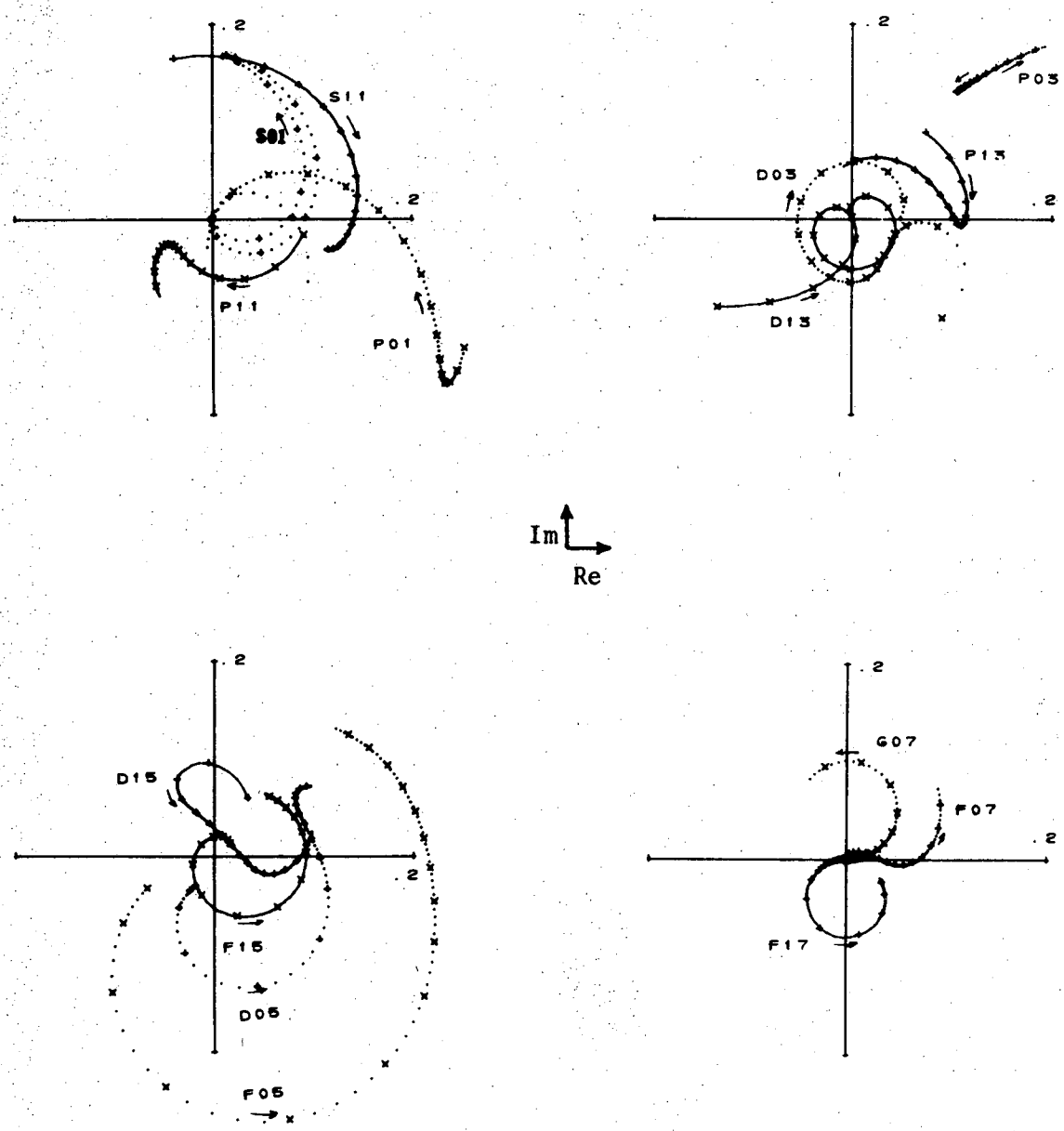

XBL 713-527

Fig. 14-B2

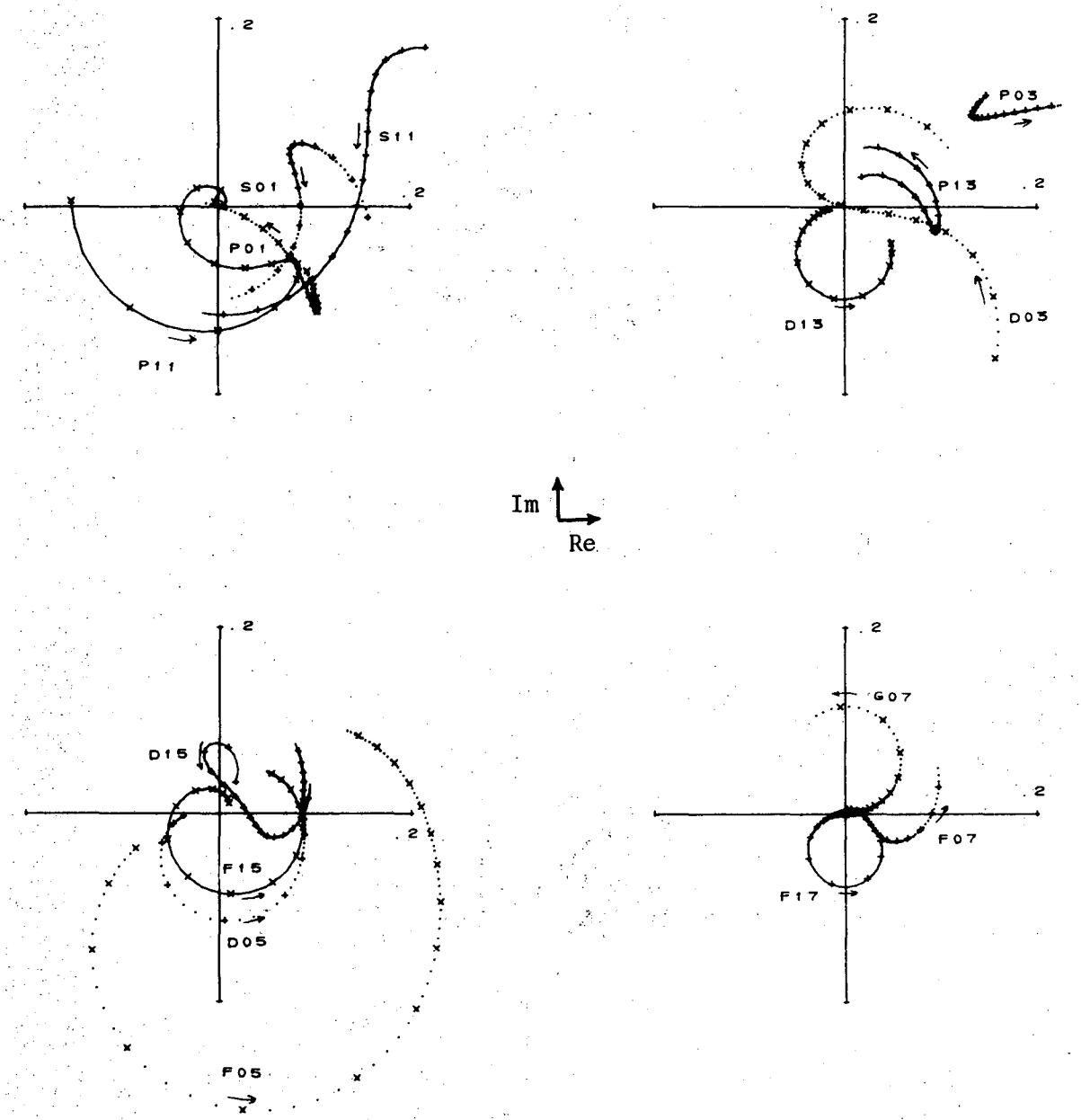

XBL 713-528

Fig. 14-C1

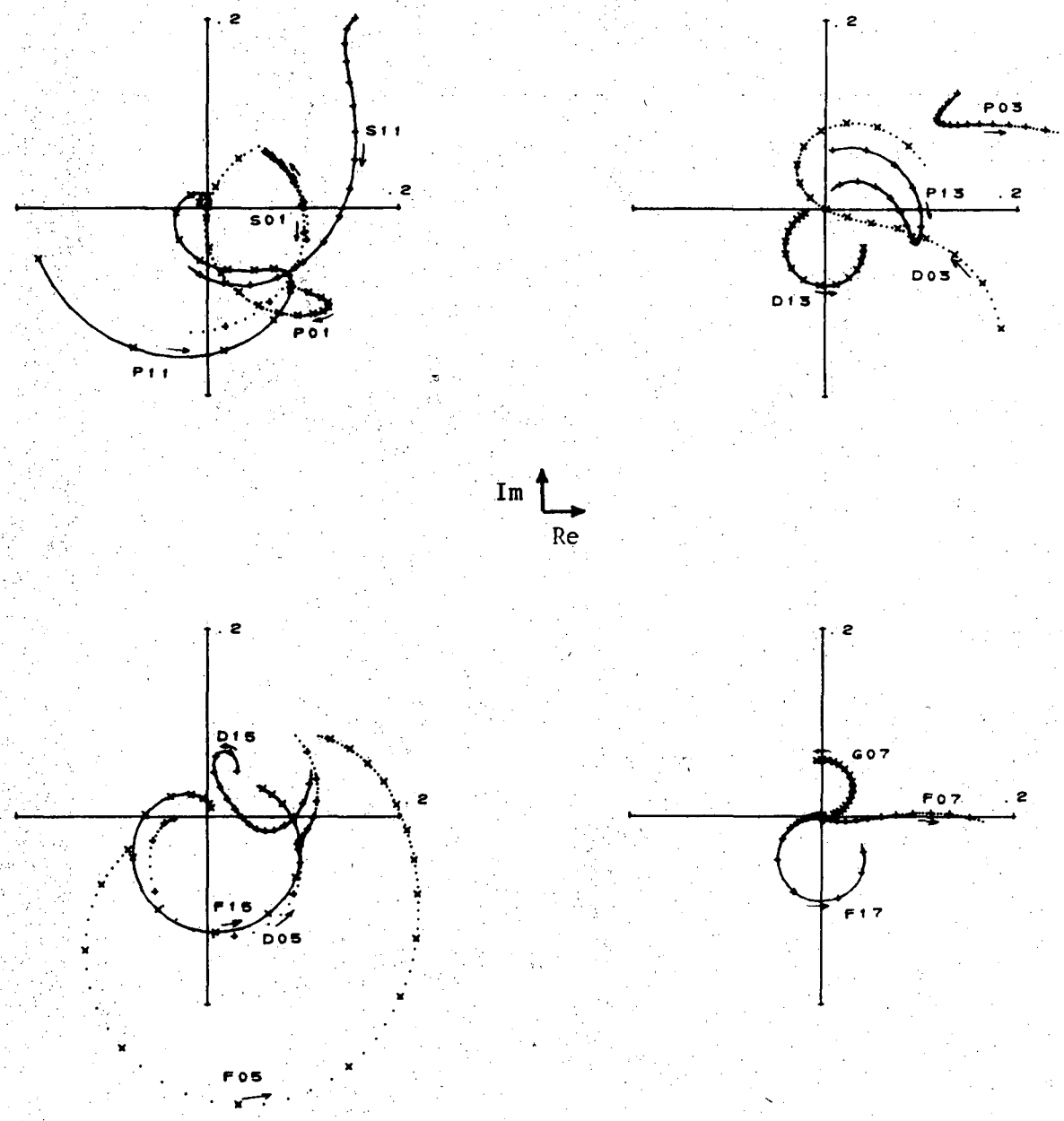

XBL 713-529

Fig. 14-CD

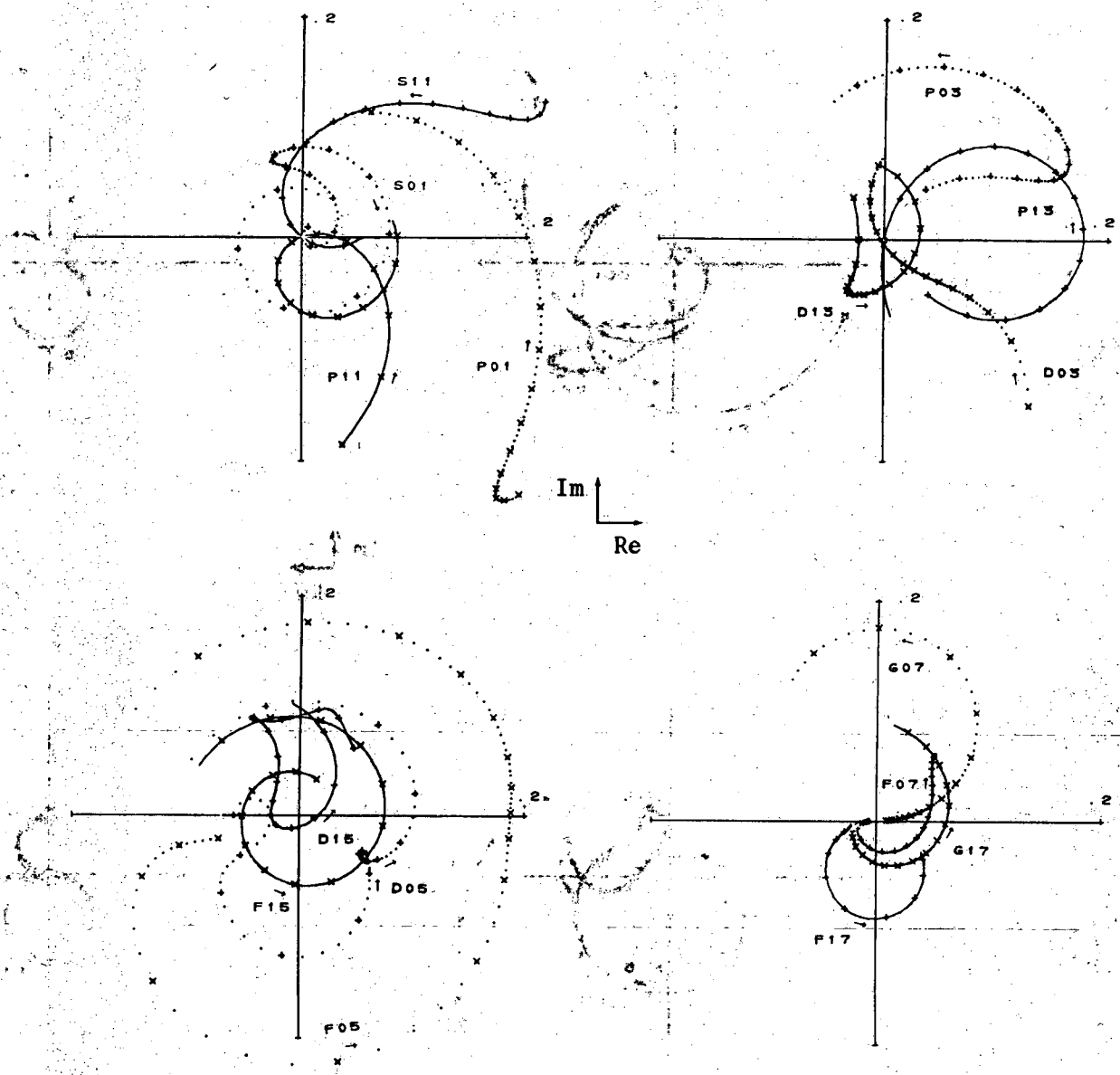

XBL 713-597

Fig. 14-E1

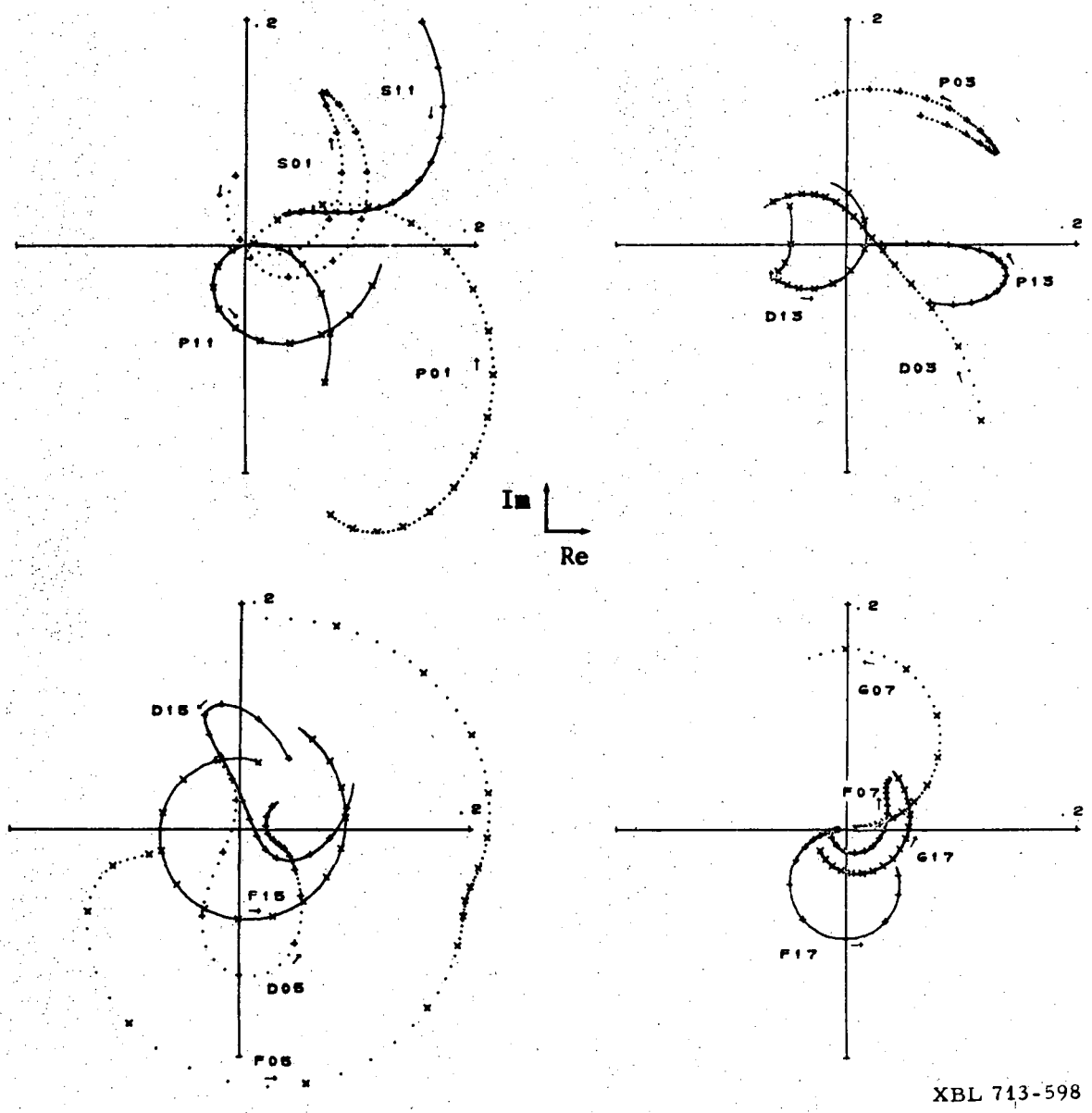

XBL 713-598

Fig. 14-EA

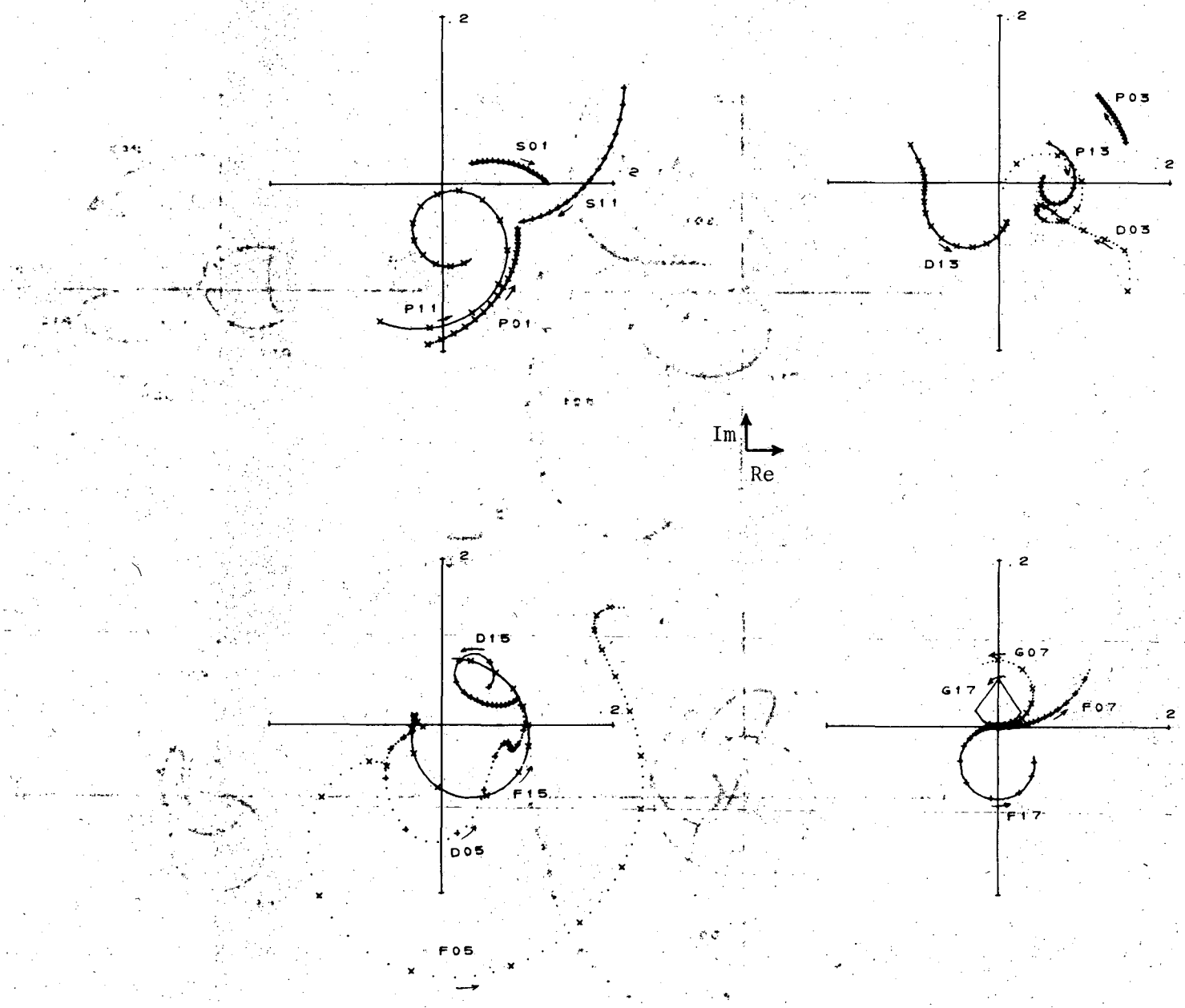

XBL 713-530

Fig. 14-G1

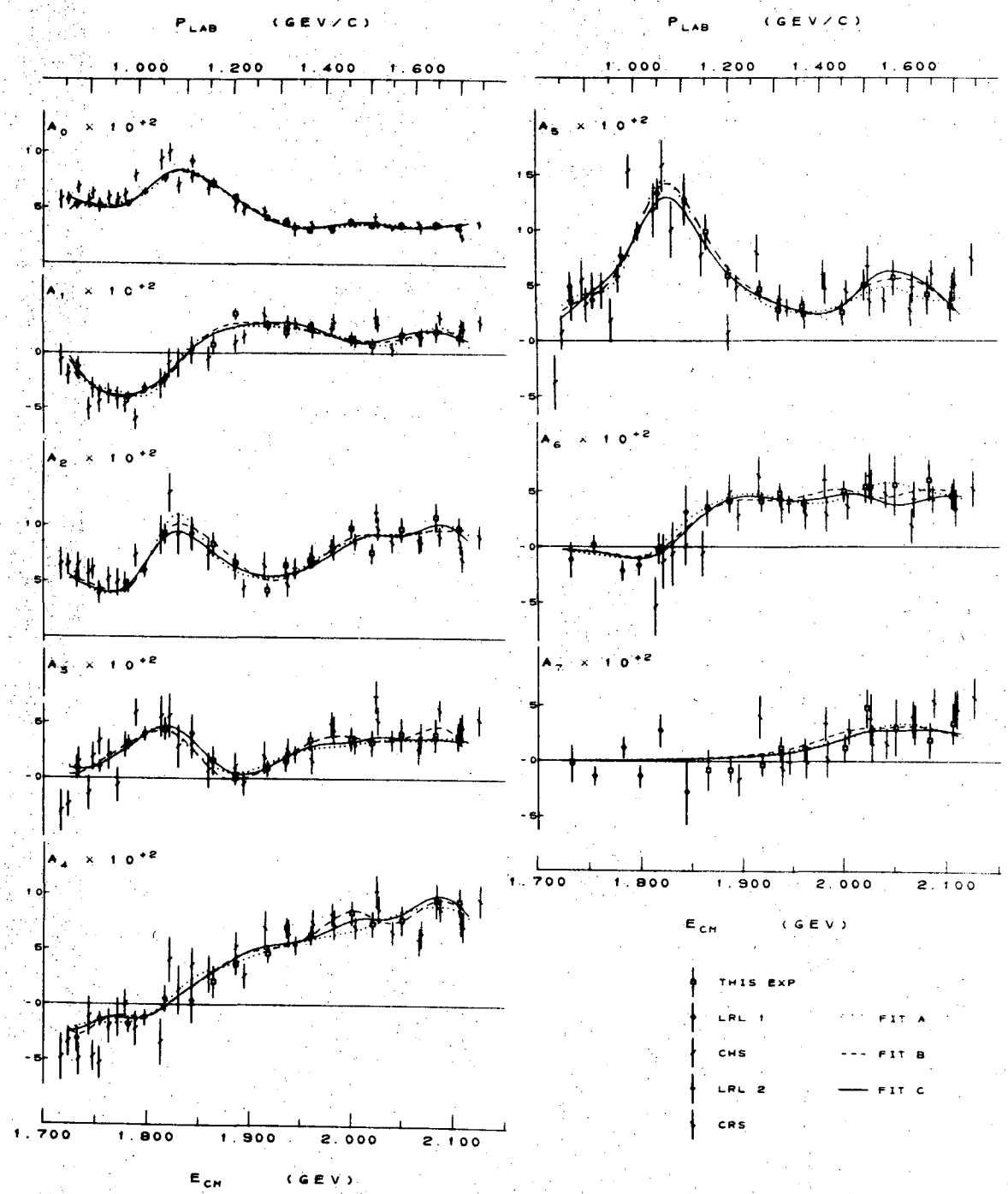

XBL 713-501

Fig. 15a. $K^-p \rightarrow \pi^+\Sigma^-$

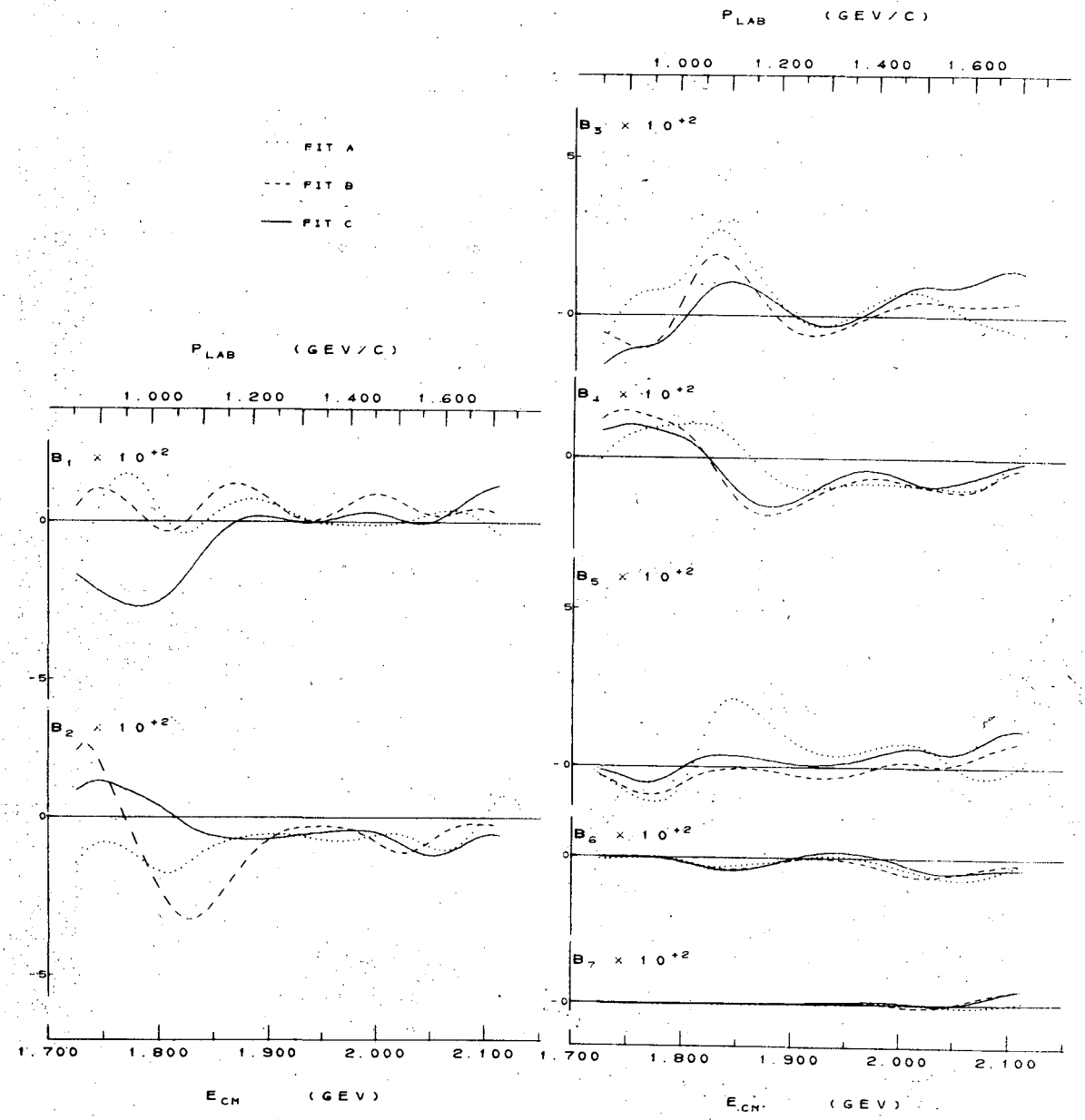

XBL 713-500

Fig. 15b. $K^-p \rightarrow \pi^+\Sigma^-$

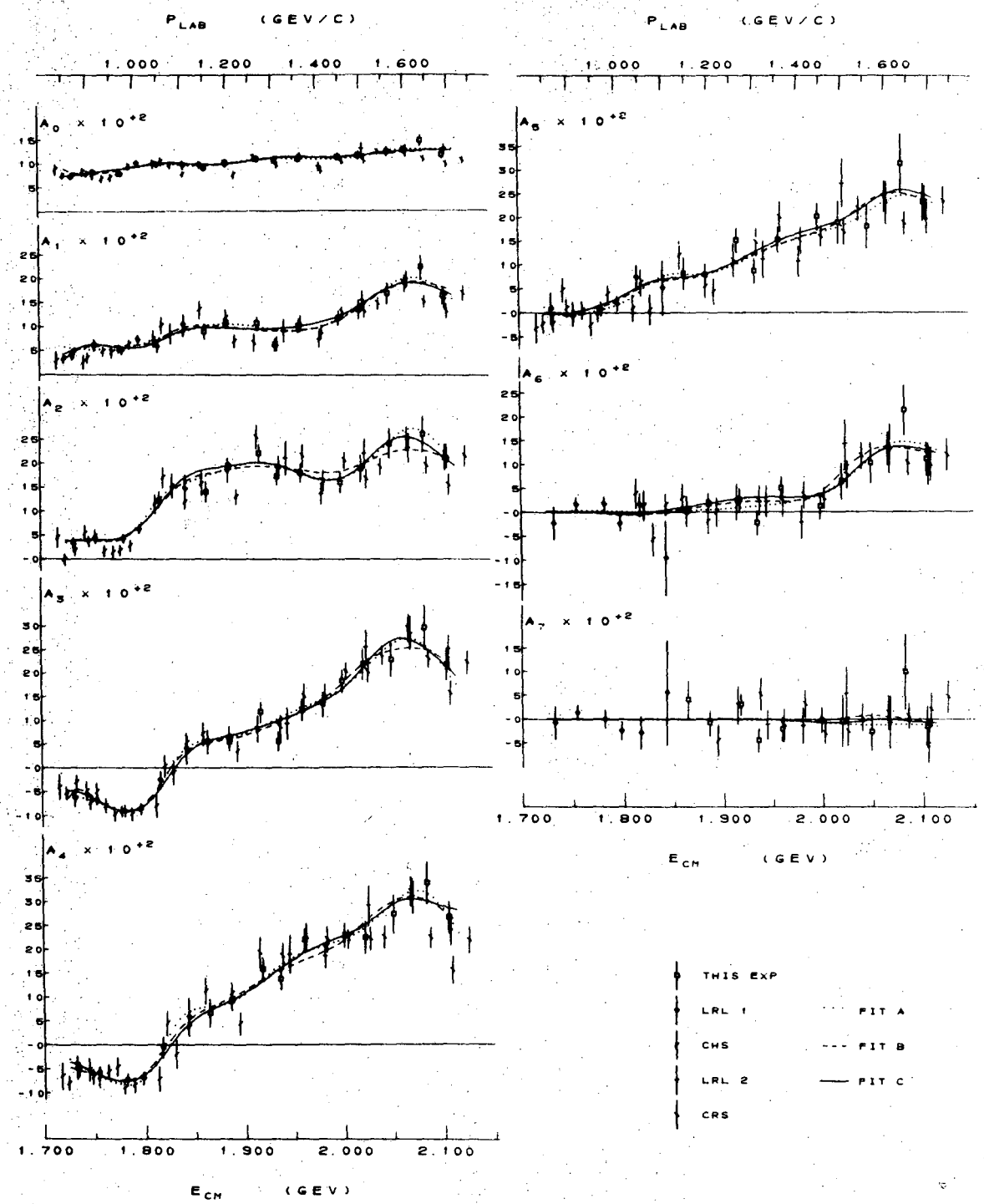

XBL 713-499

Fig. 15c. $K^-p \rightarrow \pi^-\Sigma^+$

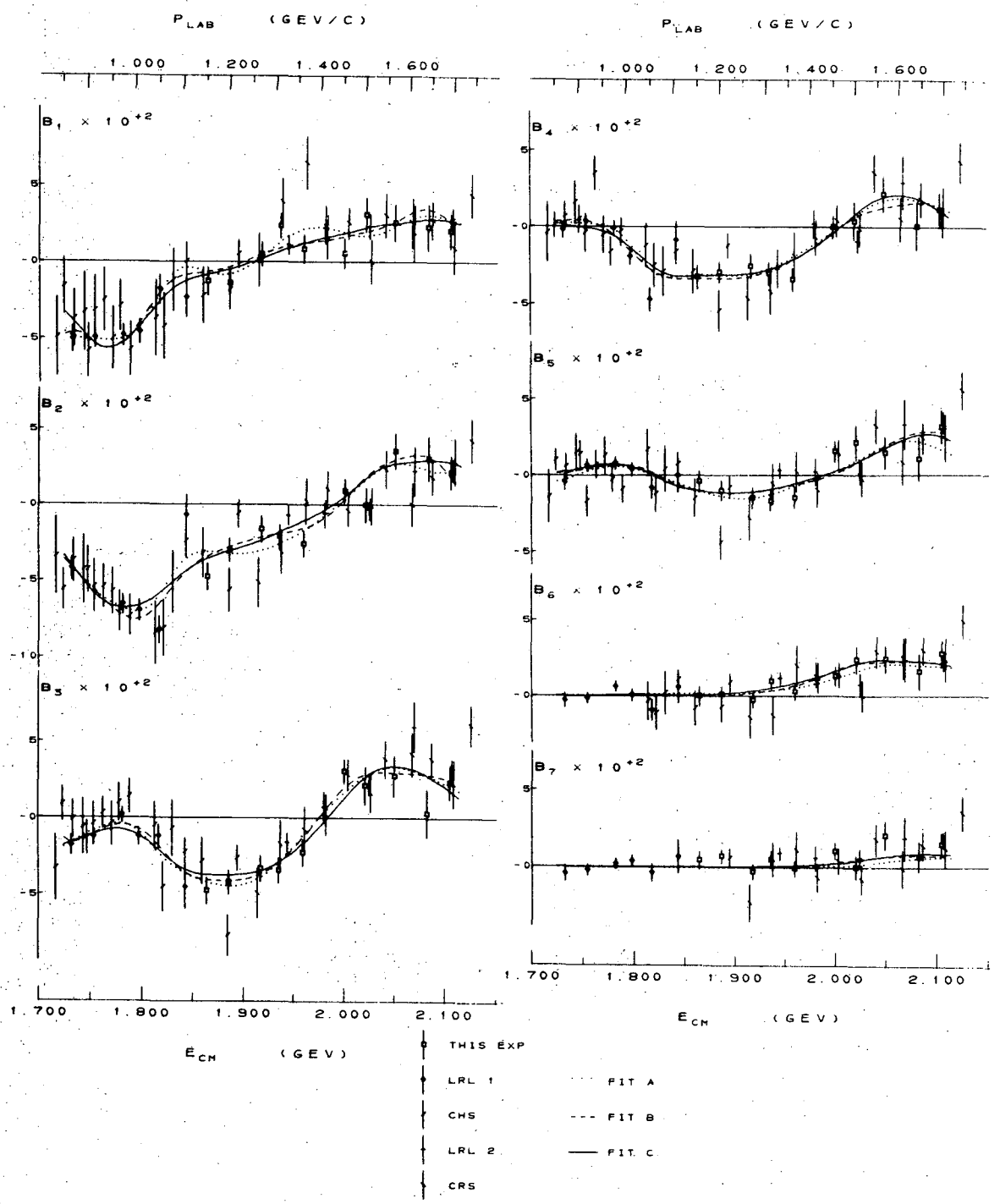

XBL 713-498

Fig. 15d. $K^-p \rightarrow \pi^-\Sigma^+$

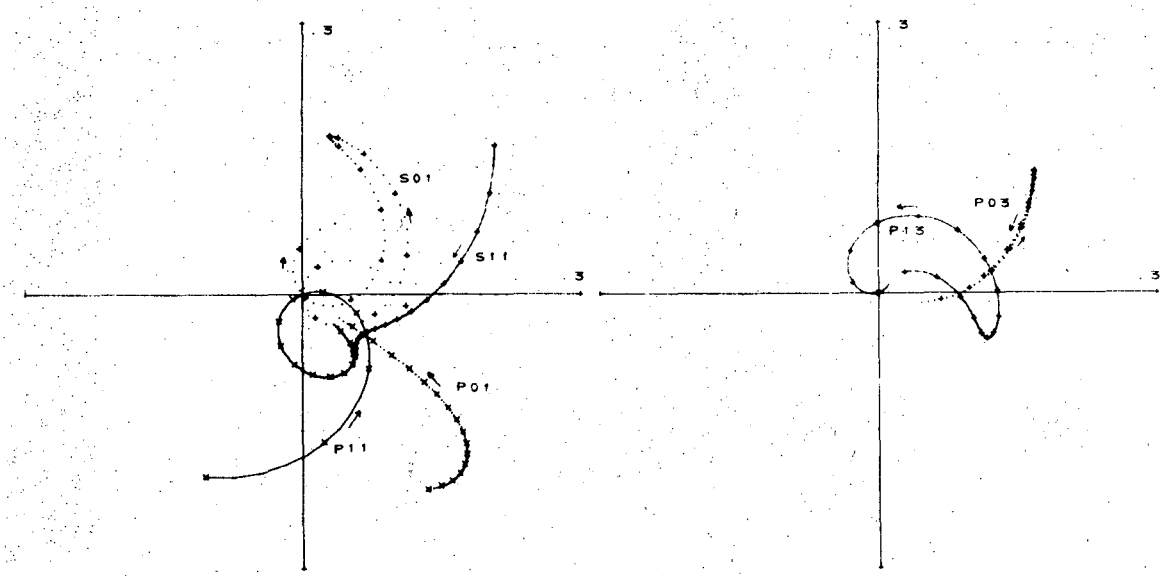

Fig. 16a

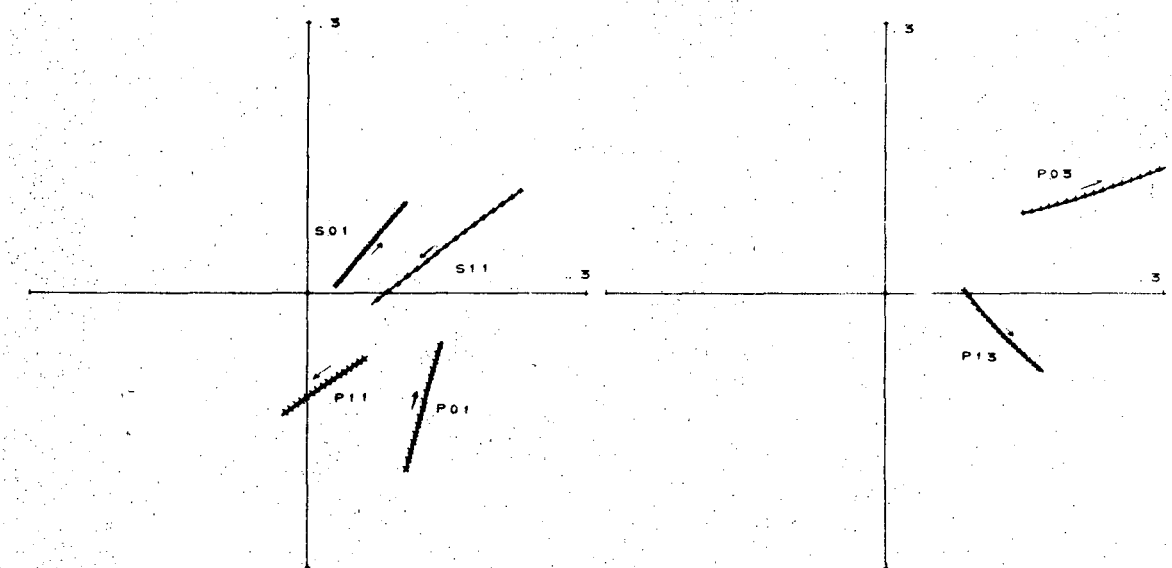

XBL 713-531

Fig. 16b

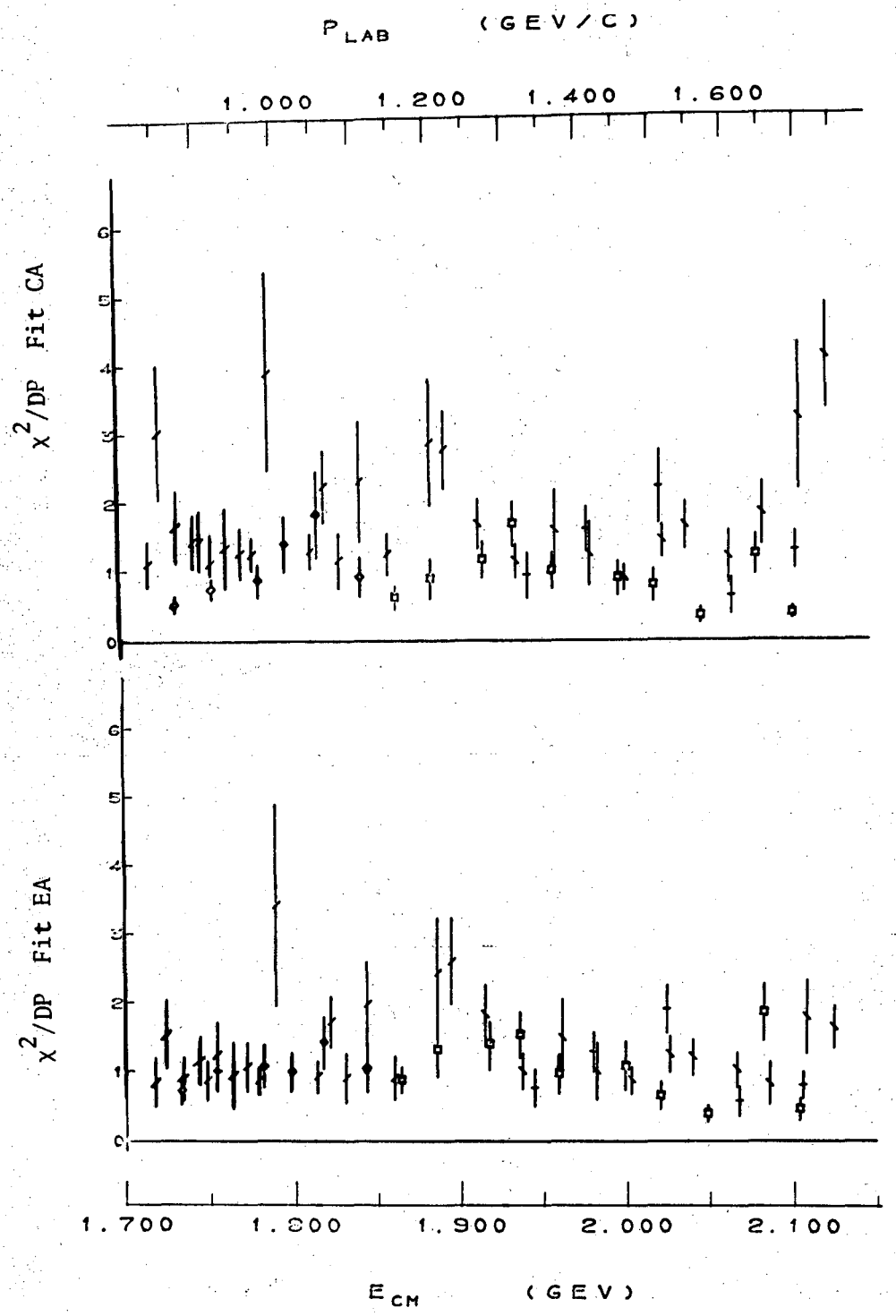

XBL 713-602

Fig. 17

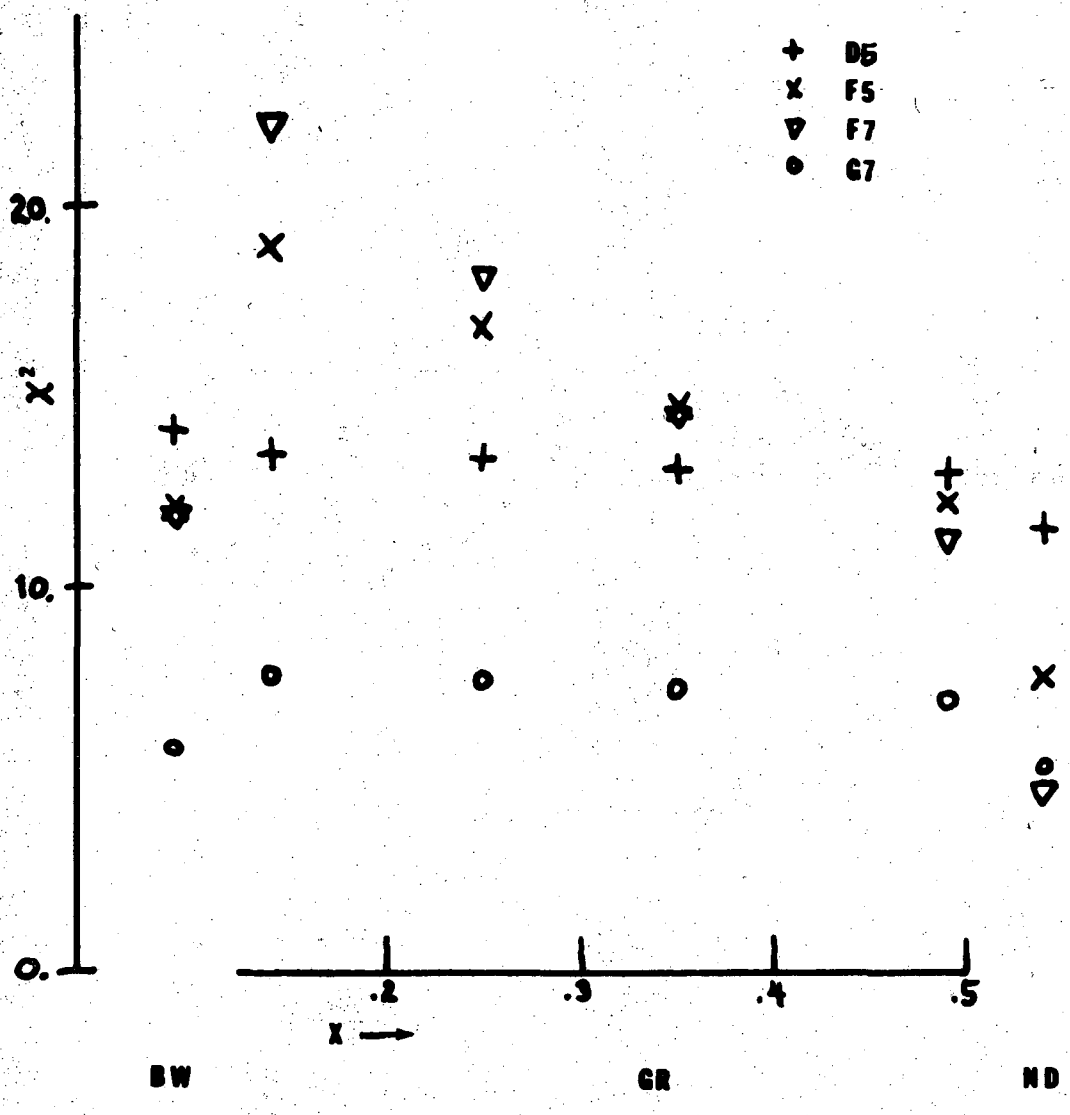

XBL 714-659

Fig. 18

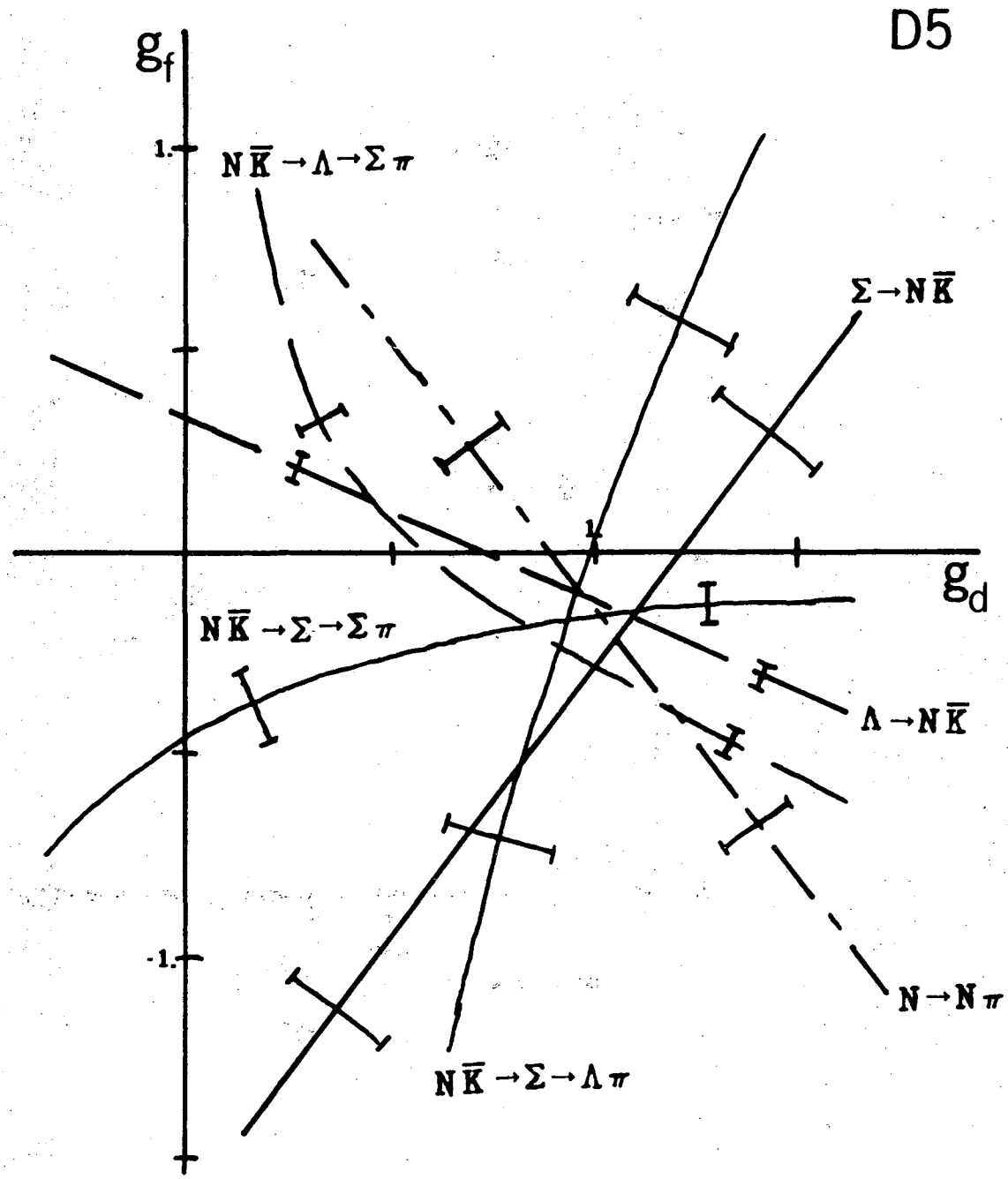

XBL 714-657

Fig. 19a

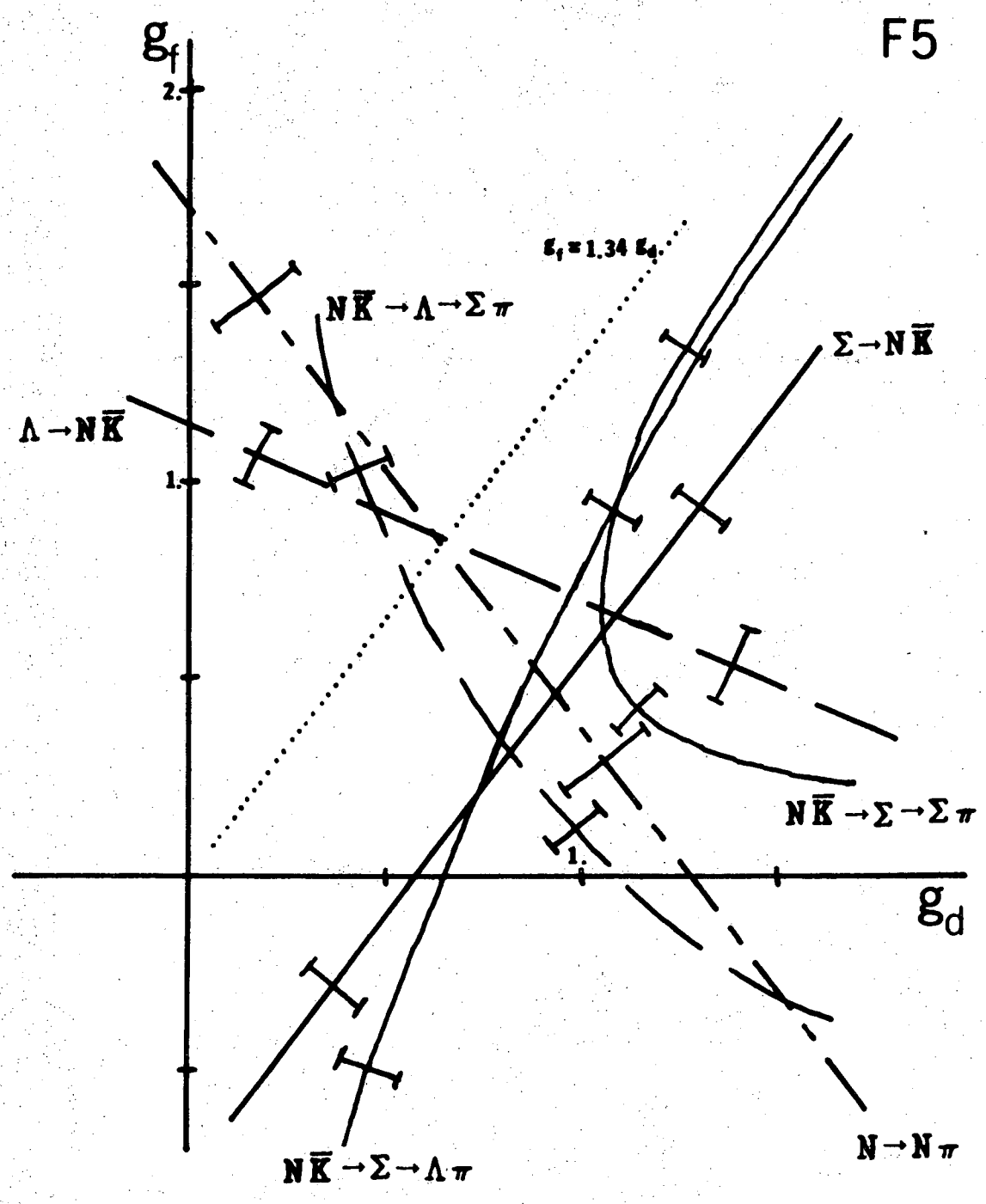

XBL 714-660

Fig. 19b

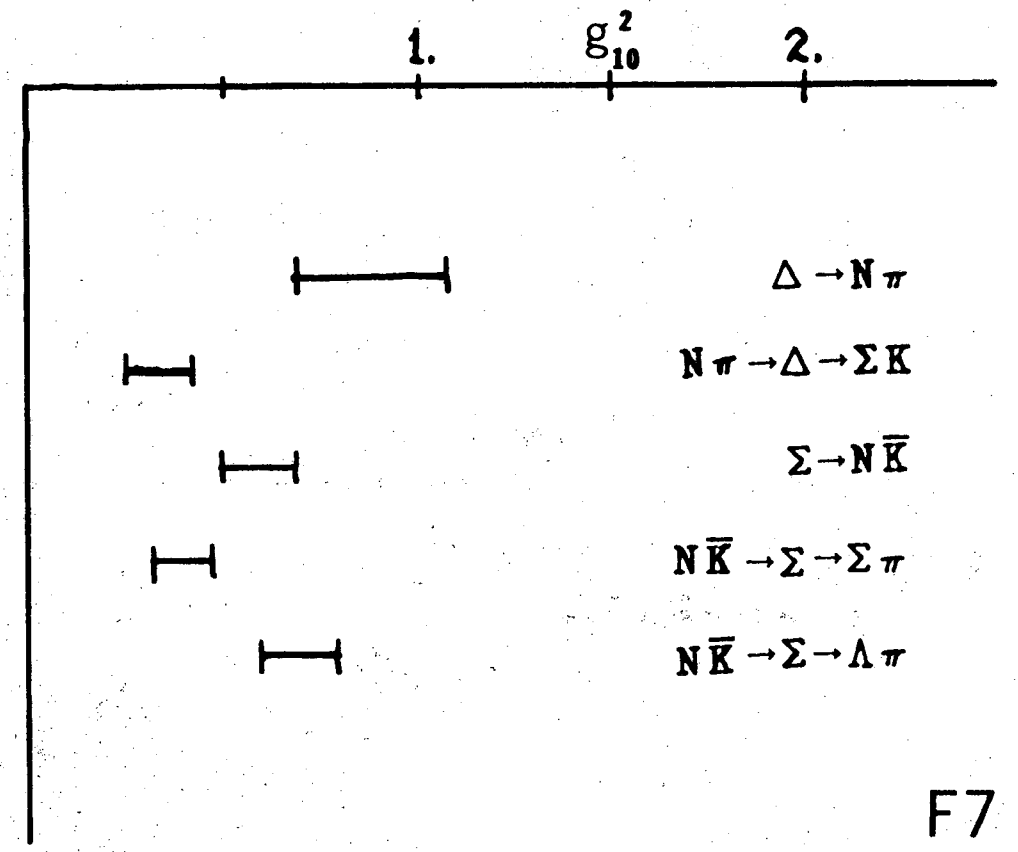

Fig. 19c

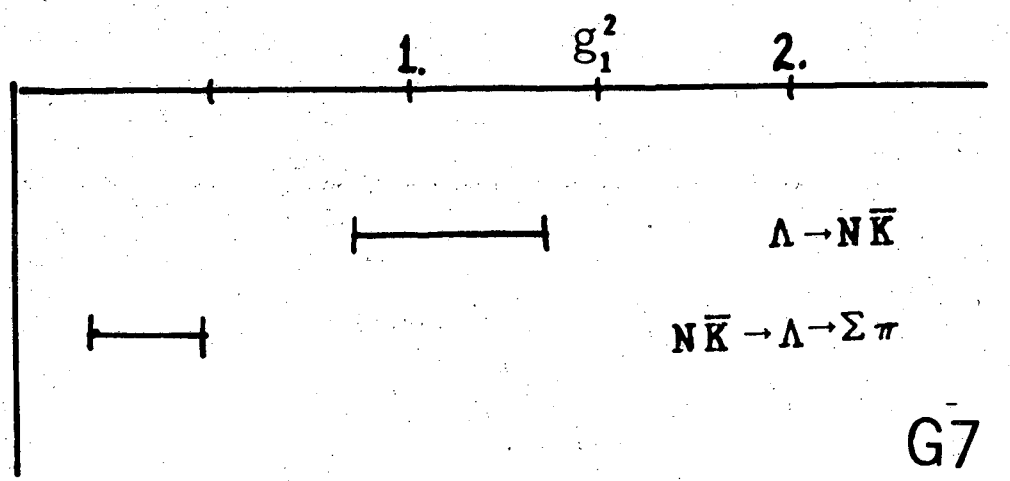

XBL 714-658

Fig. 19d

LEGAL NOTICE

This report was prepared as an account of work sponsored by the United States Government. Neither the United States nor the United States Atomic Energy Commission, nor any of their employees, nor any of their contractors, subcontractors, or their employees, makes any warranty, express or implied, or assumes any legal liability or responsibility for the accuracy, completeness or usefulness of any information, apparatus, product or process disclosed, or represents that its use would not infringe privately owned rights.

TECHNICAL INFORMATION DIVISION
LAWRENCE RADIATION LABORATORY
UNIVERSITY OF CALIFORNIA
BERKELEY, CALIFORNIA 94720